Final Report

Simulation and Analysis of Factors Leading to High PM_{10} Emissions Fluxes at Owens Dry Lake Using an Environmental Wind Tunnel

by

Bruce R. White
Principal Investigator

and

Jason Roney
Graduate Research Assistant

January 15, 2000

University of California at Davis
Environmental Aerodynamics Laboratory
Mechanical and Aeronuatical Engineering
Davis, California 95616

Prepared for

California Air Resources Board
(CARB)
Sacramento, California

Executive Summary of Report

- Four soils instrumental in fugitive dust emissions at Owens Lake were identified.
- The soils were tested in a laboratory environmental boundary layer wind tunnel at the University of California at Davis, where a control volume approach was used to establish emission rates for each soil.
- Conditions of the test bed were varied to simulate aspects of the variable conditions at Owens Lake (wind shear velocity, turbulence, saltation, moisture content, and surface conditions).
- Loose soils had the highest emission rates while crusted soils had the lowest emission rates.
- Emission increased substantially when soil particles were introduced upwind of the soil test area to simulate saltation effects.
- The highest emissions rates were 28000 $\mu g/m^2s$ for North Sheet Simulation (saltating sand over the loose soil).
- Moisture content was significant in the measured emission rates with a 10% increase in moisture corresponding to an order of magnitude decrease in emissions.
- Up to 30% of the measured PM_{10} emission can be attributed to $PM_{2.5}$.
- Of the soils tested, the most emissive soils contained high levels of Arsenic.
- Unexpectedly, one of the sandy soils (from the South Sheet) was nearly as emissive as the finer non-sand soils under the same conditions which could impact control strategies.
- The results help provide an understanding of the mechanisms that can lead to high PM levels from windblown dust episodes and show that it is possible to characterize the potential of PM generation based on the physical properties of the soil and soil surface.
- Although not a complete simulation of the actual in-situ emissions, the methods developed allow comparisons of the relative emissions potential of different soils when acted upon by winds.
- Finally, the results of this study provide information which characterizes the differing emissions potentials of Owens Lake soils which may prove useful in identifying control strategy measures.

Abstract

Factors leading to high PM_{10} emissions fluxes at Owens Dry Lake, an EPA Superfund Site for particulate matter, were investigated using an environmental laboratory wind tunnel. Four soils believed to be causal in fugitive dust events at Owens Lake were transported back to the University of California at Davis and tested under varying conditions in the Saltation Wind Tunnel (SWT), an environmental laboratory wind tunnel. The variable conditions tested include increasing the wind shear velocity and turbulence, enhancing saltation, varying moisture content, changing the surface condtions, and simulating atmospheric instabilities by heating the tunnel floor.

A control volume approach in the tunnel was used to establish rates of entrainment of PM_{10} and $PM_{2.5}$ for the soils under these variable conditions. The measurements necessary for the control volume approach were obtained with two aerosol monitors using a light scattering photometer technique to measure concentrations. Also used were two pressure transducers to obtain wind velocities for inlet and outlet flows. All data was collected in real time with an acquisition system in order to obtain mass fluxes from which the emission rates were calculated.

The highest emission rates produced were for a loose soil from the northern end of Owens Lake with saltation at the estimated equivalent 10 m wind velocity of 21 m/s (North Sheet Simulation). The before mentioned case corresponds to a Northerly blowing wind at Owens Lake. The emission rate for this soil under these conditions was found to be 27,600 $\mu g/m^2s$ for PM_{10} with about 30% of these emissions being $PM_{2.5}$. Moisture content played a significant role in reducing the emission rates; a 10% increase in moisture content in the air-dried soils can reduce the emissions by an order of

magnitude. Loose soil surfaces with and without saltation had the highest calculated emission rates. A hard crust surface without saltation had the lowest emission rates.

The results from the Saltation Wind Tunnel testing suggest that knowing and predicting trends are imperative in successfully modeling dust emissions from Owens Lake. The wind tunnel is thus one tool which can establish baseline quantities for expected emission rates at Owens Lake for variable conditions; however, it can not be expected to reproduce exact meteorological conditions. The usefulness of the wind tunnel is thus in quantifying the expected behavior of the near surface where dust emissions begin in order to develop control strategies.

Table of Contents

Table of Contents

Table of Contents

List of Tables

List of Figures

List of Figures

List of Figures

List of Figures

List of Figures

Figure Page

List of Figures

List of Figures

List of Figures

List of Figures

Figure Page

List of Figures

Figure Page

Section 1. Introduction Summary

- The Owens River diversion and desert environment lead to a dry lake.
- Owens dry Lake is an EPA Superfund Site for particulate matter as a result and requires a control strategy.
- The dry lake has many variable conditions that have not been studied or are not well understood.
- If a control strategy is to be implemented, these variables must be understood.
- The goals of this research project are then to study systematically those variables that are believed instrumental in creating large PM events.

1. Introduction

1.1. *Background*

The Los Angeles Department of Power and Water started diverting Owens river water from Inyo county to Los Angeles County with the completion of the Los Angeles aqueduct in 1913. The primary source of water for Owens Lake was thus diminished if not completely halted. Geologically, Owens Lake had slowly (thousands of years) been drying up naturally due to climatic conditions and desertification of the area; however, this slow process would have allowed stability to be reached. After the Owens River diversion, it was only a matter of years until the lake was completely dried up leaving unstable alkali soils which are susceptible to becoming airborne during wind storms. The desert climate as well as the rain shadow effect of the Sierra Nevada allowed evaporation of the remaining water (Figure 1 and Figure 2). In addition, due to the meteorology of the area, intense storm events occur due to lee cyclogenesis and intense winds blow either north or south through the Owens valley over the lake playa. These storms cause intense dust storms which transport high concentrations of PM_{10} (particulate matter of 10 μm or smaller aerodynamic diameter) into the atmosphere with estimated amounts to be 100,000-400,000 tons of particulate matter per year. In fact, by one estimate the figures go as high as 900,000 to 8,000,000 metric tons per year (Gill and Gillette, 1991). These airborne particles are small enough to travel great distances and can be inhaled deeply into the human respiratory tract creating a potential health hazard. The EPA uses PM_{10} levels as an indicator of air quality and classified the Owens Lake area as a "serious" non-attainment area. The National PM_{10} Concentration clean air standards on a 24-hour average are 150 $\mu g/m^3$ while the California standard is 50 $\mu g/m^3$. Research has shown that the Owens Valley region PM_{10} concentrations are as much as ten times the national standard on a nearly daily basis during active storm periods. In addition, the EPA is adding new fine particle standards ($PM_{2.5}$) to the existing PM_{10} standards, where in this case 2.5 refers to an aerodynamic diameter of 2.5 μm. The EPA standard for annual $PM_{2.5}$ is set at a concentration of 15 $\mu g/m^3$ with the new 24-hour standard set at 65 $\mu g/m^3$. Without doubt, the Owens Lake area surely will fail to meet these new standards without proper mitigation.

The 1990 Clean Air Act Amendment mandates that all areas must attain the PM_{10} standard, and thus, California was required to file a State Implementation Plan (SIP) which describes the process of attainment. Due to the need for mitigation of the dust storms, the University of California at Davis became active in many of the research projects aimed at evaluating the problem of dust mitigation. This report describes a study funded by the California Air Resources Board (CARB) aimed at better understanding high emission rates under various conditions at Owens Lake through the behavior analysis of Owens Lake soils in a laboratory wind tunnel.

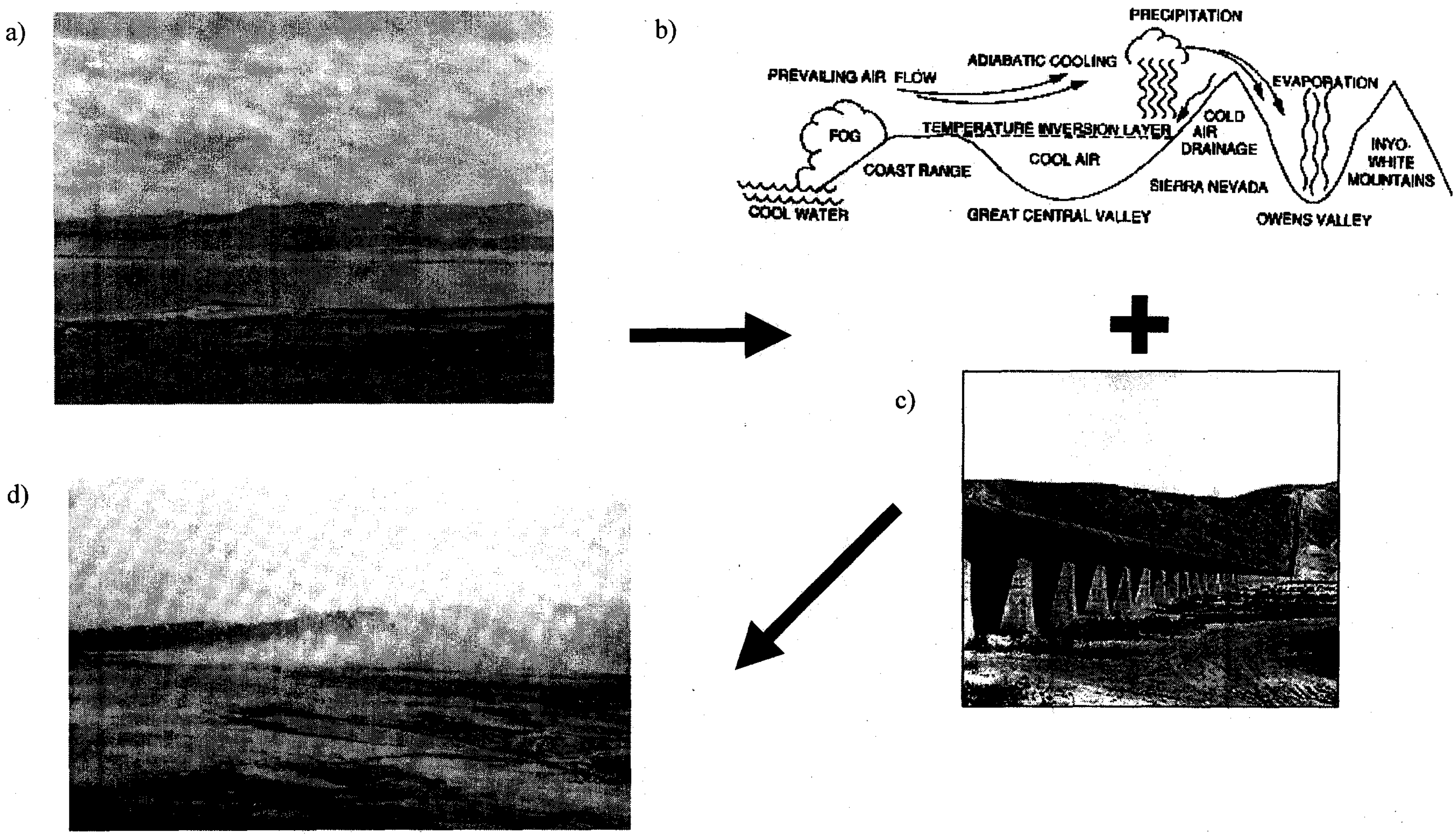

Figure 1. Owens Lake historical progression: a) a saline lake b) rain shadow effect creates desert environment c) the Los Angeles aqueduct diversion of the main source of water feeding the lake d) the present day dust storms

a)

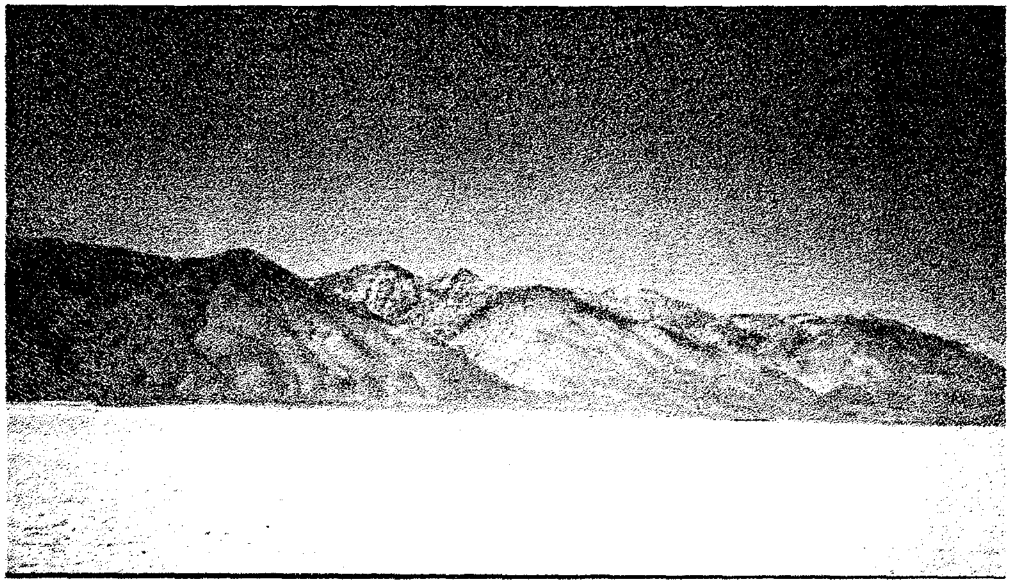

b)

Figure 2. Owens Lake: a) a clear day looking west across the lake and b) at the beginning of a dust storm.

1.2. Project Objectives and Applicability

An important component of understanding the Owens dry lake bed dust storms is determining the actual emission rates occurring during severe storm conditions--these conditions are variable and not easily characterized by a set of unique meteorological conditions. Even less clearly understood is the composition of natural surface soil when severe dust storms are initiated. It is known that there are ranges of surface conditions any of which can lead to the rapid emission of large amounts of PM_{10}. The lack of understanding of the complete emission process of Owens dry lake bed is due to the size and complexity of the lake bed. The lake bed is 110 square miles with approximately 35 square miles of the area subject to wind erosion. A more comprehensive understanding is essential if a viable mitigation plan is to occur.

The goals of this research project are then i) to rank the emissivity of different Owens dry lake surface bed types and identify those which are most susceptible to wind erosion; ii) determine the effects of enhanced soil erosion due to surface scouring by saltating particles; iii) test the effects of wind turbulence and wind gusts on erosion; and iv) test the effect of simulated unstable atmospheric conditions on the erosion processes. The hope is that, ultimately, this information can be used to develop computer models which will predict the PM_{10} flux and transport off the dry lake into the atmosphere. In order to develop and use these models, specific information about the soils and meteorology of the area must be well understood, and thus, information from and about Owens Lake must be quantifiable to improve and establish models for the dry lake.

Currently, there is a great need to be able to predict the transport of PM_{10} and $PM_{2.5}$ above 10 m heights in the atmosphere based on a 2-3 m height sampling. The effect of surface variability on dust entrainment is imperative in determining concentration levels in the atmosphere. Owens Lake is a prime example in surface variability where dry seasons and wet seasons produce entirely different conditions. Note that Owens Lake is not an isolated example and that there is a need for this type of study to address several similar particulate problems, for example, the Columbia Plateau, the Great Plains, the San Joaquin Valley, and the Salton Sea. Many researchers have addressed the Owens Lake problem; even so, there are many aspects of the problems that remain unexamined or not completely understood. A physical understanding of the mechanisms of dust entrainment for Owens Lake soils is important in helping the state of California meet its air quality goals. Thus, the primary goal of this project is to provide needed insights into the mechanisms of dust entrainment at Owens Lake, a methodology which may prove beneficial at other sites around the state California as well as other desert-type regions..

Section 2. Experimental Techniques and Methods Summary

- Four Owens Lake soils were collected corresponding to regions of known emissions activity and transported back to the University of California at Davis.
- Meteorological observations were used to gage the range of velocities to be simulated with the wind tunnel.
- Soil properties were obtained through sieving as well through chemical analysis.
- The wind tunnel used in this study is an environmental boundary layer wind tunnel known as the Saltation Wind Tunnel (SWT) which is specifically designed to simulate natural soil movements.
- The measurement instrumentation consisted of two aerosol monitors and two pressure transducers to measure wind velocity which are connected to a data acquisition system using LabView® software.
- Threshold measurements were made using a Keithly Electrometer Model 602.
- Emissions estimates were obtained with profiles of PM and velocities taken at two different locations along the soil test bed.
- Where pertinent, sand traps were used to obtain the sand saltation flux over the bed.
- A method for testing moisture effects was developed.
- A method of producing a hard crust of Owens Lake soil and testing emission is described.
- The method for observing how the emissions develop with fetch is described.
- The method for testing instabilities on threshold conditions for Owens Lake soils is described

2. Experimental Techniques and Methods

2.1. Introduction

As part of the Department of Mechanical and Aeronautical Engineering at the University of California at Davis, one of our primary research tools is simulation using wind tunnels. In this way, we can study the emissive conditions present at Owens Lake by controlling the pertinent variables. R.A. Bagnold developed a technique of studying the dynamics of desert sands by employing the use of an environmental boundary layer wind tunnel. In his studies, desert sands were placed in the tunnel and the dynamics of sand movement studied. This type of tunnel has special characteristics not found in a traditional aeronautical wind tunnel. The development section is quite long to allow for the development of a turbulent boundary layer characterized by the roughness of the soil or sand as present in the atmospheric boundary layer (to establish "fetch"). In a similar fashion, the Saltation Wind Tunnel at the University of California at Davis is designed to simulate this same type of flow (Figure 3) and can be used to establish emission rates with pertinent Owens Lake soils.

After establishing the boundary layer dynamics, the primary focus of this wind tunnel study is then to match wind conditions with those that occur near the surface in the Owens Valley. From previous studies, the mechanisms of wind development in the valley occur due to primarily four mechanisms with North/South winds being the primary effect. Other effects produce intense storm events through Sierra Waves with large down drafts. In addition, the meeting of North/South air masses lead to a lee forming horizontal cyclonic eddy. In the winter, down-valley drainage flow is the predominant weather pattern; in spring, there is combination of both down-valley drainage and up valley surface winds; and in the summer, the winds are primarily due to local heating differential causing an up-valley flow (Figure 4). This previous mechanism accounts for winds exceeding 10 mph or 4.5 m/s only 20 percent of the time (Aeroenvironment, 1992, GBUAPCD, 1994). A less common wind pattern, but far more extreme is produced by mountain lee waves (Sierra Waves). When strong Westerly winds blow over the Sierra Nevada, air masses rapidly descend into the valley warming and picking up speed, often creating rotors which churn up dust (Figure 5). These wind velocities can be as high as 45-68 mph (20 – 30 m/s) at a 10 m sampling height taken by meteorological stations. Likewise, occasionally a cold front from the north with strong northerly winds will collide with southerly winds producing a horizontal cyclonic eddy lifting dust high into the air (Figure 6).

From these extreme weather values, we obtain the upper limit on the range of velocities that the wind tunnel must be able to represent, around 30 m/s at a 10 m height. Finally, our study becomes a matter of collecting the correct soils and testing them under the variable conditions related to the meteorology.

a)

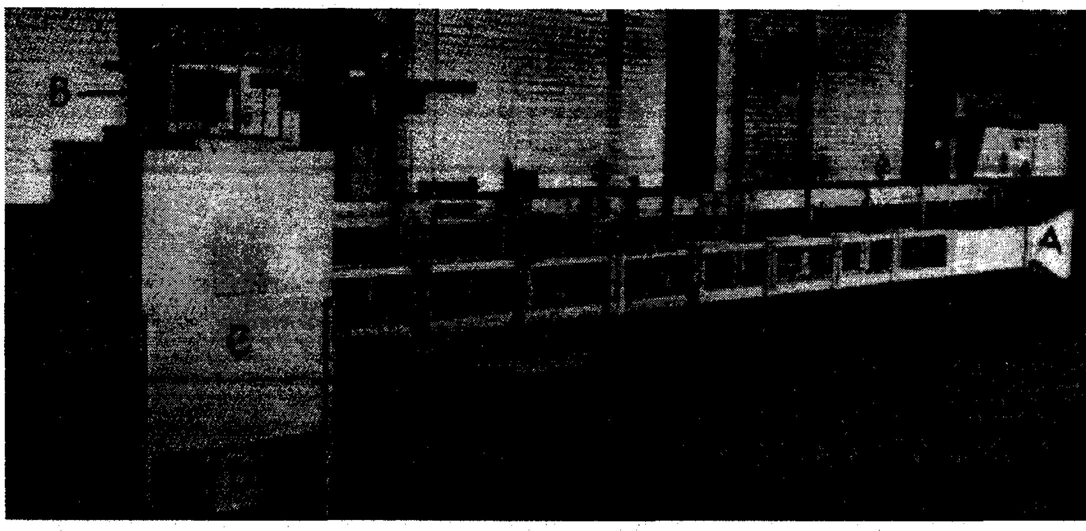

b)

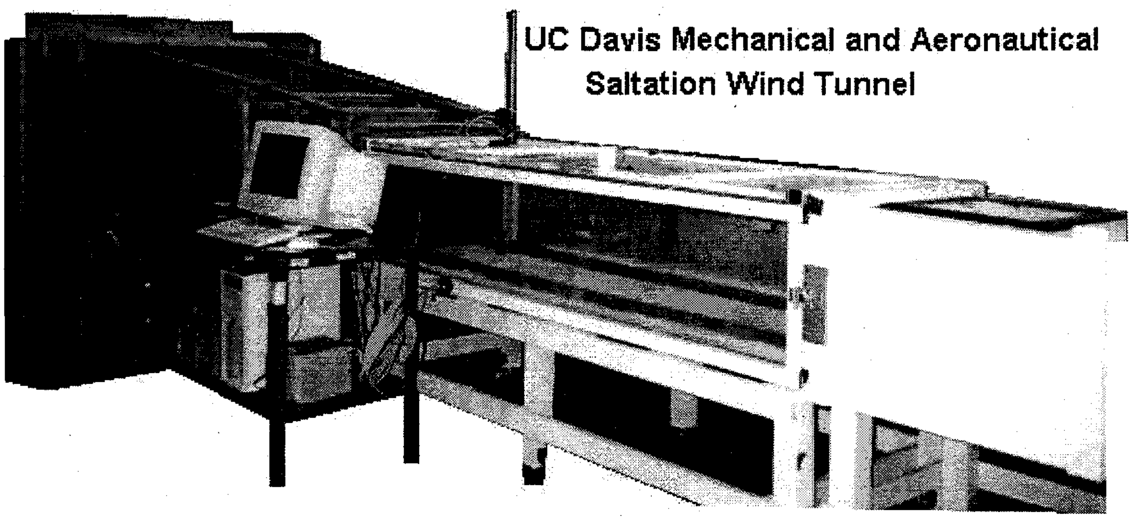

Figure 3. Saltation Wind Tunnels: a) Bagnold's wind tunnel to study sand movement and b) theUniversity of California at Davis Saltation Wind Tunnel to study dust and sand movement.

a)

b)

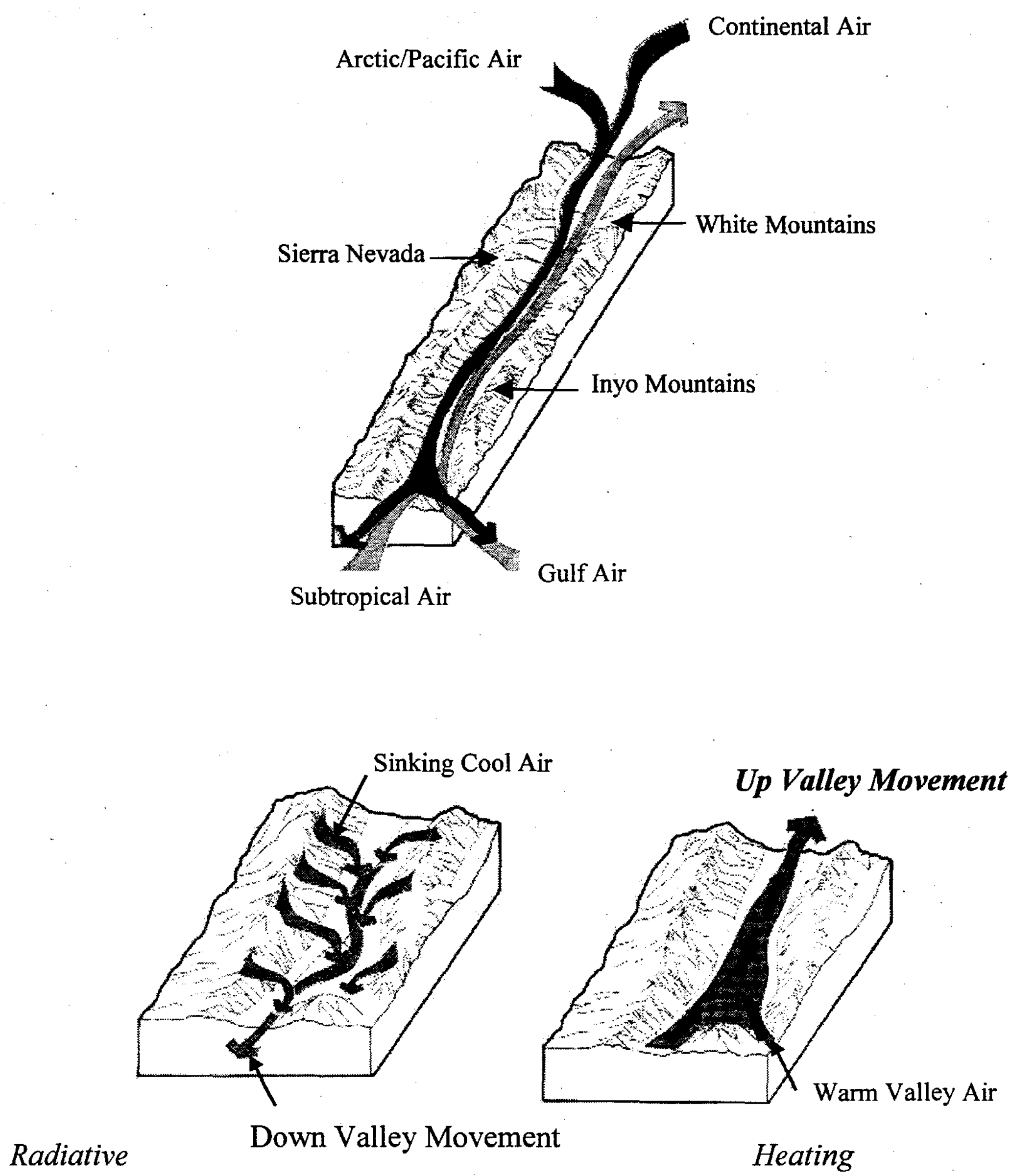

Figure 4. The primary modes of wind development in the Owens Valley: a) North/South wind patterns are produced year round by various meteorological systems, and b) they physically produce either radiative cooling in winter or a heating differential in summer or a combination of both in spring and fall. However, this mechanism is rarely responsible for the most intense storm events.

a)

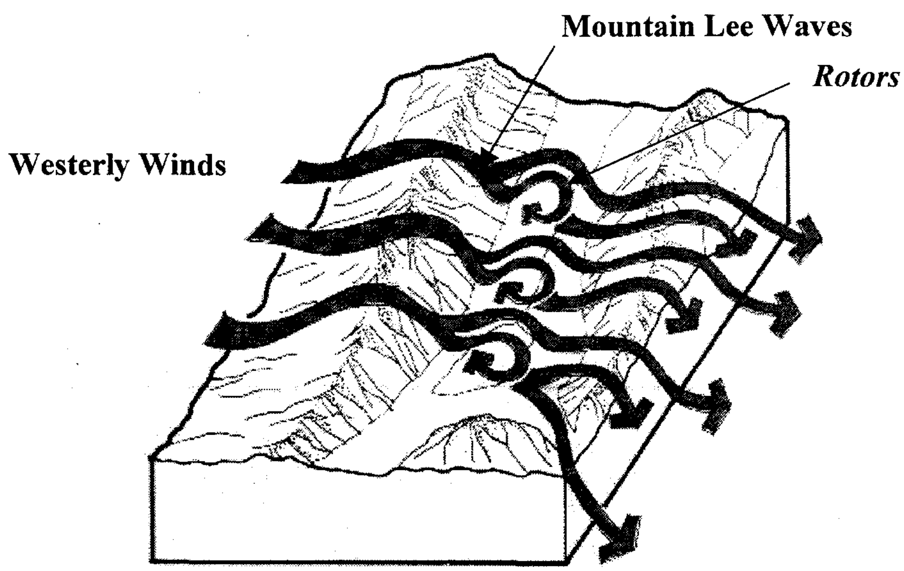

b)

Figure 5. The mechanism for intense dust storms and extreme winds in the Owens Valley a) a schematic showing the process of Sierra Waves (lee waves) and b) a photograph showing this mechanism creating a large dust storm.

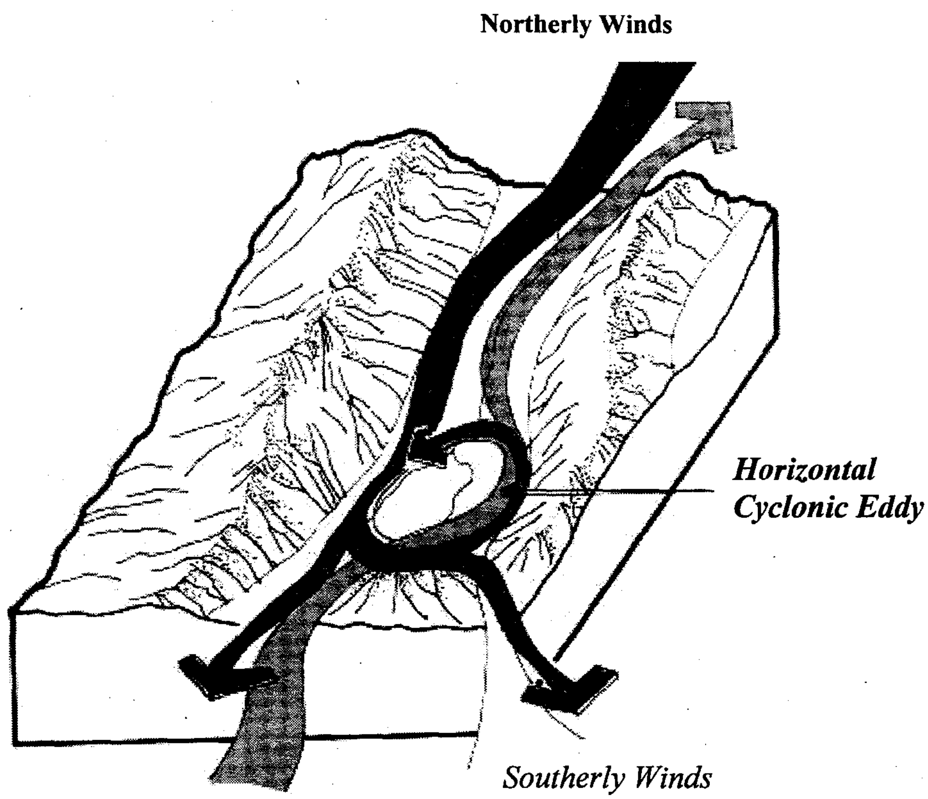

Figure 6. The process of formation of a large horizontal cyclonic eddy. This eddy can produce large amounts of dust transport off Owens Lake.

2.2. Soil Collection

In September of 1999, approximately five tons of soils were collected at Owens Lake for use in wind-tunnel simulations to be performed at the University of California at Davis. Previous field studies by Niemeyer, 1996, Cahill, 1994, Great Basin Unified Air Pollution Control District (GBUAPCD), 1997, and the California Air Resources Board, CARB, 1997 indicated the locations of the dry lake which appeared to be most emissive (Figure 7). Logically, these areas were then targeted for soil collection and located using a Global Positioning System (GPS) instrument. The locations of soil collection are shown and corresponding pictures shown on the following pages (Figures 8 and 9).

At each location, the very top surface, about 2.5 cm, was scraped off and then soil collected to depths of approximately 10 to 25 cm to ensure that only that material most susceptible to erosion was collected. The 2.5 cm layer was discarded because it corresponds to the hard crust which must be broken mechanically if the loose soils below are to be exposed to wind. The hypothesis then is that the loose soils are the major culprit of fugitive dust events with the exception of efflorescent salts, and thus, the Owens Lake soils should be tested primarily as loose soils in the wind tunnel

Soil was collected at four separate locations as indicated and labeled on the map, Figure 8. In the north part of the lake, sand from the North Sand Sheet (Soil #2) was collected as well as a more emissive soil directly to the south of the sand near the Old Wooden Pipe Line (Soil #1). The soil collected in this part of the lake was moist, with the emissive soil appearing to have the most moisture. In the south part of the lake, sand from Dirty Socks Dune (Soil #3) was collected as well as an emissive soil directly to the north of the dunes near the University of California at Davis sand fences (Soil #4). The soil in these locations appeared quite dry. The exact GPS coordinates are shown in Table 1. These soils were then transported back to the University of California at Davis to be used in the wind tunnel studies.

Table 1. GPS locations for the four soils collected at Owens Lake.

Designation	Description	Suspected Type	GPS Lat.	GPS Long.
Soil # 1	Old Pipe Line	Emissive Soil	36°28.808 N	117°54.649 W
Soil # 2	North Sand	"Sand"	36°29.194 N	117°54.655 W
Soil #3	Dirty Socks Dune	"Sand"	36°20.391 N	117°57.681 W
Soil #4	UCD Fence	Emissive Soil	36°21.411 N	117°57.467 W

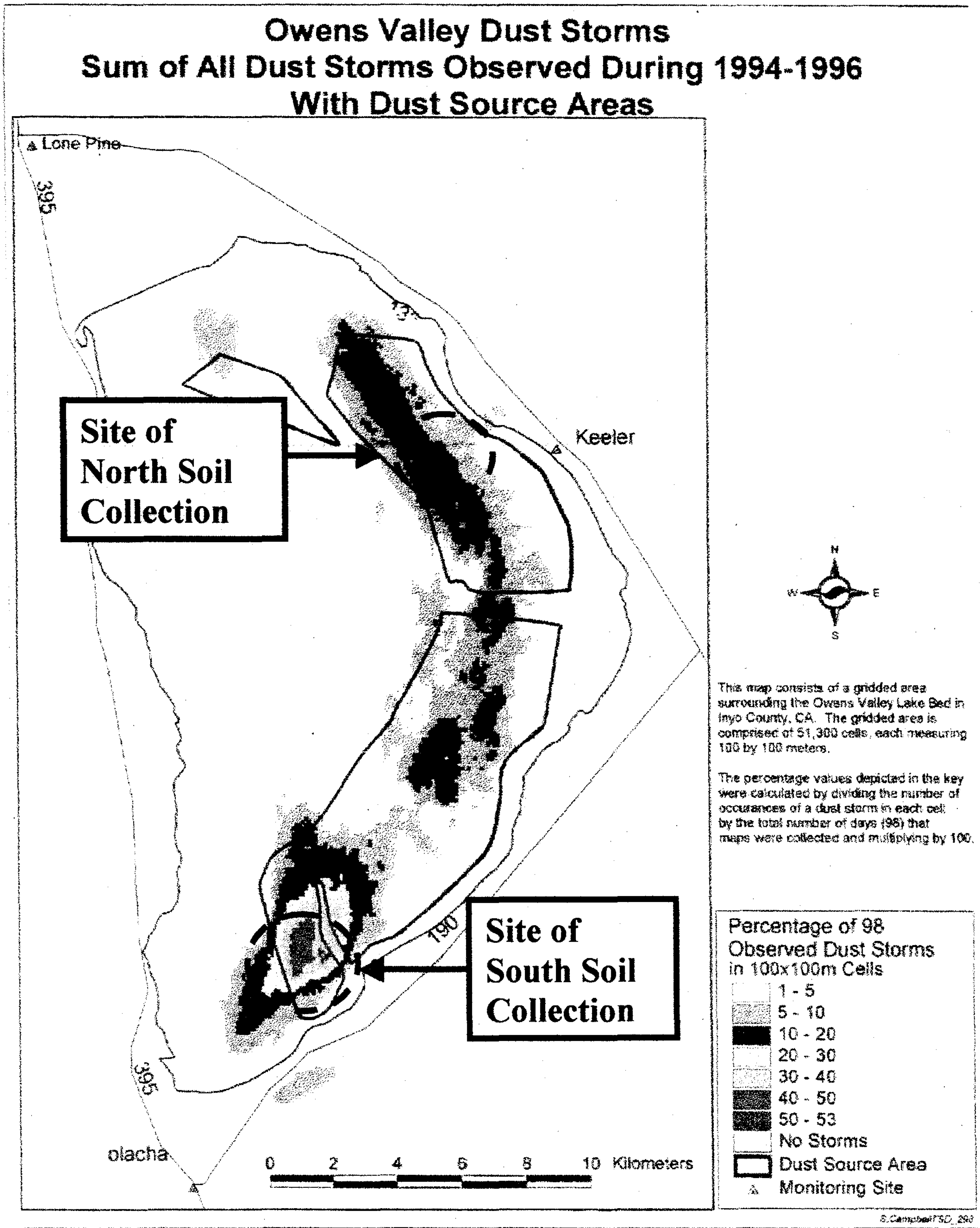

Figure 7. The above map shows the frequency of storms and the approximate locations of soil collection.

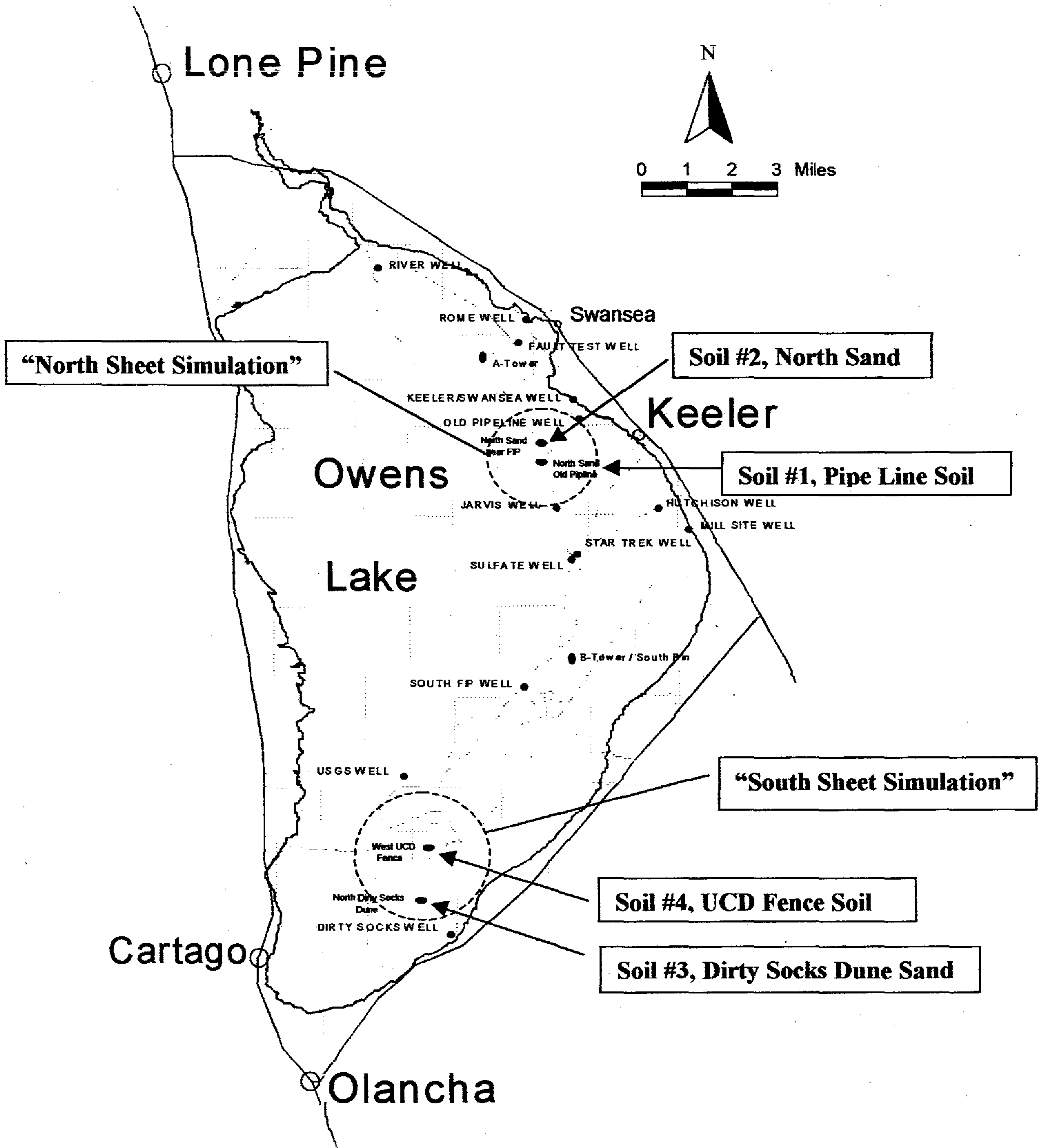

Figure 8. Sites of soil collection for Emission Inventory of PM 10 and PM 2.5 at Owens Dry Lake

a)

b)

c)

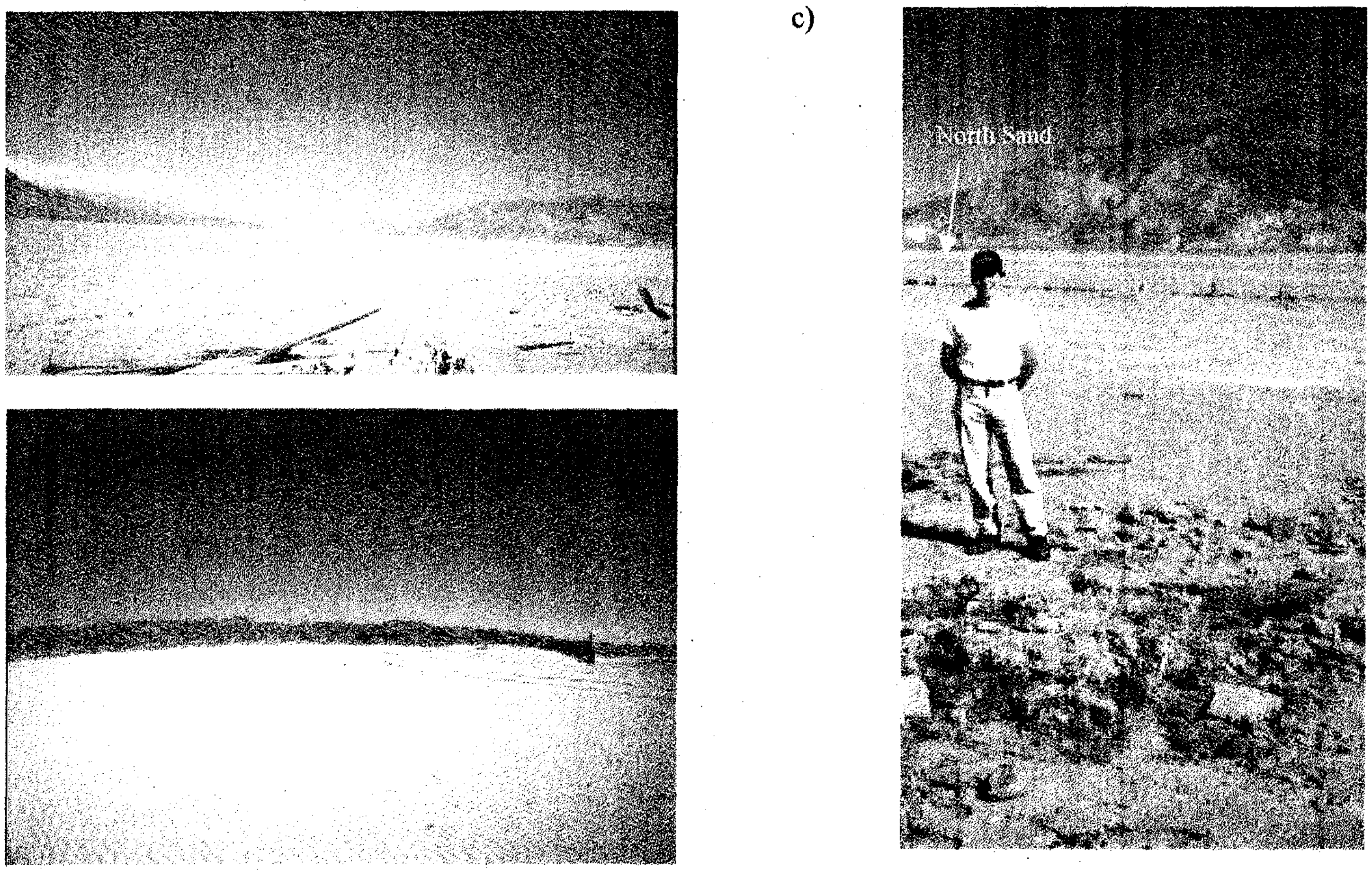

Figure 9. Photographs of the locations of soil collection a) Soil #4, emissive soil near the UCD sand fences, b) Soil #3, Dirty Socks Dune Sand, and c) North Sand (Soil #2) and the emissive soil near the Old Wooden Pipe Line (Soil #1)

2.3. Soil Properties

Properties of the soils were obtained once back at the University of California at Davis. Specifically, the particle size distribution of each soil was obtained using a sonic sieve (Figure 10). The sonic sieve works by vibrating/shaking the soils through the sieve network as well as emitting an occasional pulse to break up agglomerations which are held loosely together. In this process, 30 grams of each dry soil were sieved through the following stack of sieves: 0.841 mm, 0.500 mm, 0.420 mm, 0.354 mm, 0.297 mm, and 0.180 mm, and the fines collected. The fines were then sieved through a second stack of sieves: 0.125 mm, 0.088 mm, 0.053 mm, 0.044 mm, and 0.008 to 0.012 mm. The amount retained in each sieve was then weighed to an accuracy of 0.01 grams and recorded. This procedure was repeated a total of three times for separate random samples of the same soils and then averaged together to obtain a gradation curve, a distribution of size of particles passing through a certain size sieve. A gradation curve for each soil was obtained in this way. At the same time, samples of each soil were sent to Wallace Laboratories for a chemical analysis (See Appendix F for detailed chemical analysis of the soil). The soils were then ready to be tested in the Saltation Wind Tunnel with the applicable variables applied.

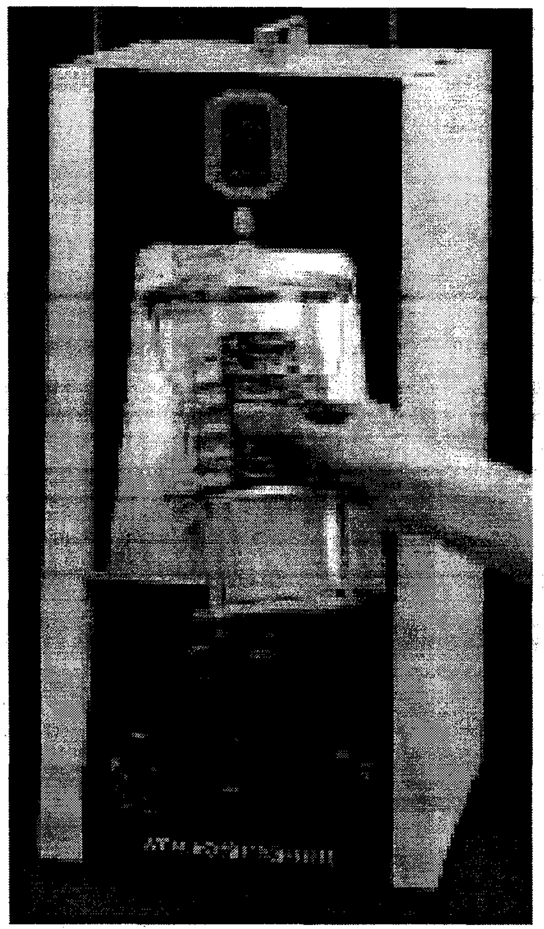

Figure 10. Sonic Sifter with a typical sieve stack arrangement used to do particle size analysis.

2.4. Wind Tunnel

Quantification of the conditions for high emissions of PM_{10} for various Owens Lake soils is addressed experimentally with a wind tunnel. Soils collected from Owens Lake which are believed to be causal in the extreme PM_{10} and $PM_{2.5}$ emission conditions were collected and tested in the tunnel.

Measurements are made with the Saltation Wind Tunnel, an Environmental Boundary Layer Wind Tunnel at the University of California at Davis (Figure11). This open circuit wind tunnel is specially designed to simulate particle flows or saltation movement, and thus, it is ideal for simulating the emission of dust from the surface of Owens dry lake. The tunnel has a long section to develop a turbulent boundary layer characteristic of the surfaces of desert playas. In order, to establish this, a set of small pebbles are affixed to the bottom surface in the first five meters of the development section of the tunnel and evenly spaced, but randomly oriented such that a well-developed two-dimensional boundary layer will form prior to impinging on the soil. The next two sections contain the soil of interest and the boundary layers are fairly closely matched due to the similar roughness characteristics. In this section, to conserve soil and maintain an even depth, a trough 0.25 m x 0.30 m wide was used with the sides containing rough sand paper to match the roughness of the soils.

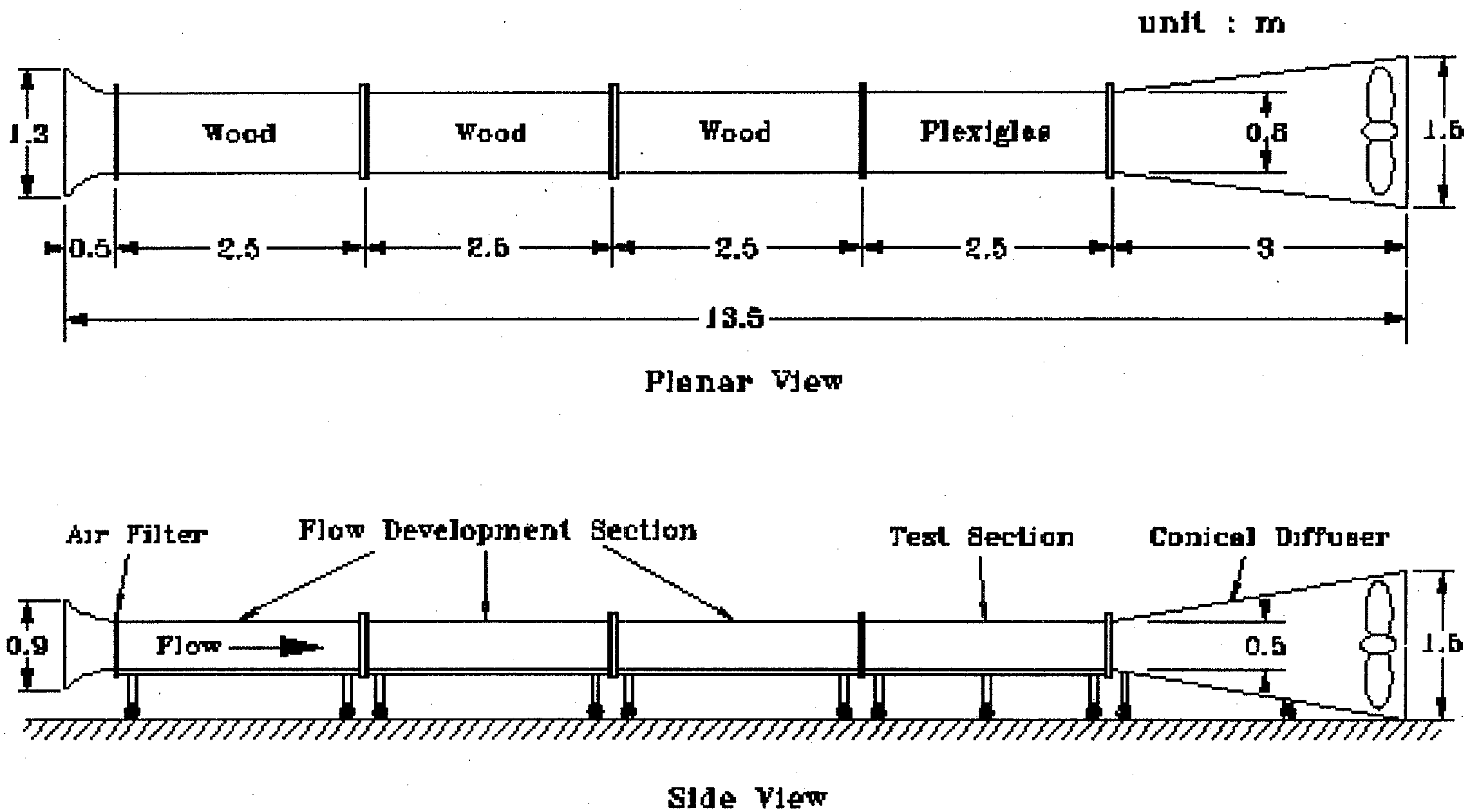

Figure 11. Schematic of the Saltation Wind Tunnel at the University of California at Davis showing dimensions.

2.5. Measurement Instrumentation

The measurement instrumentation consisted of two traversing DustTraks™, each measuring PM_{10} or $PM_{2.5}$ concentration (mg/m^3) levels at two different centerline downstream locations, a traversing pressure transducer to measure the velocity field, and a Pitot-static tube to measure the mean velocity. In addition, an Electrometer instrument could be placed in the tunnel to detect the moment when soil movement begins, measuring the threshold friction velocities of the soils. The threshold friction velocity was defined as the critical point in the friction velocity at which the particles on the surface start to move.

2.5.1. Aerosol Sampling: DustTraks™

The two traversing DustTraks™ measure the concentrations through a sampling tube inserted into the flow with a cross-sectional opening perpendicular to the incoming flow. The cross-sectional area of the tube is 31.67 mm^2 and the tube pulls in air at a sampling rate of 1.7 L/minute or 472 mm^3/s corresponding to a sampling velocity of approximately 14.9 m/s. Thus, all measurements are not isokinetic, meaning that the velocity of the flow and the sampler are not the same velocity. In our experiments the maximum velocity encountered in the wind tunnel is around 13.5 m/s. At first glance this seems to show that our aerosol samplers are actually taking conservative estimates of the concentrations. When the external speed is less than the inlet velocity, particles with high inertia will not be able to follow streamlines and will pass outside the sample wall so that the particles are under-sampled. Likewise, an initial bend in the tubing leading to the DustTrak™ is another location in which particles can be lost. Whenever an aerosol is forced to change directions, particles entrained in the airflow are forced to change direction. Small particles with their low inertia follow this change in direction better than larger particles. Any initial bends in the tubing were completely eliminated such that a build-up of particles bigger than PM_{10} size does not occur. Since, our primary concern is an accurate assessment of PM_{10} we note that the sampled particles are going to be primarily of the small inertia type and will easily be entrained in the air going to the DustTrak™ aerosol sampler.

The DustTrak™ aerosol sampler is a direct-reading aerosol monitoring instrument using a light scattering photometer. The light scattered by ensembles of particles passing through an optically defined measurement volume is related to the concentrations of PM_{10} or $PM_{2.5}$. Light scattered by particles in the sensing zone fall onto a receptor which is positioned off the optical axis. As the number of particles increase, the light reaching the receptor increases. The light intensity reaching the receptor is then predicted with Mie theory or Rayleigh theory (Nichols, 1998) which relates light intensity to particle size. The DustTrak electronics automatically uses this technique to send a concentration value in mg/m^3 to the LCD screen as well as to the computer data-acquisition system where it is recorded. In addition, the DustTrak™ has specialized orifices to selectively choose the size range of particles reaching the sampler. There are orifices specifying the following size ranges: particles less than 10 μm, particles less than 2.5 μm, and particles less than 1.0 μm.

The DustTrak™ instruments are more sensitive to low concentrations as compared to a gravimetric means (using filters as the means of measuring concentration), since the light scattering signal can be detected with greater sensitivity. However, this increased sensitivity at low concentration levels comes at the expense of having an upper concentration limit. For the DustTrak™ the upper concentration limit is 100 mg/m^3 to maintain this sensitivity. Again, we note that if this device was being placed directly in an industrial smoke stack this may have been a problem for our application; however, rarely, in the measurements performed in the wind tunnel were the dust concentrations near the surface measured to exceed this upper limit. The concentrations then decrease with height away from the surface.

Finally, we note that both DustTraks™ were cleaned and factory-calibrated by TSI (the manufacturer) before beginning this study (Figure 12) (See Appendix G for calibration certificates). The calibration of these instruments is done with Arizona Road Dust by TSI. It is assumed that Arizona Road Dust is representative of most fugitive dusts; however, the chemistry and morphology of the dusts being sampled are also important in any photometric analysis method, and thus a cautionary approach would be appropriate. The Great Basin Unified Air Pollution Control District (GBUAPCD) has recently presented that in side by side sampling of Owens Lake fugitive dust emissions at the site, the DustTrak™ and TEOM measure differing amounts. The DustTraks™ measures approximately one half the concentration of the TEOM (Ono, 1999). In a more comprehensive study, these sorts of differences are seen between the TEOM and many other types of PM monitors at Owens Lake (GBUAPCD, 1999), thus the question as to what monitor represents the most accurate description is debatable. However, all the monitors measure the same range of values, and thus, for this study, where baseline quantities and comparisons to obtain physical insight about PM entrainment are important, the exact amounts are less crucial than the physics. This statement does not concede that the DustTrak™ readings are wrong; but however, cautions that the readings should not be considered absolute until further studies clarify the ambiguity of the PM monitors and Owens Lake soils.

2.5.2. Velocity Measurements: Pressure Transducers

Years of measuring fluid velocities experimentally in either wind tunnels or water tunnels has yielded many technologies to measure velocity; however, many of these technologies are not valid in "dirty" environments. For this reason, the pressure transducer was chosen over hot-wire anemometry or Laser Doppler Velocimetry (LDV). Hot wires, which are used extensively, can easily be broken or deteriorated by the saltating particles and dust in the tunnel. Laser Doppler Velocitmetry, on the other hand, could be used, but the flexibility in traversing the height simultaneously with the aerosol sampler is lost. Additionally, modern pressure transducers have a more than adequate response time and are reliable for measuring mean velocities in a wind tunnel; therefore, these devices appear to be the logical choice for the "dirty" environment.

Two pressure transducers were used to determine velocities in the wind tunnel, the Validyne P305D and the Setra 239. The Validyne P305D pressure transducer fitted with a 0.125 psid diaphragm is used to determine the free stream velocity and is attached to a Pitot probe approximately 0.22 m from the bottom surface of the wind tunnel and facing parallel to the flow direction. The pressure obtained by the Pitot tube was sent to the differential transducer containing a diaphragm and circuitry as shown in Figure 13. The movement of the diaphragm was related to the pressure difference and created a voltage from –2.5 to 2.5 V which was correlated to the pressure. The correlation of pressure was obtained by calibration in a wind tunnel over a range of operating velocities with a Meriam micromanometer, which gives pressure readings in terms of column height of oil in a U-tube. The pressure for this instrument is considered the standard and was calculated as follows:

$$p - p_\infty = gh(\rho_m - \rho_f) \quad , \tag{1}$$

where p is the applied or total pressure, p_∞ is the free stream static pressure, g is the gravitational constant, h is the displacement height from reference in the manometer, ρ_m is the density of the manometer oil, and ρ_f is the density of the air or fluid transmitting pressure. This pressure was then plotted versus the voltage output given by the Validyne Pressure Transducer and a calibration curve established (Figure 14). The pressure was then related to the velocity through Bernoulli's equation, which for our simplified case becomes the following:

$$u_\infty = \sqrt{\frac{2(p_0 - p_\infty)}{\rho}} \tag{2}$$

where u_∞ is the free stream velocity, p_0 is the total or stagnation pressure, and ρ is the density of the fluid media (air). The calibration equation was programmed into the data acquisition software to automatically calculate the free stream velocity as voltages from the transducer were data acquired. The maximum velocity for the Validyne is approximately 36 m/s.

Likewise, the Setra 239 is a very sensitive velocity instrument and was attached to a total pressure probe and a static port to give a differential pressure. The Setra 239 was calibrated in the same way as the Validyne and the calibration curve shown in Figure 14. The Setra 239 has a similar operating principle except the voltage is created by a capacitive transducer as shown in Figure 15. The movement of overlapping plates due to the pressure differential gives rise to the voltage. The total pressure probe attached to the Setra 239 is traversed vertically above the centerline of the tunnel to obtain velocity profiles. The voltage output is again data acquired and turned into a velocity automatically using the LabVIEW® data-acquisition software. The maximum velocity of the Setra 239 is approximately 10.5 m/s over 2.5 volts. This poses a problem for those velocities exceeding 10.5 m/s in the tunnel (above threshold conditions). We note however, the pressure differential was more important than the velocity and we can obtain a pressure differential between the free stream total pressure and the traversing pressure that was always less than the maximum range of the transducer. The pressure differential then was used along with the pressure differential given by the Validyne for free stream to obtain a pressure differential corresponding to the traversing velocity.

2.5.3 Data Acquisition

All of the measurements with the aerosol samplers and transducers were then collected in real time with a LabVIEW® data-acquisition program. This presents exact time correlation between the velocity and the PM_{10} measurements, and the velocity and the threshold velocity measurements. From the acquired information, the PM_{10} and $PM_{2.5}$ flux from the soil surface was calculated for various wind velocities and conditions. The contribution of each soil to total Owens Lake dust emissions could then be estimated.

a)

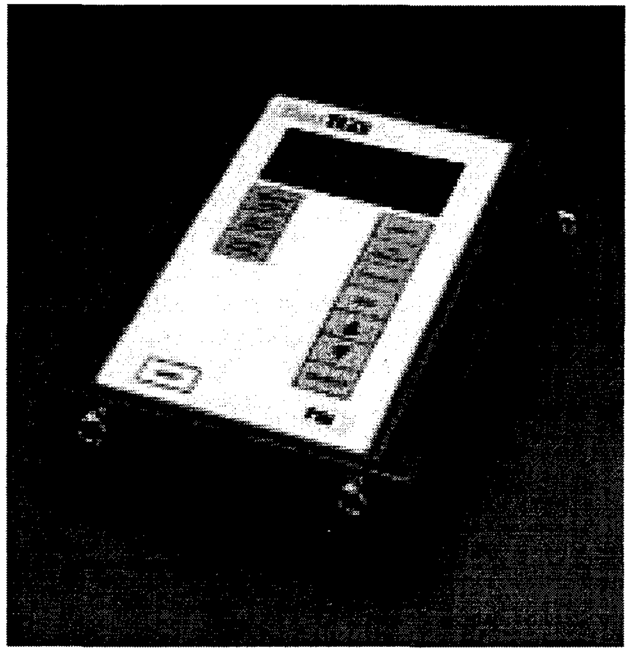

b)

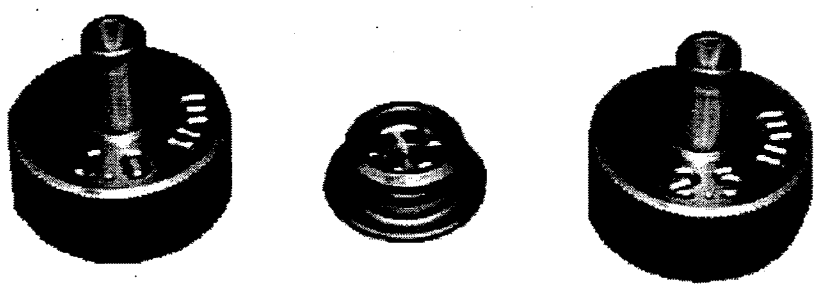

Figure 12. TSI DustTrak used to measure PM_{10} and $PM_{2.5}$: a) the recording unit b) the orifices used to measure differing sizes of particulate matter.

a)

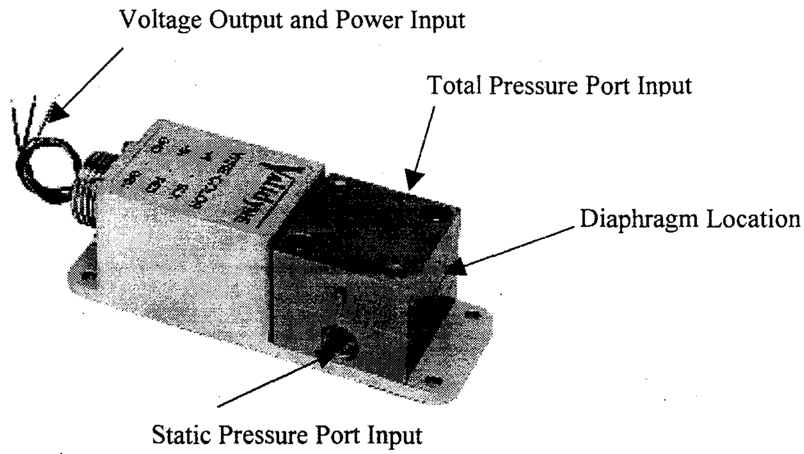

b)

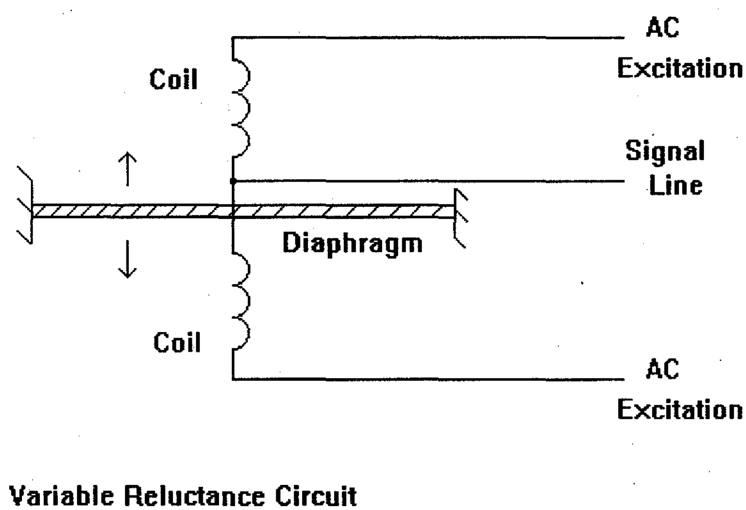

c)

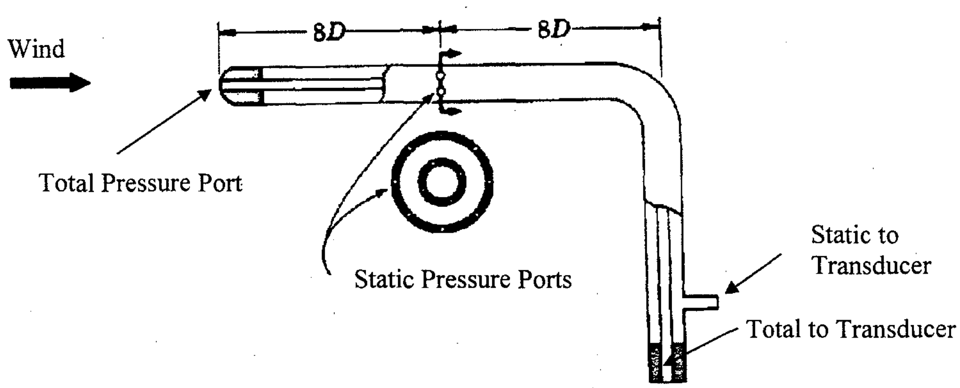

Figure 13. The Validyne pressure transducer: a) photograph showing general characteristics, b) the circuit showing the general theory behind voltage correlating to a pressure differential displacement, and c) a schematic of the attached pitot-static tube.

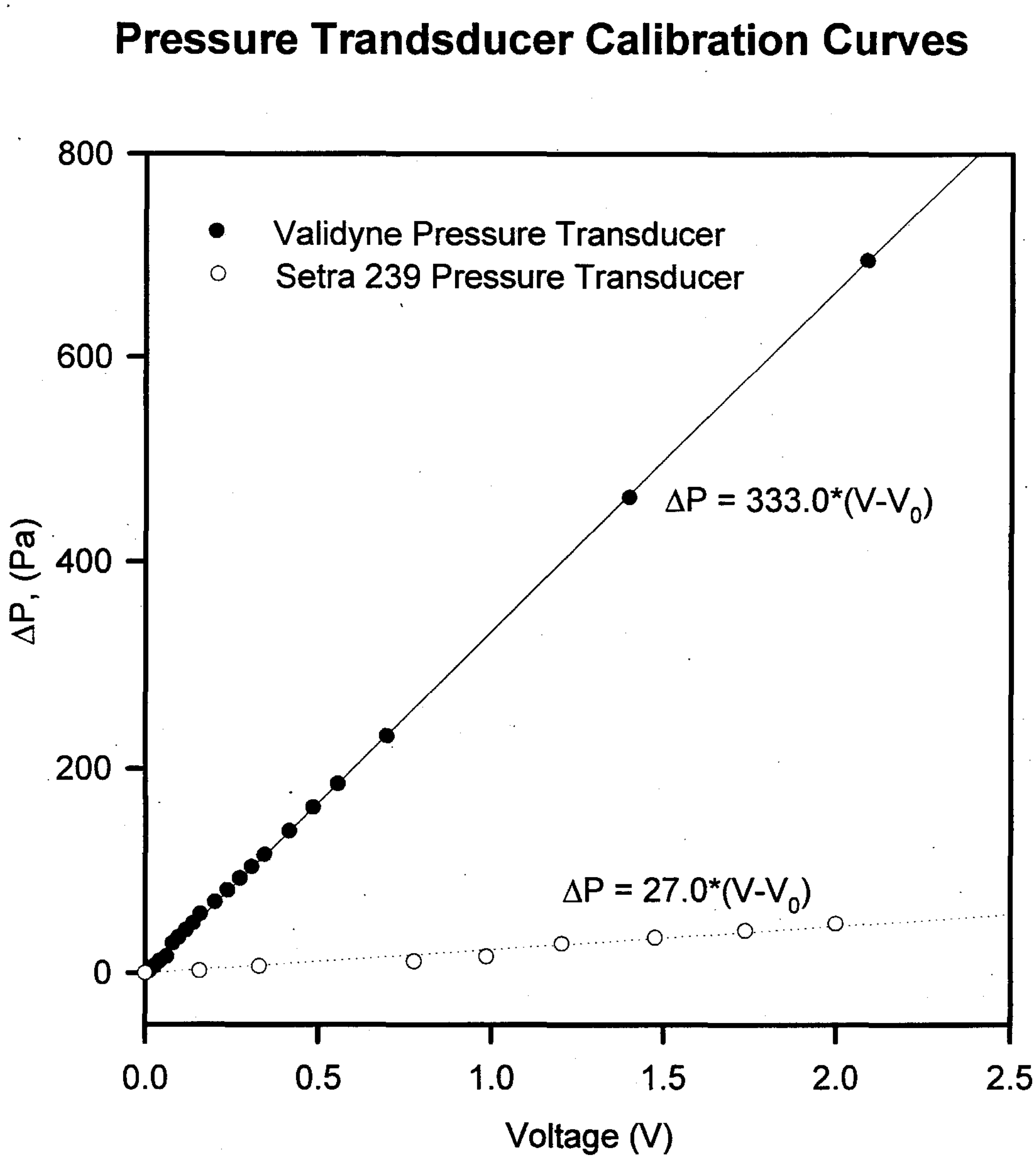

Figure 14. Experimental calibration curves showing the relationship between differential pressure and voltage for each of the two transducers. These equations were then used to automatically change voltages into velocities with the LabView™ program used for data acquisition.

a)

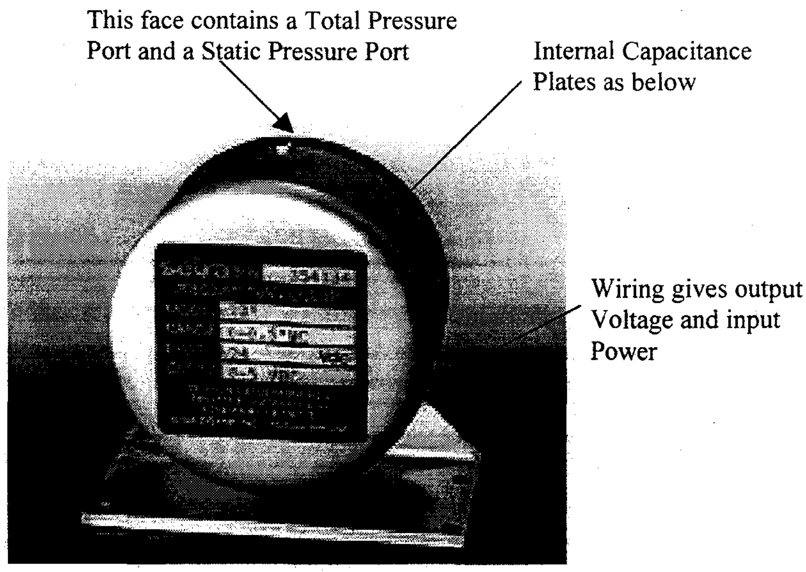

b)

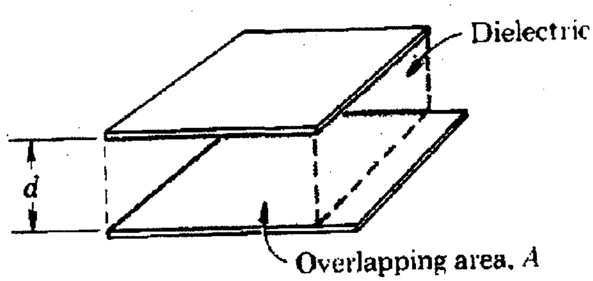

Figure 15. Setra 239 Pressure Transducer: a) photograph showing the various parts and b) a schematic showing in general how capacitive transducers work.

2.6. Measurements

2.6.1. Threshold studies

The threshold velocity is defined as that velocity at which the particles on the surface begin to move/creep and saltate leading to emissions (Figure 16). For this part of study, a Keithly Electrometer Model 602 is placed in the diffuser section of the wind tunnel where it was connected to a voltmeter that recorded a positive voltage when particles impact on the metal plate. The metal plate was perpendicular to the wind velocity as shown in Figure 17. The voltage was then recorded simultaneously along with the velocity acquired with the free stream Pitot-static tube pressure transducer. The velocity corresponding to a rapid increase in the voltage was thus taken as the threshold velocity and can be correlated to a 10 m height corresponding to common meteorological observations or a near surface height.

2.6.2. Roughness Height z_0 and Friction Velocity u_*

Every surface has a physical characteristic roughness height z_0 which can be determined from conditions prior to threshold. After threshold, saltating particles will effect the surface characteristics. In addition, the shear velocity u_* for any given flow can be calculated. Both z_0 and u_* are determined by using mixing-length theory as prescribed by the following equation:

$$\frac{u(z)}{u_*} = \frac{1}{k}\ln\left(\frac{z}{z_0}\right), \qquad u_* = \sqrt{\frac{\tau_w}{\rho}} \tag{3}$$

where u(z) is the velocity at some height z above the surface, u_* is the friction or shear velocity, k is the von Karman constant equal to 0.419, z_0 is the aerodynamic roughness, and τ_w is the wall shear stress. This well known equation was originally developed by Prandtl for any two dimensional turbulent boundary layer and later modified to incorporate roughness elements. The premise of the equation is that the turbulent flow is characterized by the surface, which creates a logarithmic velocity profile. Likewise, if we measure the velocity profile, it is possible to obtain the aerodynamics characteristics of the surface. The characteristic roughness of many different surfaces have been obtained experimentally, and these are often used as benchmarks to determine if the tests are consistent with these values. In order to obtain both z_0 and u_*, experiments must be used in combination with mixing-length theory. By obtaining a series of velocity profiles below threshold for the boundary layer, z_0 is obtained in the spirit of Bagnold, 1941 (Figure 18), where the intersection of the curves along the z-axis represents the z_0 value. By obtaining the slope of the each curve, u_* can be obtained for each case as well.

The experimental method was as follows: first, a specific soil is placed in the test bed; second, a specific free stream velocity below threshold is reached in the tunnel as indicated by the free stream Pitot-static tube; and finally, the traversing mechanism is used to record the velocity as a function of height with the total pressure tube and static port read by the Setra 239 pressure transducer. The traversing probe was used to measure 19 different centerline vertical velocities obtained by vertically traversing the probe logarithmically and leaving it at each location for ten seconds at a sampling rate of 1000 Hz giving 10000 data points which were then averaged together. This procedure was repeated for up to four more free stream velocities below the known threshold. This procedure did not give the correct roughness height once saltation began, since movement of particles changes the effective roughness. This procedure was used for all four different soils and variations of them. z_0 and u_* were then calculated using the above theory.

2.6.3. Loose Soil Emission Measurements

The next step in this study is to calculate emission rates of the loose soils above threshold velocity. First, the soil was placed in the test bed (5.0 m long, 0.025 m deep and 0.30 m wide) if no preconditioning was necessary (Figure 19). Only one of the four soils had to be preconditioned before testing as a loose soil: Soil #1 (Old Pipe Line) had to be air dried for a week and then clumps mechanically broken down with a coarse sieve (Figure 20). A sample of the soil was then run through the sonic sieve to ensure that its gradation curve remained the same as previously measured.

With the soil in place, emission rates were obtained experimentally by simultaneously vertically traversing two DustTraks™ logarithmically at 2.65 m and 4.38 m from the leading edge of the soils for a set of the same ten heights at velocities above threshold (Figure 21). The velocity measurements were made in a similar fashion as in the previous section. The DustTraks™ record concentration at each location in mg/m^3 with the information sent to LabVIEW® and the PC. Each traversing height was sampled for ten seconds. To obtain an emission rate, a control volume analysis was used between the various inlet and outlet measurements (Figure 22). The emission rate was defined as the mass emitted in a unit area per unit time or $[M/L^2T]$ or $[mg/m^2s]$. The control volume was defined as w x l x h where w is the width of the soil bed, l is the length of the soil bed or length between probes, and h is the height of the tunnel. The mass outflux from the control volume was defined as $\dot{m}_{exit}$ and the mass influx $\dot{m}_{inlet}$. E was then the emission rate for the control area A = l x w, and applying a mass balance on the control volume the following equation describes the emission rate:

$$E = \frac{1}{A}\left[\dot{m}_{exit} - \dot{m}_{inlet}\right] \qquad (4)$$

Since the aerosol sampler measures in terms of concentration, the mass flux rates must be described in terms of concentration as the following:

$$\dot{m}_{exit} = \int_0^h c_{exit}\, u_{exit}\, w dz \quad , \qquad \dot{m}_{inlet} = \int_0^h c_{inlet}\, u_{inlet}\, w dz \qquad (5)$$

where u and c represent velocity and concentration respectively, and the subscripts represent inlet and exit (outlet) locations. The revised emission rate equation becomes

$$E = \frac{1}{L}\int_0^h \left(c_{exit}u_{exit} - c_{inlet}u_{inlet}\right)dz \qquad (6)$$

For a simplified analysis, emissions upwind of the soil bed were assumed to be zero. Likewise, the velocity profiles are assumed equivalent at the inlet and outlet when the inlet was at 2.65 m and the outlet was at 4.38 m. These assumptions do not compromise the data, since the concentrations being measured were found to be several orders of magnitude greater than the upwind concentrations; and, the change in mean velocity profile between the downstream distances of 2.65 and 4.38 meters was negligible. Once the velocity and concentration profiles were obtained, emission rates were calculated from Equation (6). Regression curves were fit to each PM_{10} profile and velocity curve and then integrated numerically to obtain an emission rate per unit area. This procedure was repeated for up to five velocities above threshold for each soil, and the emission rates calculated.

2.6.4. Sand Flux

For the two sands (Soil #2 and Soil #3), the sand flux was obtained by using 15 sand traps stacked on top each other with each having a frontal sampling area of 1 cm x 2 cm. The traps were then placed at the exit of the test section near the diffuser with the frontal area perpendicular to the wind velocity. The trap is approximately an isokinetic sampler as the air is allowed to freely move through the sampler, and thus, is taken in at the same rate as the wind velocity (White, 1982). All particles smaller than sand easily flow through the trap (Figure 23). The mass in each trap was weighed and the time of collection was recorded. A sand flux was then obtained in the following way at each height:

$$q_i = \frac{m_i}{tA_i} \tag{7}$$

where m_i is the mass collected in each sand trap at each location, A_i is the frontral area of the trap, and t is the time of collection. Once the sand flux had been obtained a total flux was obtained with the following equation:

$$Q = \sum_{i=1}^{15} q_i h_i \, , \tag{8}$$

where h_i is the height of the trap.

Finally, these results can be compared to other empirical equations for total sand flux to verify that the mechanism of sand flux is following a similar trend. White (1979) presents the following equation for total sand flux:

$$Q = 2.61 \frac{u_*^3 \rho}{g}(1 - \frac{u_{*t}}{u_*})(1 + \frac{u_{*t}}{u_*})^2 \qquad (9)$$

where u_{*t} is the threshold friction velocity.

This sand flux calculated was important in quantifying the saltation rate for various wind velocities for each sand as well as for the cases in which sand is allowed to saltate over the soils.

2.6.5. Fetch Studies

Results from the loose soil emissions indicated that some of the soils of interest may have the ability to quickly get into the air before the 2.65 m sampling location and then incur some sort of fall-out due to saturation of the wind tunnel. If this was the case, it then became important to be able to recognize what happens from the beginning of the fetch to the 2.65 m location and beyond; therefore, new locations were sampled for this portion of the experiment and the emission rates obtained as decribed. The amount of material in the air was then plotted against fetch distance and the dynamics of how the material became airborne investigated.

2.6.6. Saltation Studies

Saltation is an important effect at Owens Lake. There is a North and South sand sheet at each end of the lake providing saltating particles which scour the surface of Owens Lake during North/South storm events. This scouring is believed to produce higher emissions of PM_{10} than could wind stresses alone, i.e., in the absence of saltating sand. The effect of saltating particles on soil erosion was addressed by introducing coarse Owens Lake sand (Soil #2 and Soil #3) upstream of the test bed containing the emissive soils (Soil #1 and Soil #4) and measuring the PM_{10} levels (Figure 24). The upwind saltating material having the most substantial scouring effect was determined. In addition, a ratio of sand flux to PM_{10} was obtained by introducing the sand traps above threshold. This procedure was repeated for various soils and surface conditions.

2.6.7. Moisture Studies

The effect of moisture on the most emissive soils (Soil #1 and Soil #4) was conducted by testing the two soils with varying moisture contents at an extreme emissive velocity. First, the soil was placed in the bed, and three samples of approximately 30 g removed from the bed, at 1.0 m, 2.5 m and 4.4 m. These are immediately weighed and the value recorded as the "wet" weight. The soil samples are then kept in a sealed container and the experiment in the wind tunnel conducted as before. Immediately, any loss in soil due to the experiment was replenished in the bed. Then, moisture was added by evenly spraying the surface with water and mixing the soil into the layer underneath. Again, the surface was sprayed with an even coat and mixed with this process continuing until there was a noticeable increase in moisture. Again, three samples were collected and weighed and placed in a sealed container. The wind tunnel test was then conducted. This procedure was repeated for up to six different moisture contents for each soil.

The moisture content was then determined for each test by taking the soil from the sealed containers and placing them in a small oven to dry. The oven drying was rapid and not in accordance with the ASTM standard which requires oven drying at a moderate temperature for up to 24 hours to ensure that all possible moisture content is released. Instead, the procedure used in the wind tunnel laboratory followed the sand-bath method which is used for quick multiple sets of laboratory results. In this procedure, a bunsen burner or small electric stove can be used instead of the larger stove producing results in about 10 minutes for each sample. The sacrifice is that the results are only good to about $\pm$ 1% instead of the $\pm$ 0.1% with the ASTM method (Head, 1992). For our case, the greater accuracy was not imperative. In fact, often the quick results were used to gage how much moisture to add to the next test. After drying in the oven, the dry weight of each sample was noted and compared to the "wet" weight to obtain the moisture content with the following formula:

$$Moisture \quad Content = \frac{m_w - m_d}{m_d} x100\% \quad . \tag{10}$$

where the subscripts "w" and "d" refer to wet and dry. The moisture content for each study was the average of the three samples taken along the test bed. The emission rate as a function of moisture content was then plotted.

2.6.8. Crust Studies

Another aspect of significant importance in understanding the emissions at Owens Lake is the surface conditions of the lake. If a hard crust has formed on the lake, almost no emissions are observed. However, in intense winter and spring storms these crusts quickly become abraded by saltating sand. In order to simulate this process, crusts were formed in the wind tunnel and the mechanism of abrasion studied. Crusts were formed by simulating the natural diurnal cycle of the soil, ultraviolet exposure in the day, night time cooling, and the introduction of moisture. The majority of crusts produced followed a hard crust cycle and not the efflorescent crust cycle (Figure 25).

The procedure of crust formation is explained briefly in this paragraph. The soil was saturated all the way through simulating an intense rain storm reaching the ground water level and seeping water back up to the surface such that puddles form on the surface. This process suspended very small particulate in the surface water and slowly over time the particulate begin to settle out on the surface of the soil leaving a film of fine sediments—the exact time of settling was approximated with Stoke's settling velocity. After the sediments settle, a clear film of water was left above the sediment layer and was siphoned off to expedite the drying process. The soil was then allowed to dry for a week with the aid of blowing fans and heaters to simulate the drying/baking of the soil under desert conditions. The heater and fans were used each day for approximately 8 hours for 7 days. As the soil begins to dry salt crusts formed initially on the surface even though the soil's interior was still quite wet. This might correspond to the time at which PM_{10} and $PM_{2.5}$ emissions could be tested in order to observe the emissions due to the salt "fluff". Over time, the entire block of soil dries leaving a hard crust on the surface primarily composed of fine sediment particles (Figure 26).

The emission rates of the crust due to strong winds without any saltation was tested in a similar procedure as the loose soils test, where the velocity was varied through a range of values and the resulting emissions measured. However, this time the DustTraks™ as well as the velocity probes were stationary for the entire test; they were both placed at the 4.38 m location and measured only at two vertical heights 0.0127 m and 0.216 m simultaneously (Figure 27, 28, and 29). Next, the crust was subjected to saltating particles; a bed of sand was placed upwind of the crust (Figure 30). Again, the velocity was varied through a range while measuring the concentrations. A background emissions value of the saltating sand was made prior to the saltation test by covering up the crust and measuring at 4.38 m the amount of PM_{10} from the sand alone. This background test was one of the only ways that any enhanced emission can be observed due to saltation without being overshadowed by the emissions of the sand. Lastly, if the "hard crust" did not break due to scouring particles alone, the crust was broken manually and the emission amounts measured without any saltation.

The efflorescent salt crust that forms on Owens Lake was reproduced in the laboratory although on very small scales--it is known that this efflorescent salt crust when broken apart can produce high levels of PM_{10} and $PM_{2.5}$; however, this scenario could not be tested with the above development. Different conditions than are available in the laboratory would be necessary to produce such a crust (Figure 25).

2.6.9. Stability Studies

The effect of atmospheric stability on soil erosion was studied because diurnal changes in solar radiation on Owens Dry Lake set up a cycle of heating and cooling of the planetary boundary layer. This process strongly influences the wind field due to stratification. The air layer is stable during the night since the ground is cooler than the atmosphere above it. However, when the ground is subject to solar heating it quickly becomes warmer than the air and begins to transfer heat to the atmosphere above it through molecular conduction. The parcels of heated air move past the cooler gas enhancing the turbulent mixing near the surface. The heated parcels will thus enhance the aeolian surface stress as compared to an unheated or cooled surface and will become an important factor in the PM_{10} emissions as threshold velocities lessen. Experimentally, this surface condition was simulated by heating the surface of the tunnel floor to produce a minimum temperature difference between the surface and the air of 25 C. Exact simulation with regards to vertical turbulent structure would require exactly matching the Richardson numbers in the tunnel with those that occur on the surface of Owens dry lake bed. The range of testing condition in the wind tunnel thus covered all possible unstable conditions occurring on Owens Lake.

In order to simulate equilibrium stability condition in the test section, the wind tunnel floor in the test section and last flow development section were heated by electric heating plates. Pebble beds as set in the previous experiments were again used to form the proper boundary-layer flow. Figure 31 shows schematic diagrams of the wind tunnel floor bed setup for stability experiments. The overall length of the two heating floors was 5.0 m and width of the heating plates was 0.30 m. As Figure 31 indicates, the heating plates were located between two masonite plates that have insulation layers made of fiberglass. Silicone-flexible heaters were covered with aluminum plates, which have high thermal conductivity, to spread the heat onto the soil surface evenly. Another fiberglass layer and a cork sheet layer were placed on the bottom of heating plates to minimize conductive heat transfer to the surroundings (Figure 31 detail). The set of stability and dust threshold experiments was performed over an aerodynamically rough surface simulated by adhering 60-grit sandpaper to eight aluminum plates that were mounted flushed to the wind-tunnel floor. Securing the sandpaper to the hot heated floor was problematic and could only be successfully accomplished by using high temperature RTV, similar to the type used for sealing gaskets in automobile engines. This adhesive allows the sandpaper to remain attached to the aluminum plates under severe heating conditions. The plates were heated using silicone-flexible heaters that have a surface heating capability up to 230 °C; however, temperatures upward of only 50 °C were needed to obtain the 25 °C differential needed to match the conditions on Owens Lake.

For all experiments the ambient temperature, the temperature of the heating plates, the vertically local temperature locations on the thermocouple rake, and the velocity in the test section were measured and recorded via the LabVIEW® data-acquisition software. The measurements were made to obtain the velocity and temperature profiles at the same downstream location over the test bed. Velocity profiles were acquired as described in previous sections. Temperature profiles were obtained using a thermocouple rake that housed ten Type T thermocouples logarithmically spaced above the surface to a height of 17 cm. The same type of thermocouple (totaling twelve more thermocouples) monitored the surface and heater temperatures. To determine dust threshold, an electrostatic particle impact probe was installed at the end of the wind-tunnel test section as discussed in the threshold studies section. This device was connected to a Keithley Instruments Electrometer Model 602 that indicated dust suspension by measuring the electrical charge developed around the face of the probe. The electrometer does not necessarily measure the strength of the impact, but with great sensitivity detects the pressure of dust in the air stream, thus providing an accurate and repeatable dust threshold measurement. Threshold was the most vital measurement on near ground instability as it predicted when the bed begins to move due to enhanced surface stress from the instability.

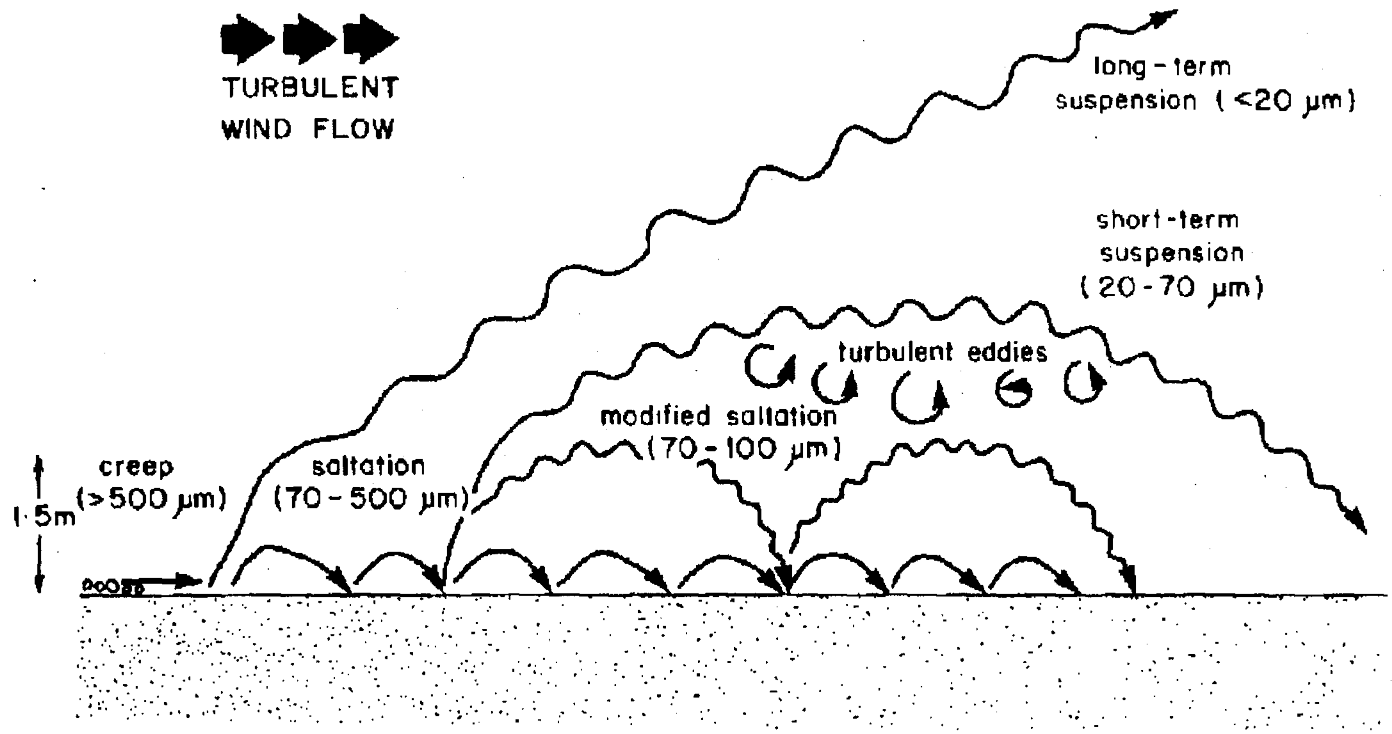

Figure 16. Schematic of the believed saltation and suspension mechanism of soils; threshold thus being defined as that moment when creep and initial saltation begin (Pye, 1987).

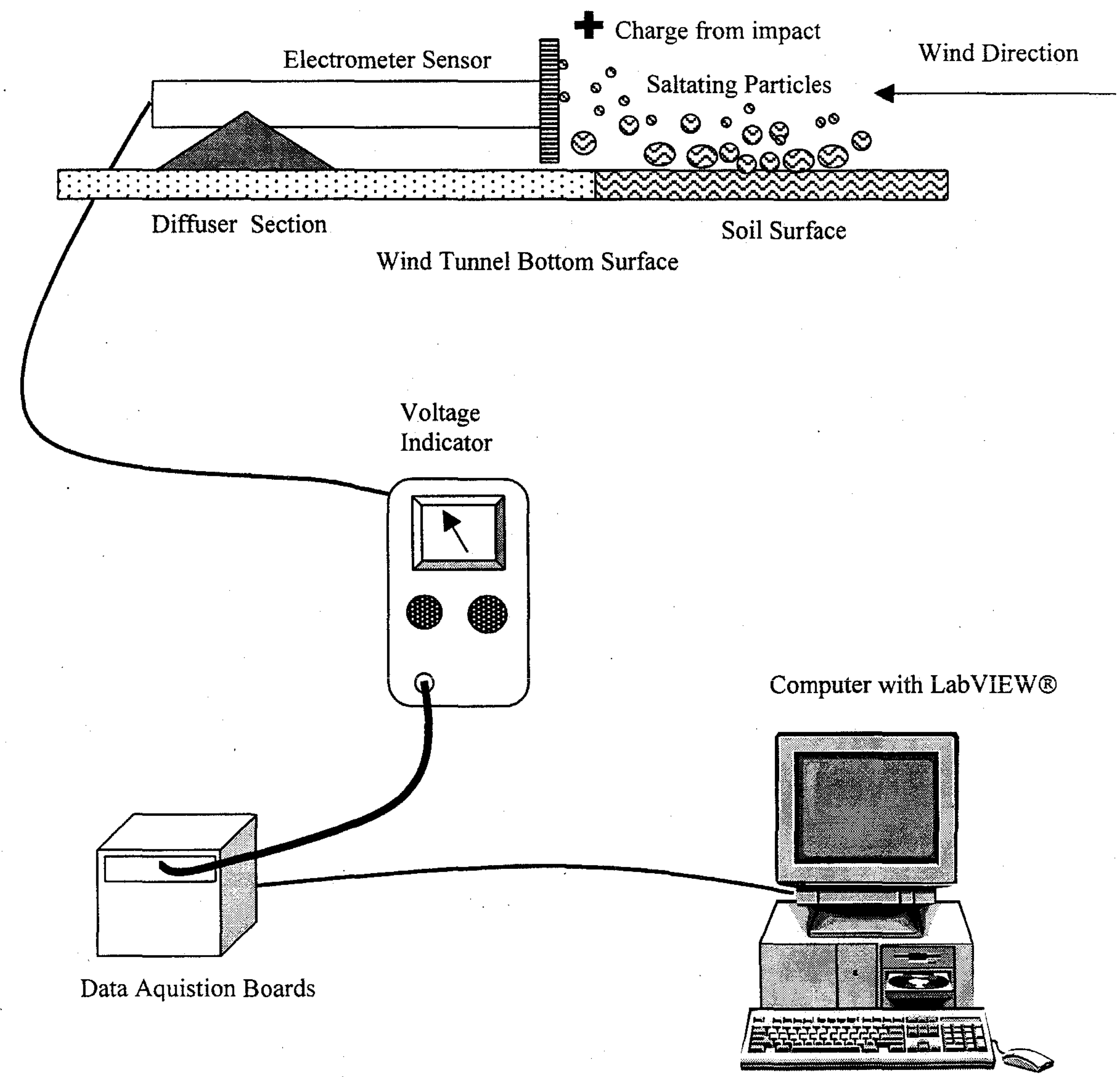

Figure 17. Electrometer Schematic showing the basic principle of obtaining the threshold velocity for each soil.

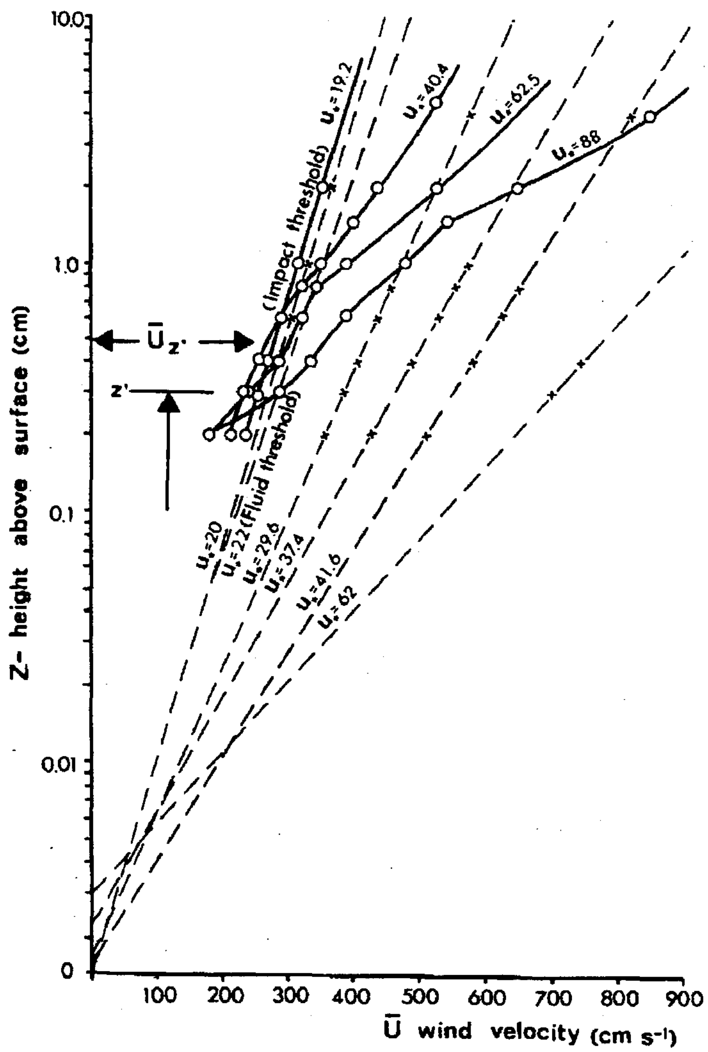

Figure 18. Bagnold (1941) experiments showing how z_0 and u_* can be found, where u_* is the friction velocity and z_0 is the intersection across or focus on the z-axis above.

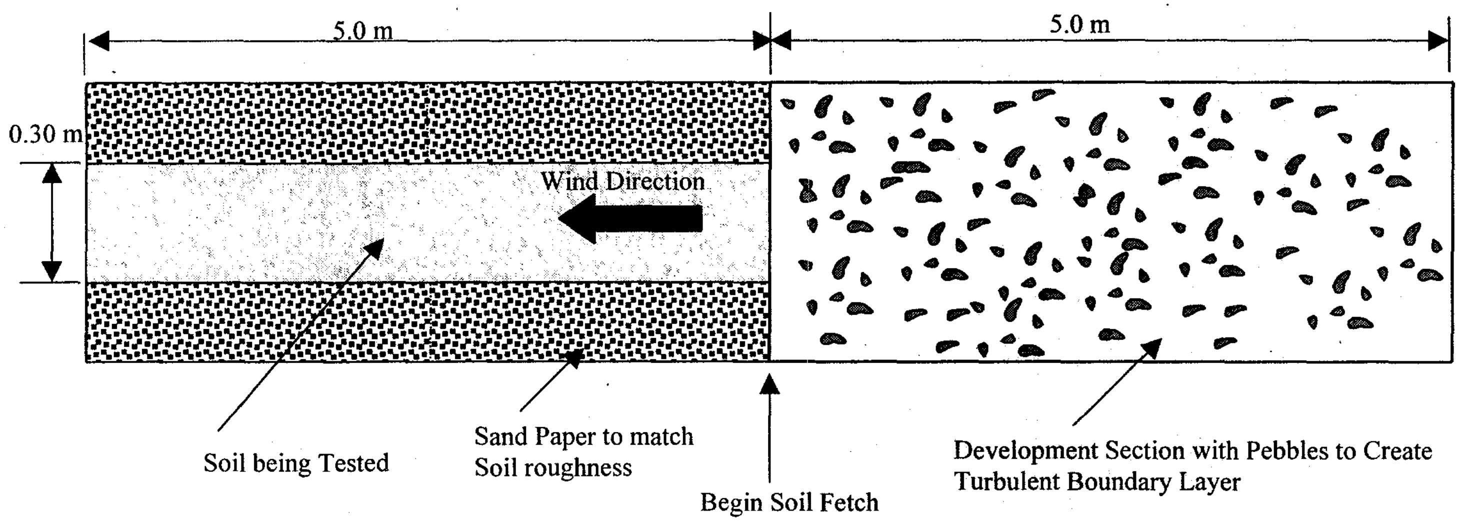

Figure 19. A schematic of the test bed showing the configuration for loose soil emissions testing without saltation.

a)

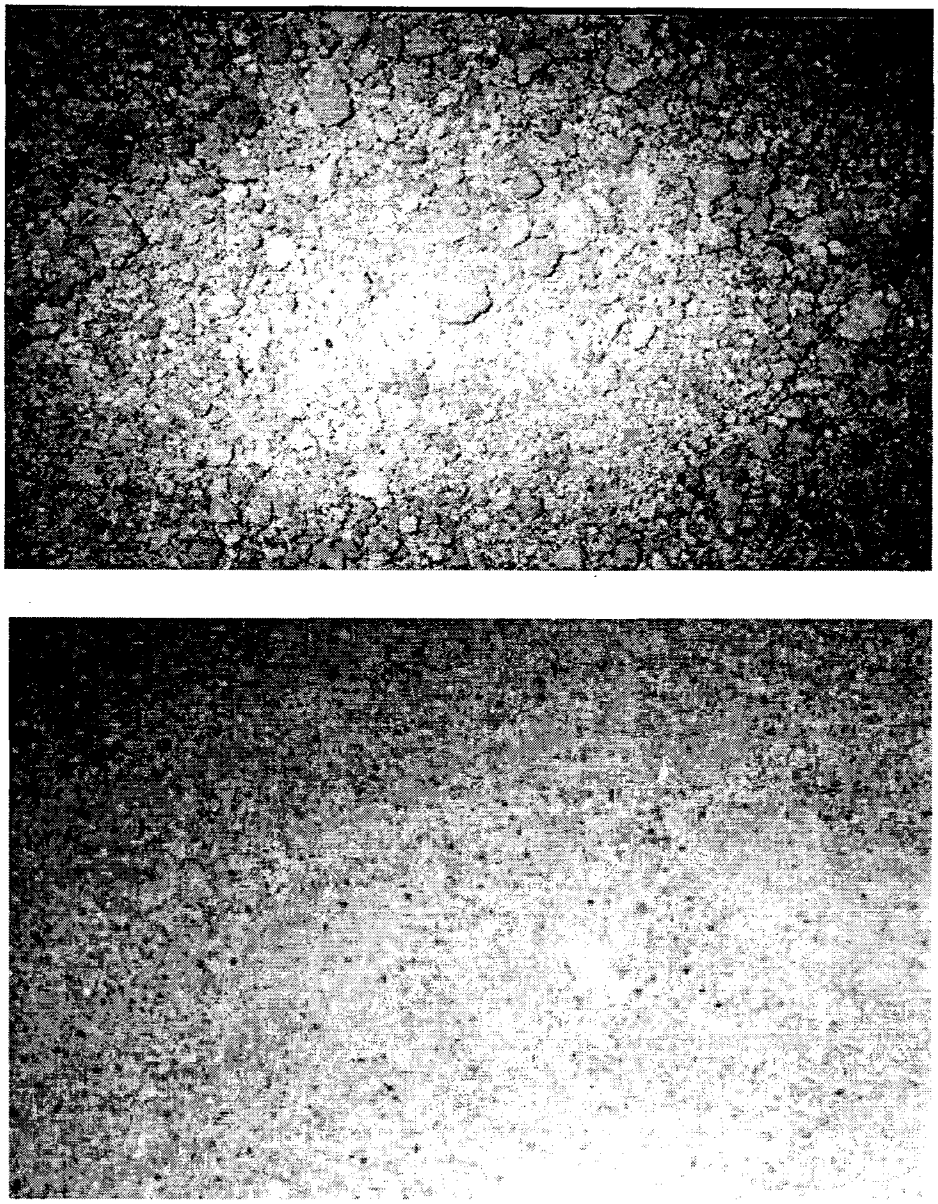

b)

Figure 20. The above figure illustrates the method of processing Soil #1 where a) is the soil as it appears air dried with large clumps and b) is the soil after being put through a coarse sieve to break up the clumps.

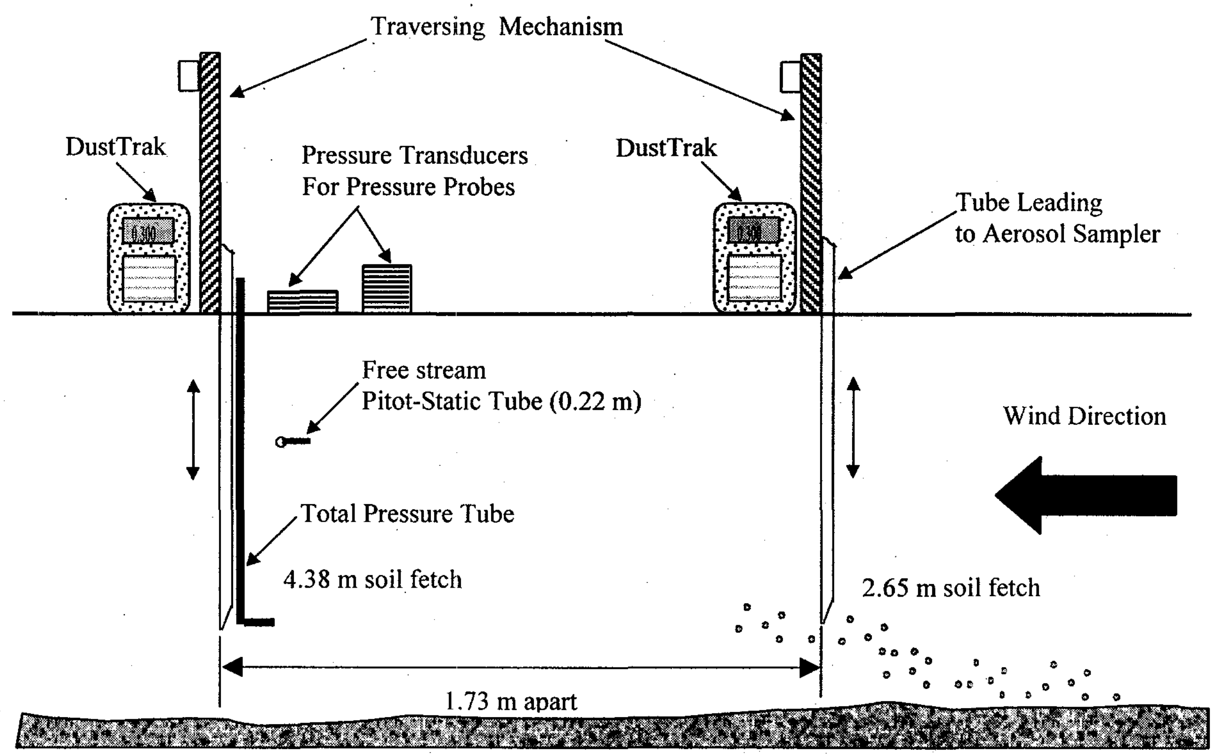

Figure 21. Schematic representing the loose soil emission testing where the pertinent instrumentation is shown. As in the threshold schematic the voltage output of each of the instruments is data acquired and recorded with a PC.

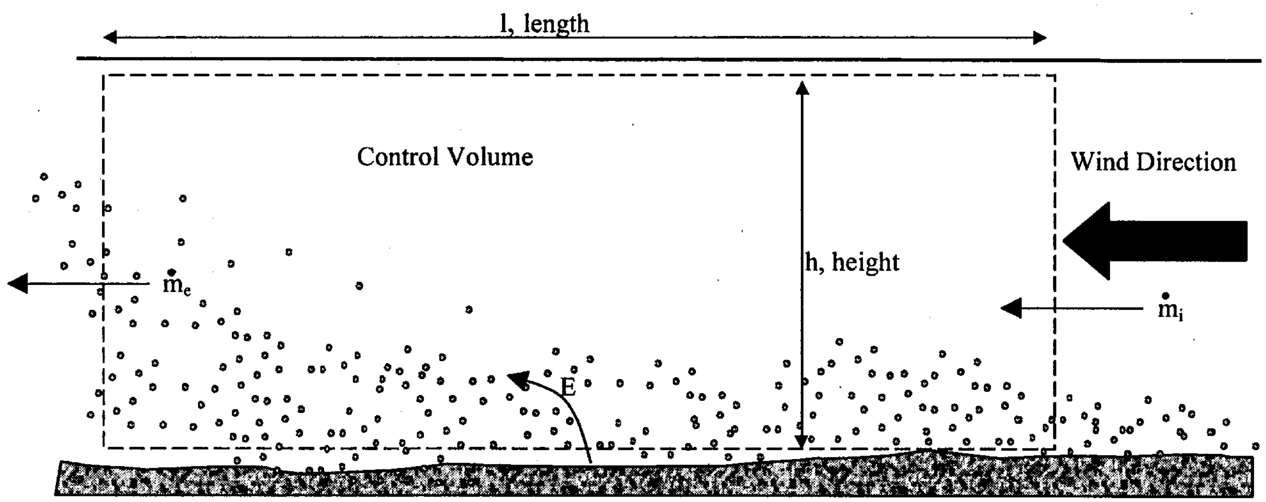

Figure 22. Schematic representing the method of determining loose soil emission rates with a control volume

a)

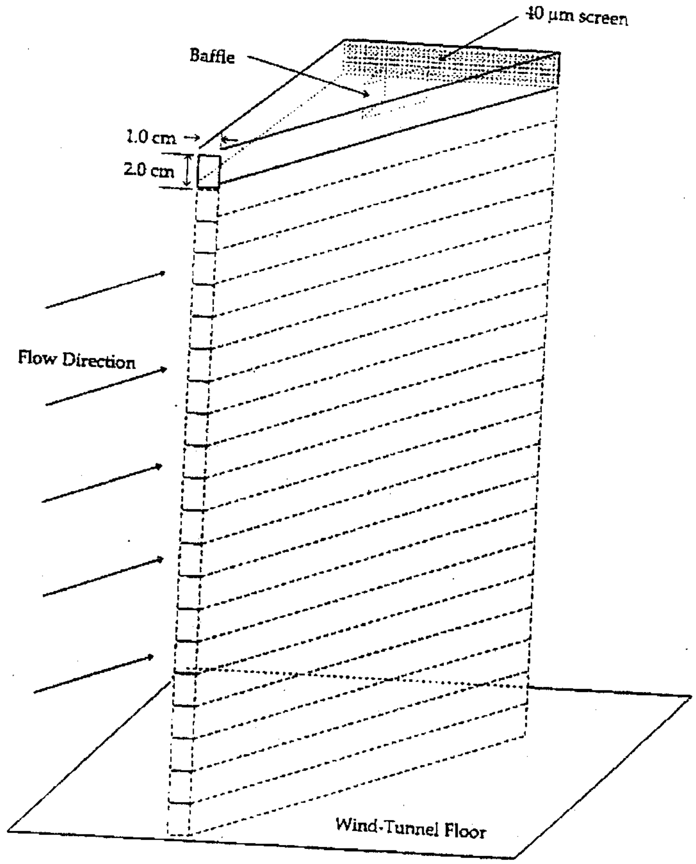

b)

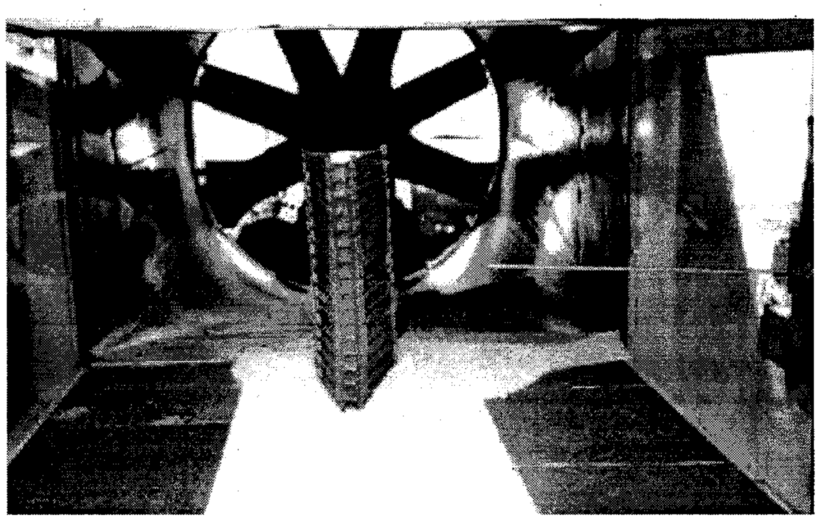

Figure 23. Sand Traps used to measure sand flux during saltation experiments: a) schematic and b) photograph.

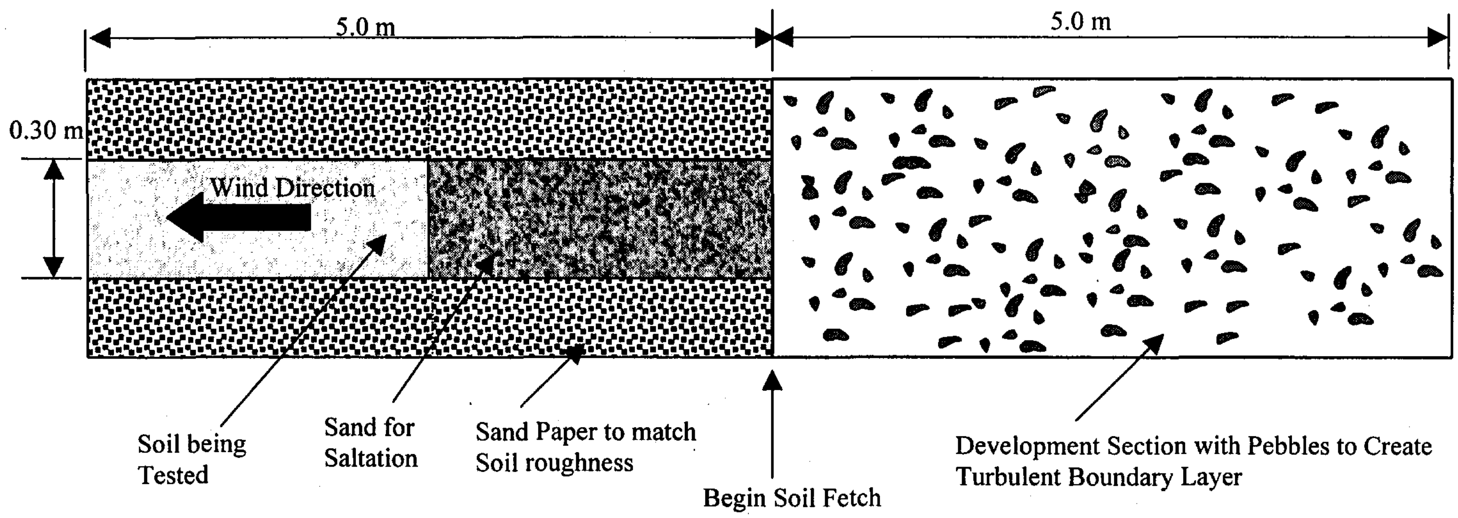

Figure 24. Schematic of the test bed showing the configuration for evaluating the effect of saltation on an emissive soil.

a)

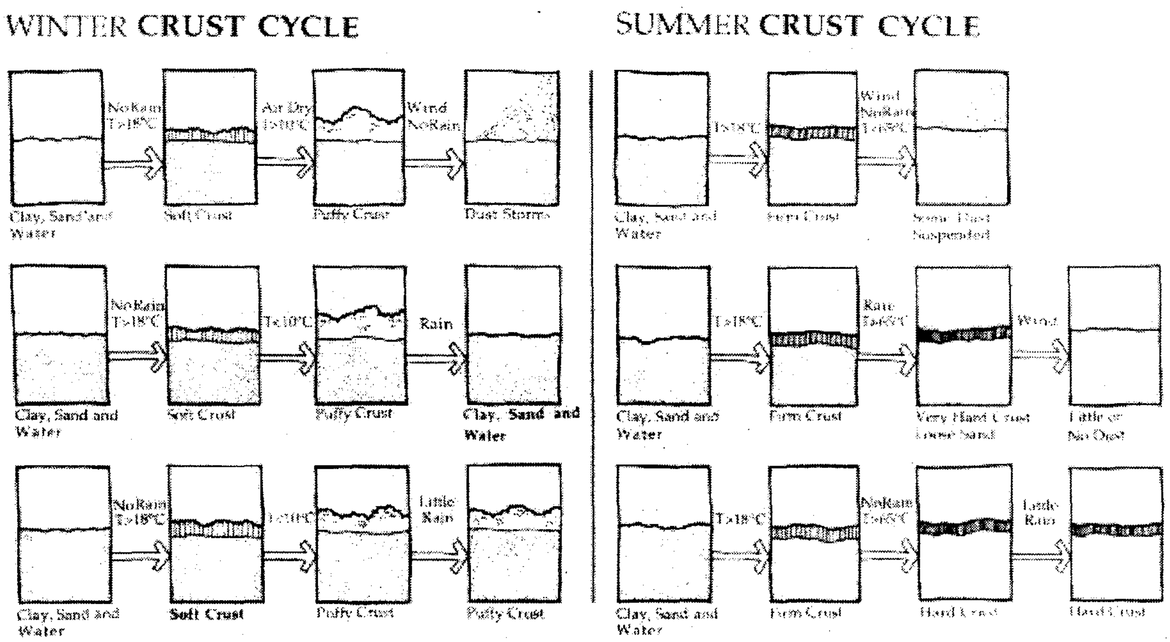

b)

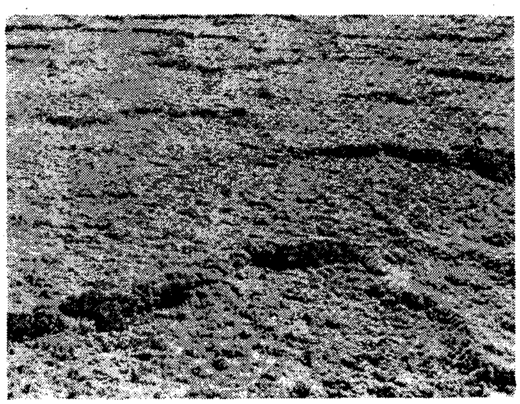

Winter Crust

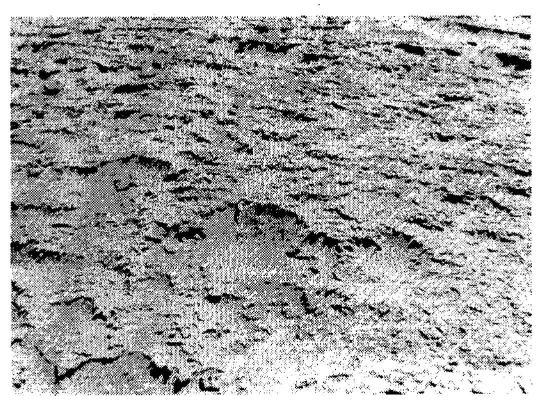

Summer

Figure 25. Owens Lake Crusts: a) proposed methods of crust development in the winter and summer and b) the resulting seasonal crusts as they appear on the lake.

a)

b)

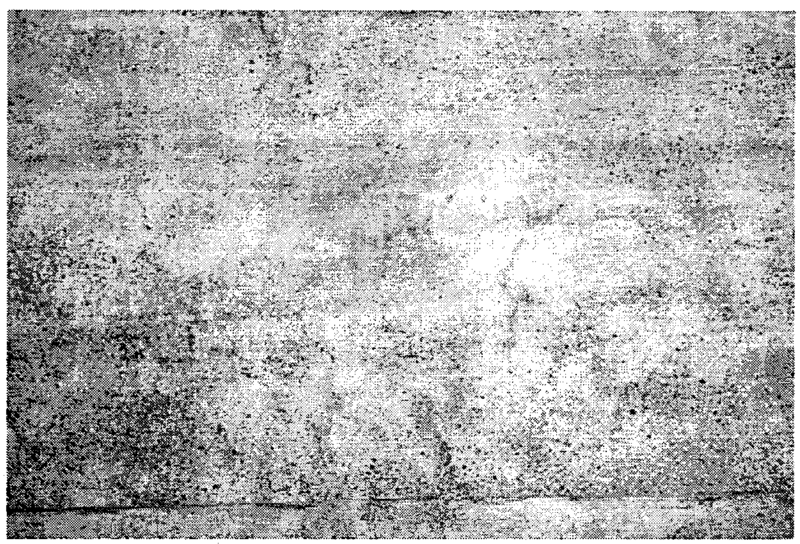

Figure 26. Photographs of the crust developed in the wind tunnel: a) the crust resting in the test bed and b) a close up showing the fine sediments crusted on the top surface. The lighter colored material is salt-like where the darker material is pure soil sediment. Underneath is a fairly loose soil with some softer crust.

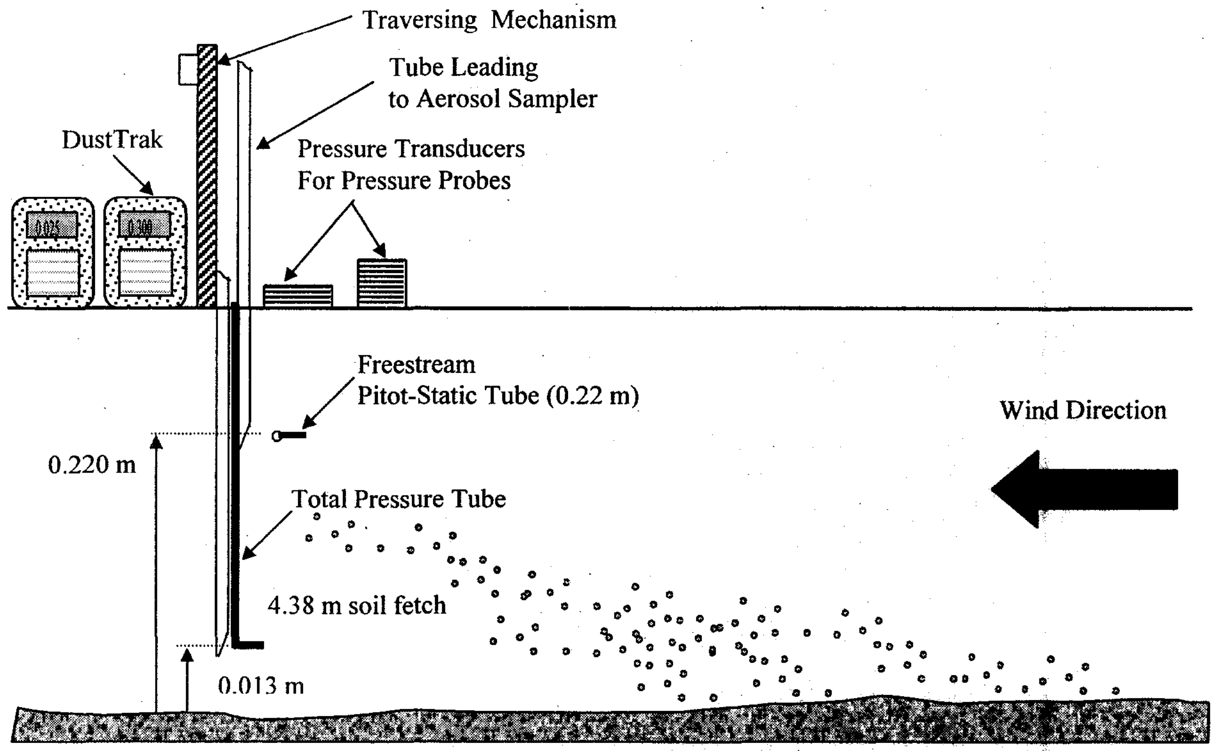

Figure 27. Schematic showing the set-up for obtaining data for the crust studies. Note, there is only one traversing location and only two locations for velocity and concentration are scanned. The wind speed is then varied for the duration of the test.

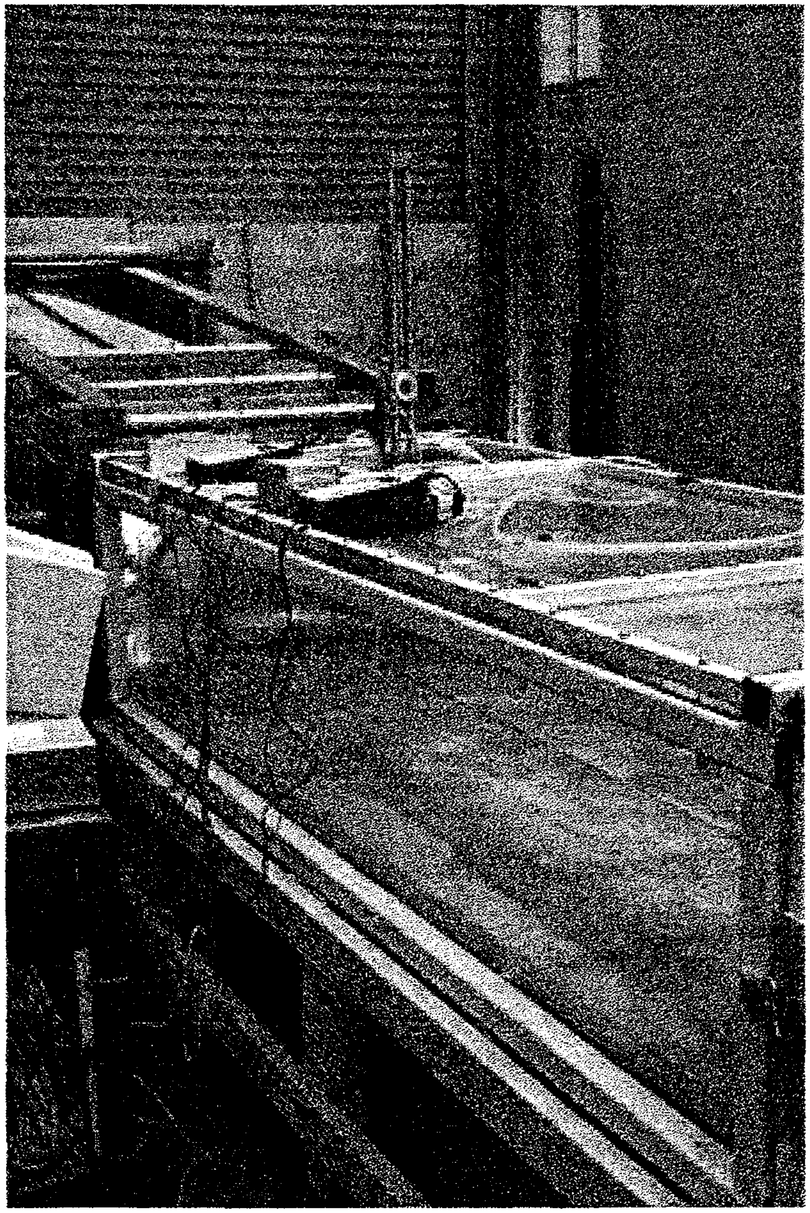

Figure 28. Photograph showing the instrumentation set-up on the Saltation Wind Tunnel for the crust studies.

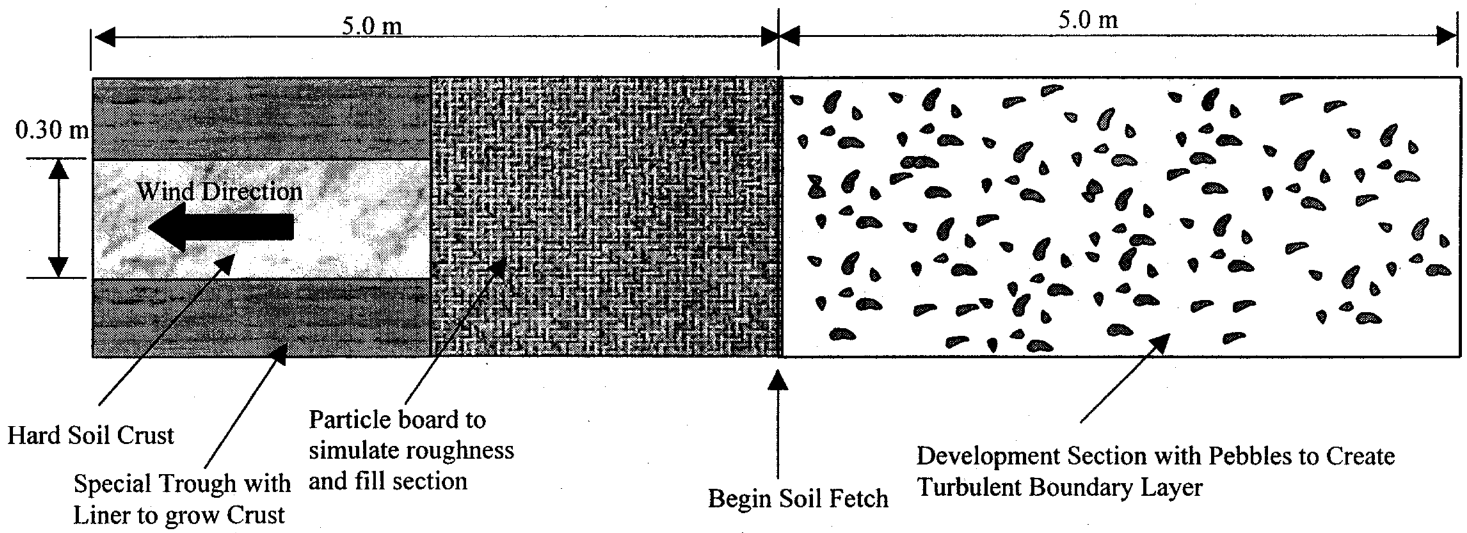

Figure 29. This schematic shows the configuration for testing the hard crust without saltation. Since a crust could only be grown in the test section, the other section had to be filled with a roughness element, in this cas a large piece of particle board.

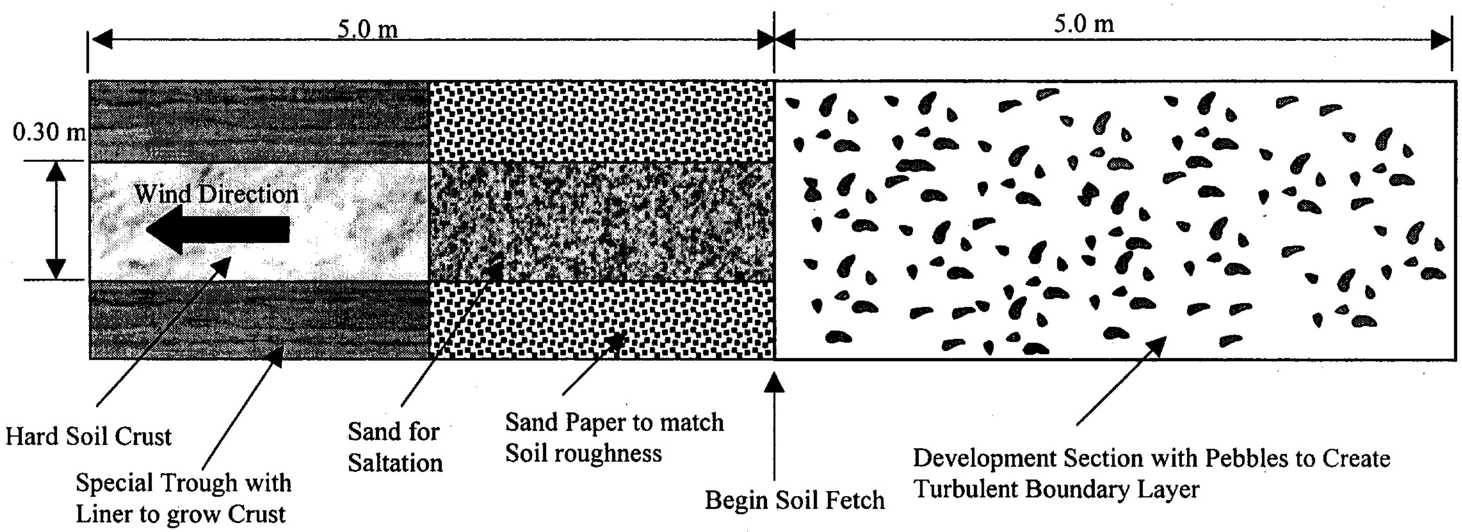

Figure 30. This schematic shows the configuration for testing the hard crust with saltating sand.

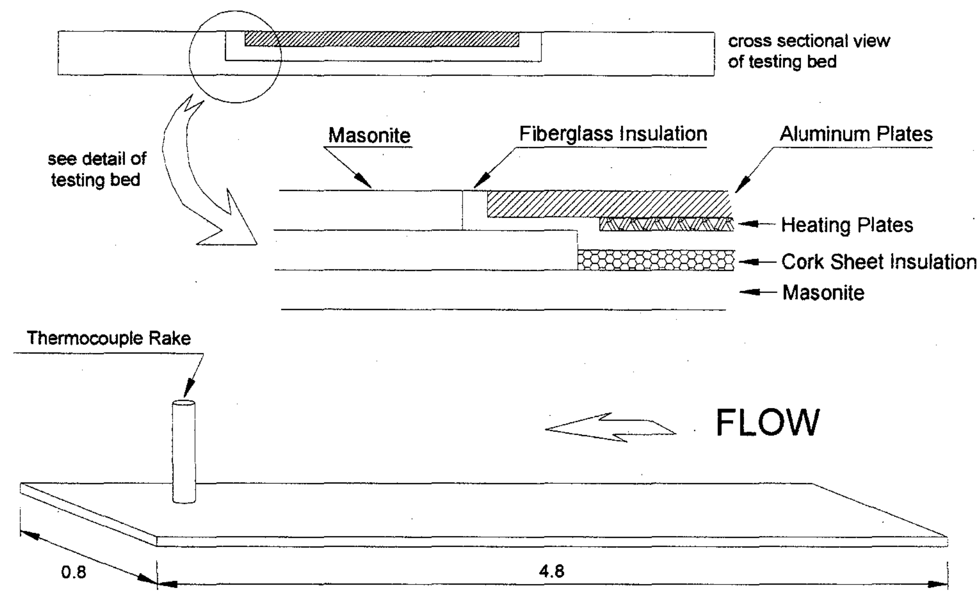

Figure 31. The experimental set-up for the stability experiments showing the method used to develop the heated bed as well as the associated instrumentation

Section 3. Results Summary

- Soil Properties: Soil #1 and Soil #4 have the most fine particulate
- Soil Properties: the emissive soils have high levels of Arsenic and salinity
- Threshold studies: the threshold friction velocity for movement of the soil beds is around 0.40 m/s for all four soils
- The surface roughness values measured in the wind tunnel are comparable to those measured on desert playas
- Emission rates for the loose soil emissions were upwards of 15200 $\mu g/m^2 s$
- The North emissive soil (Soil #1) attained the highest values
- Unexpectedly, one of the sandy soils (from the South Sheet) was nearly as emissive as the finer non-sand soils under the same conditions which could impact control strategies.
- Emission increased substantially when soil particles were introduced upwind of the soil test area to simulate saltation effects.
- The highest emissions rates were 28000 $\mu g/m^2 s$ for North Sheet Simulation (saltating sand over the loose soil).
- Sand fluxes did not follow the empirical trends because of the inhomogeneity of sizes in the soil samples.
- The fetch effect on emissions shows that at high velocities the near surface becomes saturated downstream and the rate of emission entrainment decreases or remains the same for the steady flow conditions.
- Moisture content was significant in the measured emission rates with a 10% increase in moisture corresponding to an order of magnitude decrease in emissions.
- Up to 30% of the measured PM_{10} emission can be attributed to $PM_{2.5}$.
- Hard crusts have the least amount of emissions and must be abraded and broken over very long periods of time.

3. Results

3.1. Soil Properties

3.1.1. Particle Size Analysis

The results of the particle size analysis are shown in the gradation curves shown in Figure 32. The emissive soils, Soil #1 and Soil #4 have a far greater percentage of particles in the size range less than 100 μm around 8% and 10%, respectively, while the sands, Soil #2 and Soil #3, contain 1% and 4%, respectively, in this range. This is indicative of the potential to produce PM_{10} and $PM_{2.5}$; however, agglomeration of particles in the clay-type emissive soils has to be considered as another potential site of these small particles. Thus, the sonic particle sizing can only give an estimate of the potential for emissions with the wind tunnel being more indicative of the potential for high emissions. The sifter, which was pulsed, did manage to break apart the most easily separable agglomerations, but likely the sifter could not differentiate the hard agglomerations from sand-sized particles. It is likely that some of these hard agglomerations could be abraded by saltating particles effectively enhancing emissions in the wind tunnel. In general, the gradation curve is a quick look at the potential for emissions, and also corresponds well with how the soils have been classified as "emissive" and "sand".

3.1.2. Chemical Analysis

The Chemical analysis was done by Wallace laboratories and their original two-page report is in Appendix F, so in this section only the major points of the analysis will be addressed. The soil analysis indicates all four soils have pH levels of around 11.0 meaning that they are all quite alkaline (basic)—this quantity is measured in a saturation extract. The arsenic soil concentrations of Soil #1 and Soil #4 are quite high at 25.71 g/m^3 and 19.95 g/m^3 while Soil #2 and Soil #3 are lower with 4.77 g/m^3 and 7.22 g/m^3, respectively. It is disconcerning that the "emissive" soils have the higher levels of arsenic as these pose the possibility of becoming airborne inhalants. The estimated soil texture of the soils are as follows: Soil #1 is a loamy sand, Soil #2 is sand, Soil # 3 is sand, and Soil #4 is a sandy loam. According to the chemical analysis, Soil #1 and Soil #4 have a salinity levels which are about twice that of sea water (35 g/kg) at 85.50 g/kg and 89.60 g/kg and Soil #2 and Soil #4 have a salinity level about equal to that of sea water at 38.90 g/kg and 37.50 g/kg. Like the pH values, these salinity values were measured in a saturation extract. The salinity levels play a crucial role in the formation of salt crusts at Owens Lake, thus the chemical analysis logically points to the likely formation of crusts by Soil #1 and Soil #4, again to those soils collected which are believed to be most emissive.

There is a difference in the type of salts found in the soils as well: Soil #1 and Soil #2 from the north part of the lake can be grouped primarily as chloride based salts while Soil #3 and Soil #4 from the south part of the lake are grouped primarily as carbonate salts. Also of noticeable interest is that there is relatively low organic matter in these soils, indicating essentially a "dead" lake playa in these locations. This lack of organic matter does not bode well for the introduction of plant life without means of artificially introducing organic matter for the plants to be grown.

Lastly, Wallace laboratories indicated the moisture content of the soils as the following: Soil #1 at 20.5%, Soil #2 at 2.5%, Soil #3 at 1.3%, and Soil #4 at 15.0%. As mentioned in the descriptions of the initial soil collection at Owens Lake, Soil #1 and Soil

#2 appeared quite moist with Soil #1 appearing to have the most moisture. On the other hand, Soil #3 and Soil #4 appeared quite dry. There is a good correlation with Soil #1 appearing to have a high moisture and Soil #3 having a low moisture content as per the observations. For Soil #2, the sand sent to the laboratory was from an open container which had time to dry, so we would expect it to have a low moisture content as well. Finally, the greatest anomaly is Soil #4 which appears and always has appeared quite dry to have a moisture content of 15.0%. In the studies on the effect of moisture on emissions to be presented later, the moisture content of this soil was repeated three times and agreement with this 15.0% value concurred. Most likely, this soil conceals its moisture content by containing a lot of hygroscopic moisture. Hygroscopic moisture is water which is not so tightly held that it can not be removed by oven drying, but it is too tightly held to be removed by air drying such as on a dry lake playa or in the laboratory. Lastly, the half saturation percentage is calculated for each soil and indicates the amount of moisture content necessary for half saturation of the soils. For Soil #1 the value is 19.7%; for Soil #2 the value is13.0%; for Soil #3 the value is 16.7%; and for Soil #4 the value is 23.0%. These numbers are useful for testing the effect of moisture content on emission rates as well.

In all, the soil properties obtained through particle size analysis and the chemical analysis helps to substantiate beliefs about the soils as well as give direction to some of the different emissions related studies. The size analysis helps to point to the most emissive soils, while the chemical analysis gives crucial details which aid in reproducing the variable conditions of the lake bed. The particle size analysis indicates that Soil #1 and Soil #4 are likely to be the most emissive. Likewise, the chemical analysis indicates that crust development is most likely to occur with Soils #1 and #4 because of high salinity. In addition, the chemical analysis indicates the gravity of high arsenic levels in an inhalable soil as well as the likelihood of naturally growing vegetation in these areas.

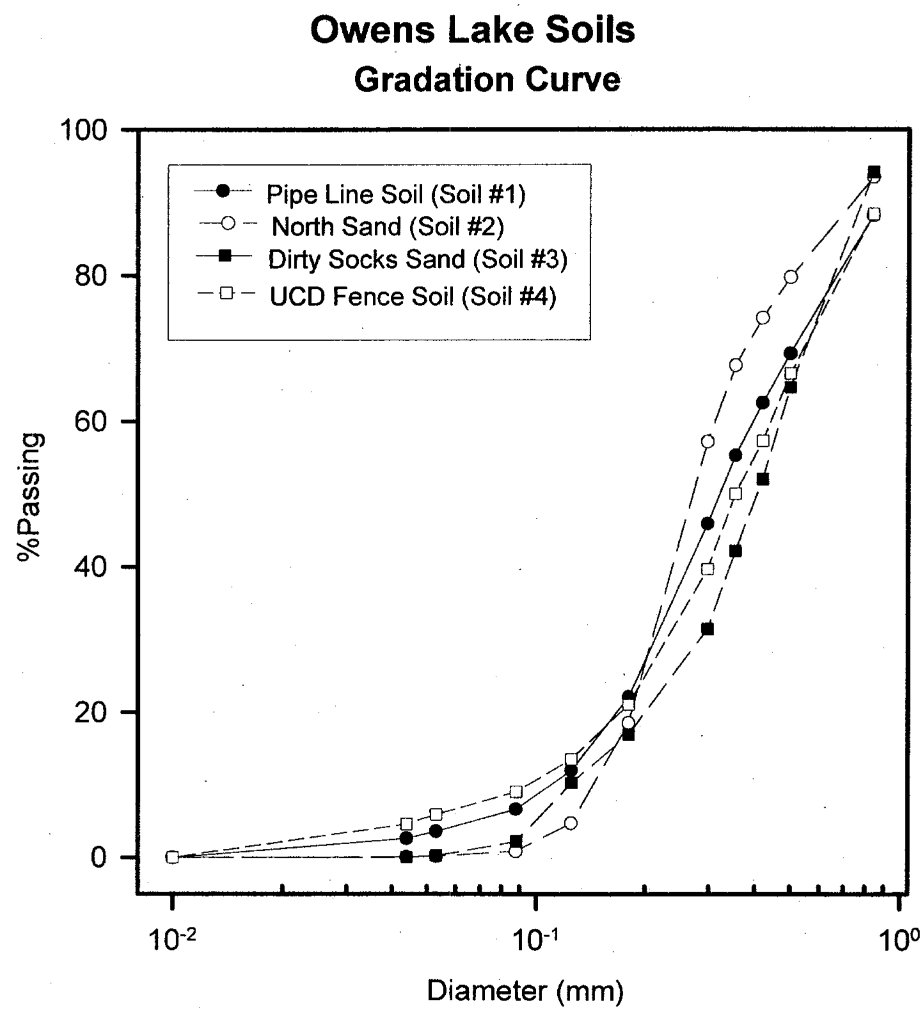

Figure 32. Particle size analysis for the four soils presented as a gradation curve. The curves show that Soil #1 and Soil #4 have a greater number of particle that are less than 100 μm or 0.1 mm indicating a greater potential for small particulate emissions (individual curves in Appendix H).

3.2. Threshold Studies

The threshold velocity of each of the four soils was obtained by correlating with the free stream velocity in the tunnel taken at approximately 0.22 m height. The results of this study are shown in Figures 33-36. In these figures, the voltage of the electrometer versus the free stream velocity is plotted indicating the threshold velocity for a 0.22 m height sampling. For all the soils the threshold velocity was found to be quite similar, around 8.0 m/s at 0.22 m height. This indicates that the surfaces of the loose soils are aerodynamically similar, and the initial movement of the surface follows a similar physical mechanism. Wind passing over the stable bed is retarded at the base by the friction imparted on the fluid by the soil particles. As the velocity increases in the tunnel, both the frictional velocity and the shear stress increase. At some critical point, grains on the bed start to move. Bagnold has shown that this movement depends on the mean grain diameter of the soil (1941), and thus since, the effective mean grain diameter of all four soils is quite similar, the threshold velocity should be about the same for our soils. Once the velocity profiles and z_0 values are established in the next section, the 0.22 m height velocity can be correlated with a near surface values or a 10 m meteorological station velocity. Likewise, the threshold friction velocity u_{*t} can be obtained.

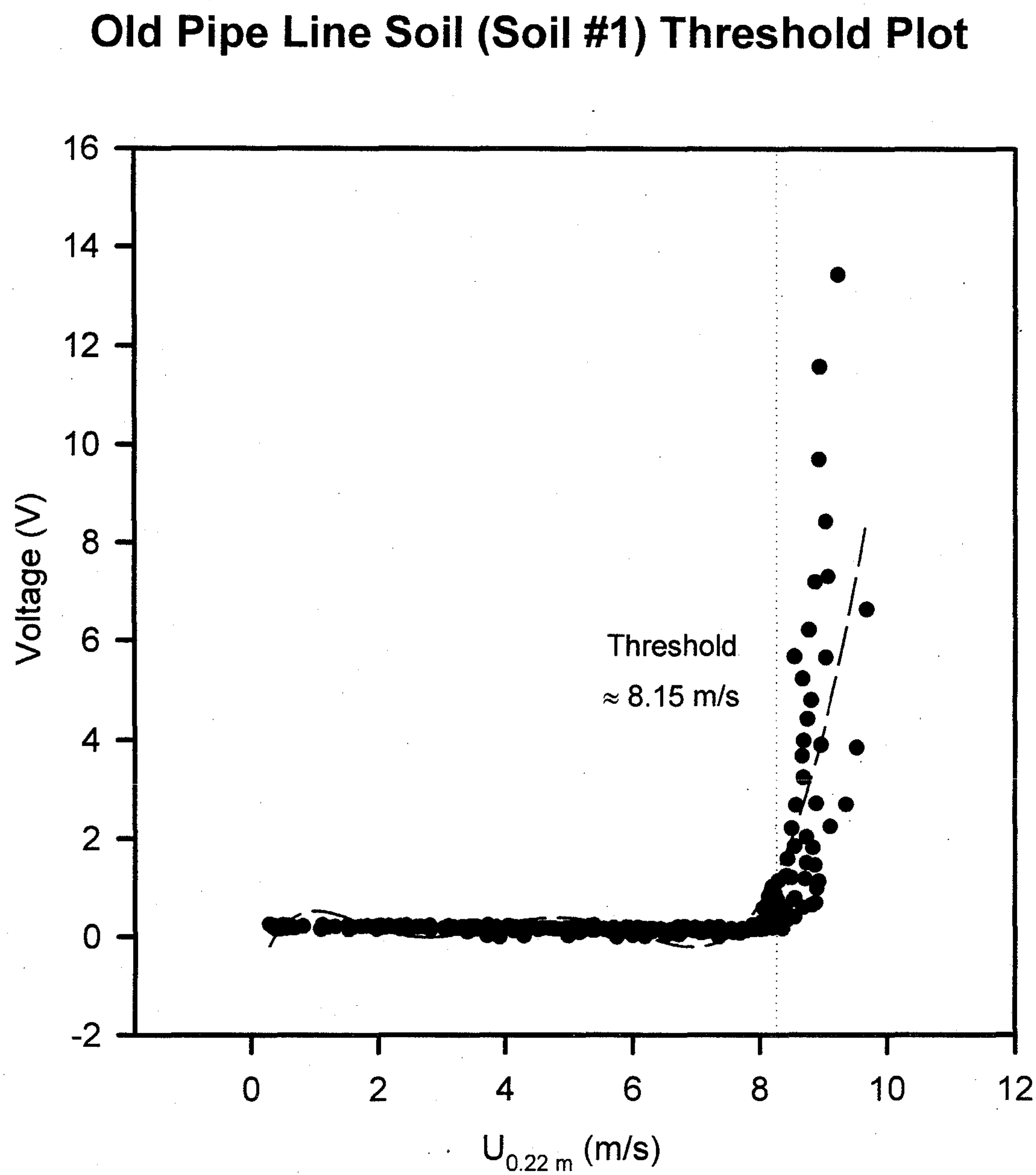

Figure 33. The threshold velocity for Soil #1 at 0.22m height is obtained above by plotting three trials on the same curving and finding the velocity where a rapid increase in the voltage of the electrometer is noted.

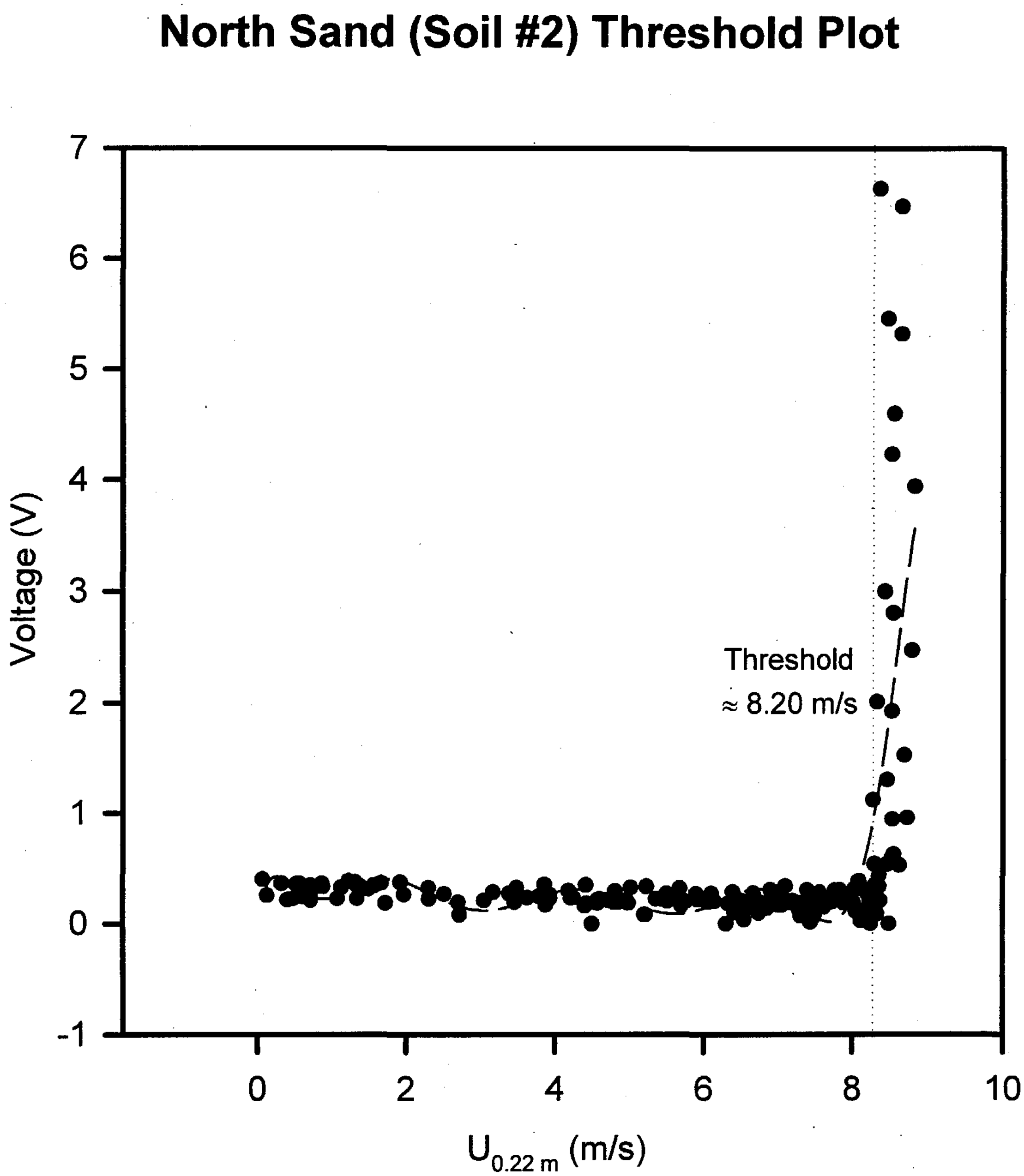

Figure 34. The threshold velocity for Soil #2 at 0.22 m height is obtained above by plotting three trials on the same curve and finding the velocity where a rapid increase in the voltage of the electrometer is noted.

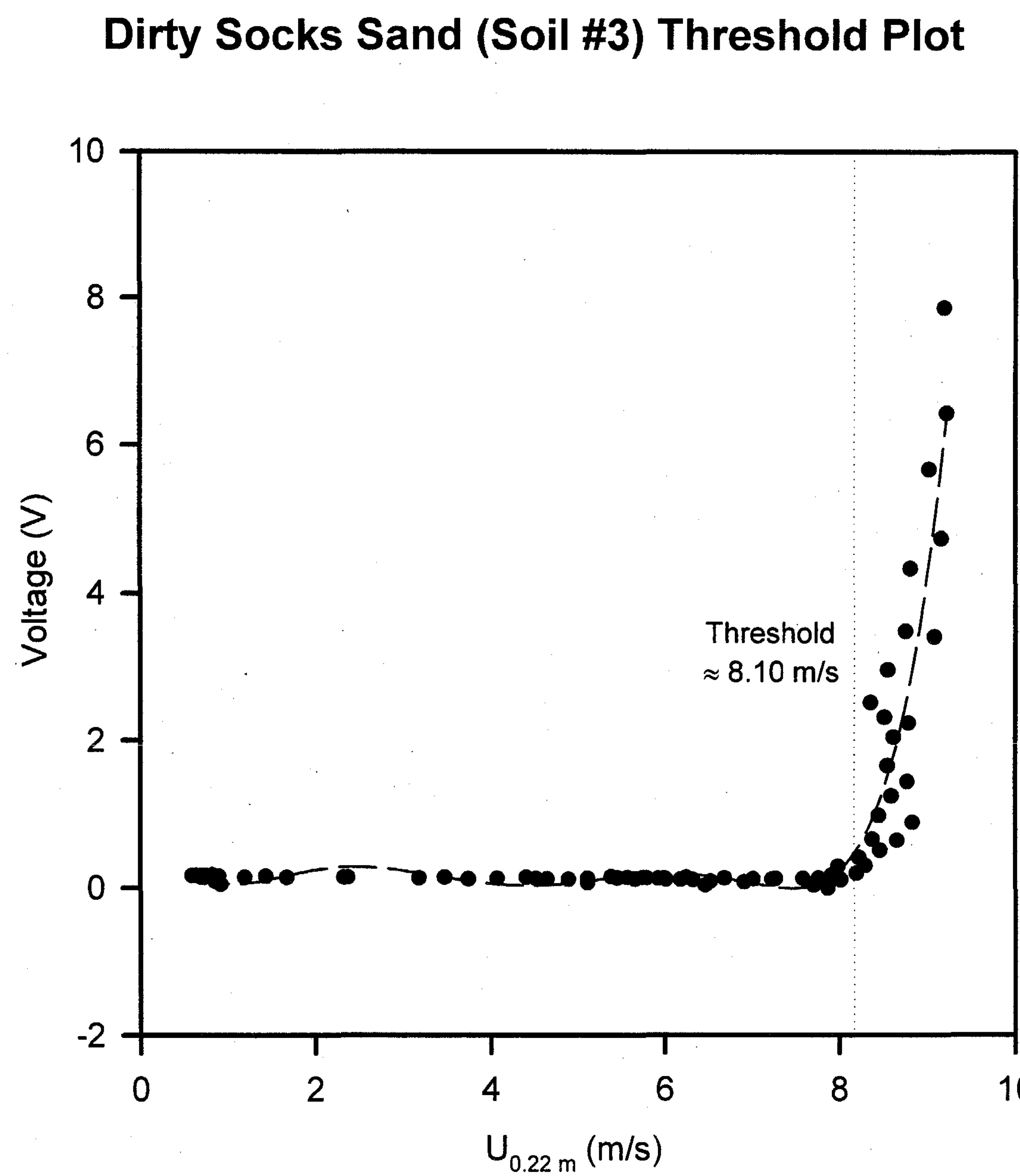

Figure 35. The threshold velocity for Soil #3 at 0.22 m height is obtained above by plotting two trials on the same curve and finding the velocity where a rapid increase in the voltage of the electrometer is noted.

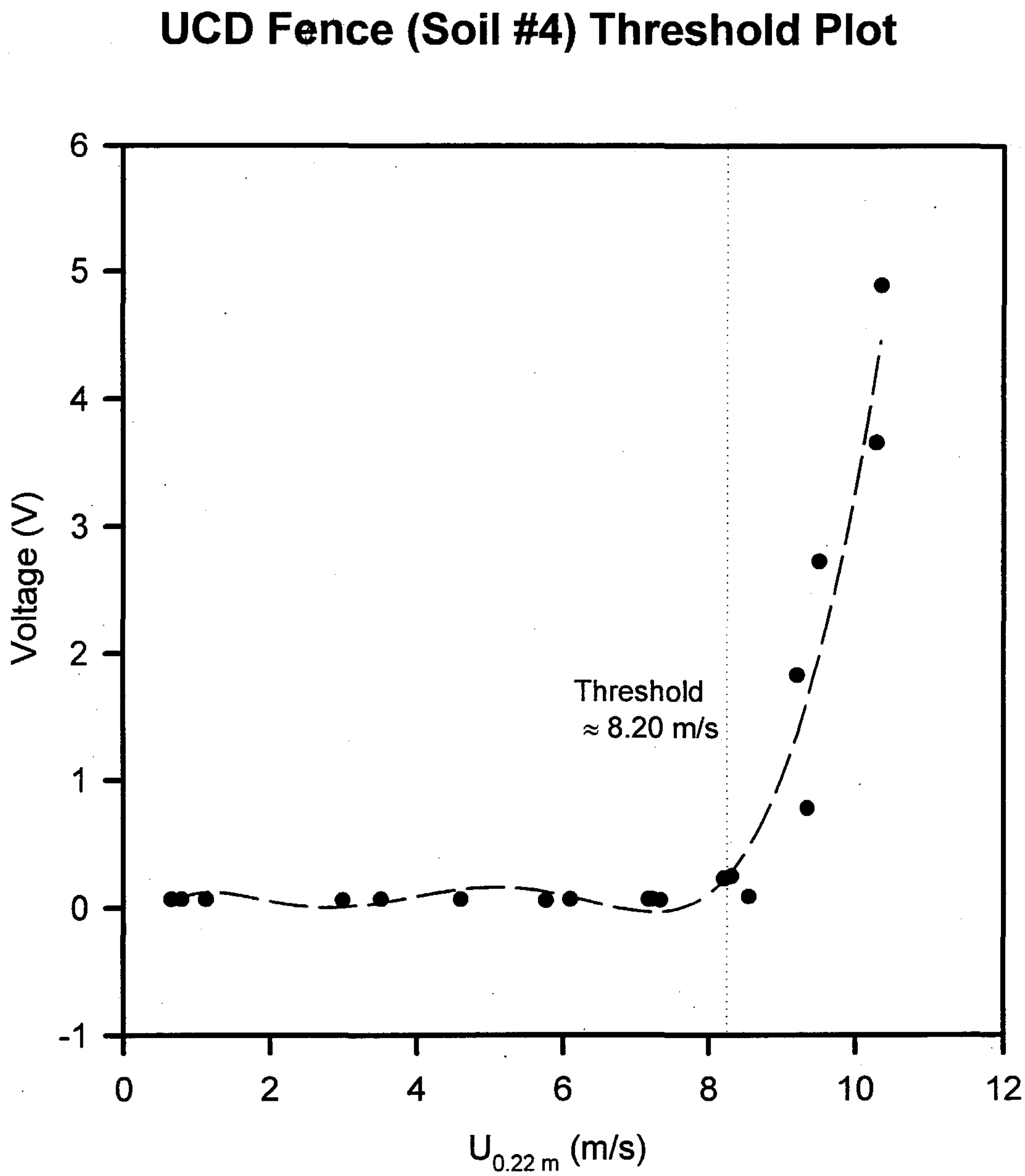

Figure 36. The threshold velocity for Soil #4 for at 0.22 m height is obtained above by averaging the results of three tests and obtaining the velocity where a rapid increase in the voltage of the electrometer is noted.

3.3. Friction Velocity u_* and Surface Roughness z_0 Measurements

The surface roughness z_0 and friction velocity u_* values are obtained for velocity values for free stream that are less than threshold initially, since movement of the soils will effect these measurements. The velocity profiles are shown in Figures 37-41. The average z_0 values for each case are shown on the plots and summarized in Table 2. The z_0 values correspond well to the established values for desert playas (Arya, 1997). The friction velocity u_* values are simply the slopes of the lines shown on the plot. The dotted lines representing the curve fit to the equation, $u = a\log z + b$, are shown on the plot and the regression coefficients "a" and "b" are used to find z_0 and u_* as in Equation (3). These lines which correspond to Equation (3) can then be used to correlate the free stream velocity in the wind tunnel to 10 m (z = 10 m) meteorological observations of the wind. In other words, the velocity increases with height throughout the boundary layer. This relation becomes more important when relating the emissions to the observed meteorological conditions.

Table 2. A summary of the experimentally obtained z_0 characterizing the surface roughness.

Designation	Description	Type	z_0 (m)
Soil # 1	Old Pipe Line	Loamy Sand	2.2×10^{-5}
Soil # 2	North Sand	Sand	4.0×10^{-5}
Soil #3	Dirty Socks Dune	Sand	6.2×10^{-5}
Soil #4	UCD Fence	Sandy Loam	2.2×10^{-5}

All of the friction velocities for all the tests (pre-threshold, loose soil emissions, Enhanced Saltation, PM_{10} and $PM_{2.5}$, Moisture, Fetch, etc.) have been compiled with respect to a the free stream velocity uref (z = 0.22m) in the wind tunnel taken by the Pitot tube. The corresponding plots of the four soils are shown in Figures 42-45. Previous experimental studies suggest that this relationship is linear; however, the plots do not show a linear relationship for the entire range of velocities investigated, but rather a bi-modal breaking around the threshold friction velocity. This form is most recognizable in the plot of Soil #1 (Fig 42). This relationship is the result of the enhanced surface shear stress as a result of saltation and the formation of ripples at the higher velocities. When saltation begins the particles can quickly sort and produce ripple beds which create a rougher surface and ultimately a higher shear velocity. The ripple beds are most pronounced at the highest velocities tested. In fact, observations suggest that Soil #1 had the quickest response to forming ripples and had the most pronounced ripple beds (Figure 46). These fits were then used to obtain the threshold friction velocity u_{*t} corresponding to the uref value obtained in the threshold studies; the values are given in Table 3.

Table 3. The threshold friction velocity value u_{*t} obtained from $uref_t$ and a curve fit to the uref versus u_* for all the cases as given in Figures 42-45.

Designation	**Description**	**Type**	**u_{*t} (m/s)**
Soil # 1	Old Pipe Line	Loamy Sand	0.39
Soil # 2	North Sand	Sand	0.42
Soil #3	Dirty Socks Dune	Sand	0.42
Soil #4	UCD Fence	Sandy Loam	0.37

The threshold friction velocity values obtained in the wind tunnel are slightly higher than those obtained by GBUAPCD; some of their studies suggest values as low as 0.24 m/s for the initiation of particle movement on the lake bed. Likely, the differences in the values are due to the differences between the lake bed conditions and the idealized uniform surface in the laboratory test bed. In the laboratory, the threshold value is taken when the entire bed begins to move under a steady wind, while at the dry lake a sudden gust of comparable or lower speed wind could dislodge loose particles initiating movement and registering a lower threshold friction velocity.

The combined saltation cases are also plotted on the individual friction velocity curves even though they do not represent strictly one soil type over the entire bed. For example, u_* values from Dirty Socks Sand (Soil #3) saltating over the UCD Fence Soil (Soil #4) are placed on the individual curves relating the friction velocity to uref for Soil #3 and Soil #4. For the case of Soil #3 saltating over Soil #4, the u_* values below threshold correspond with those obtained for the sand (Soil #3), where at higher velocity values, the u_* values correspond with the UCD Fence Soil (Soil #4). Likely, this results from the fact that there is a discernible roughness difference between Dirty Socks Sand and UCD Fence Soil of approximately three times greater roughness for the sand. At the lower velocities, at the 4.38 m sampling point, the flow development has not completely transitioned from the turbulent characteristics of the rougher sand behind to the UCD Fence Soil in front. At the higher speeds, the transition to turbulence from one rough surface to the next is much more rapid and the limited fetch of new soil does not become a factor. The characteristic roughness and shear velocity of that soil (UCD Fence Soil) closest to the probe is the one measured. However, the North Sand saltating over the Old Pipe Line Soil does not show this same trend. The roughness of the North Sand and the Pipe Line Soil are about the same—the sand is almost twice as rough as the soil. At low speeds, the characteristics of the friction velocity u_* are about the same for both soils, and thus, prior to threshold the values could fit either curve. Likewise, above threshold, the same conclusion is reached.

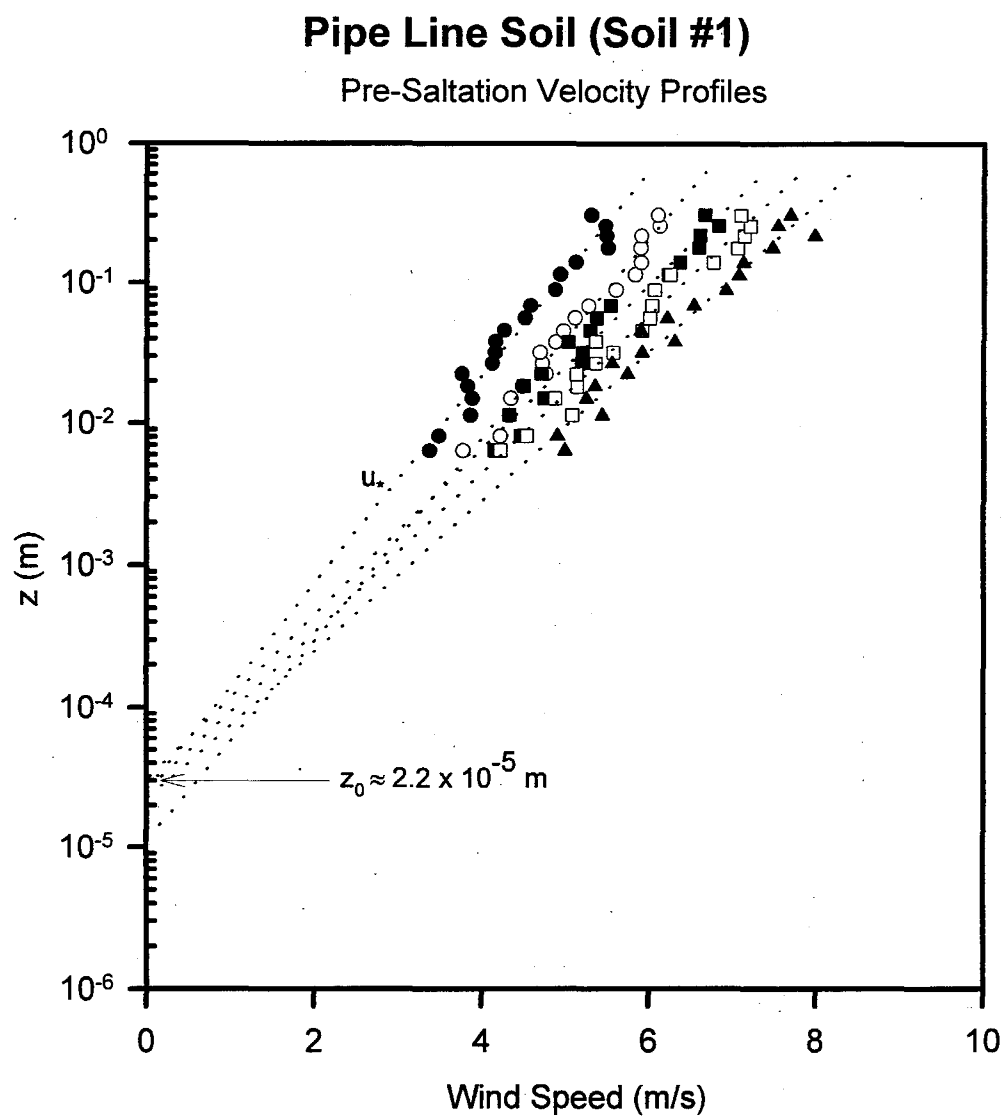

Figure 37. The pre-saltation velocity profiles for Soil #1 indicating the value of z_0 obtained by the intersection of the z-axis. The slope of the velocity profiles then corresponds to a frictional velocity u_* which is related to the shear stress on the soil surface.

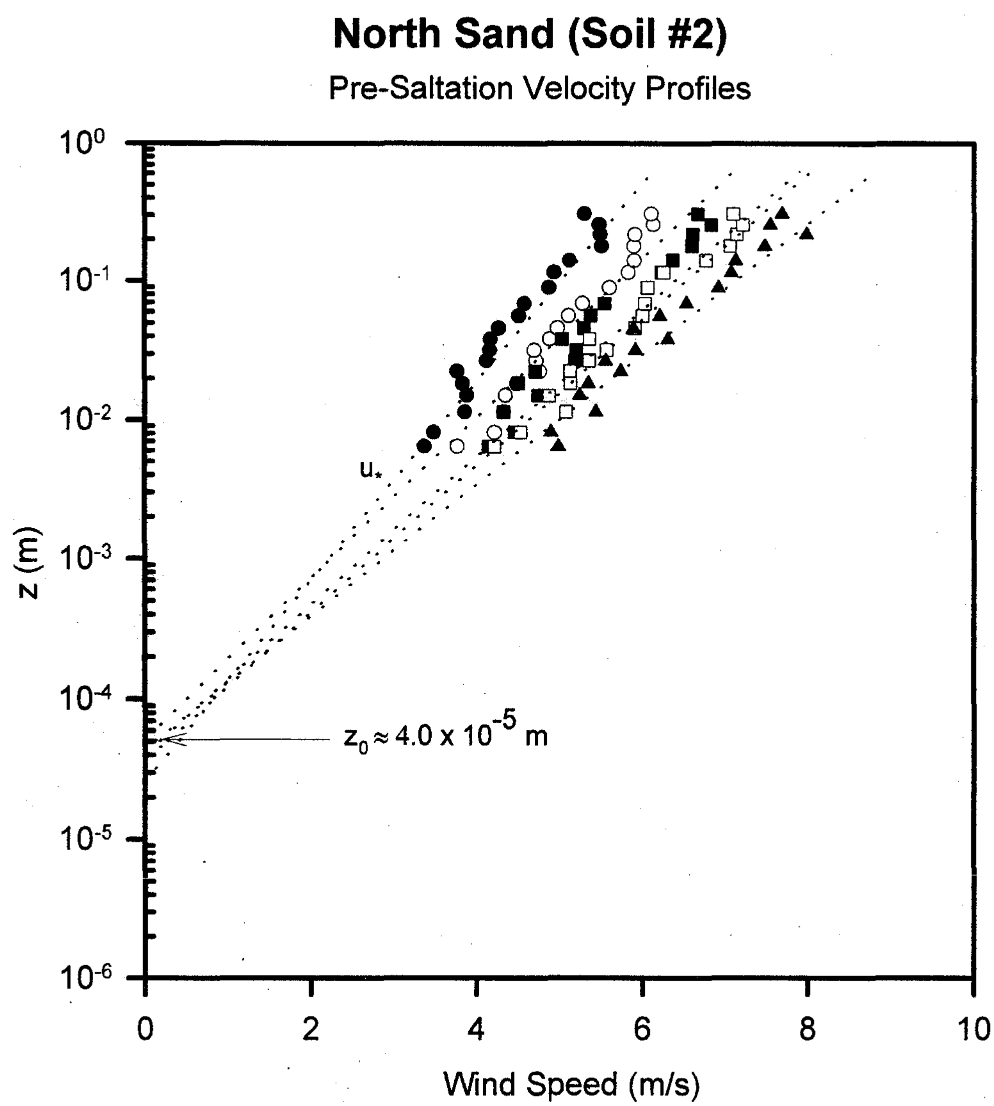

Figure 38. The pre-saltation velocity profiles for Soil #2 indicating the value of z_0 obtained by the intersection of the z-axis. The slope of the velocity profiles then corresponds to a frictional velocity u_* which is related to the shear stress on the soil surface.

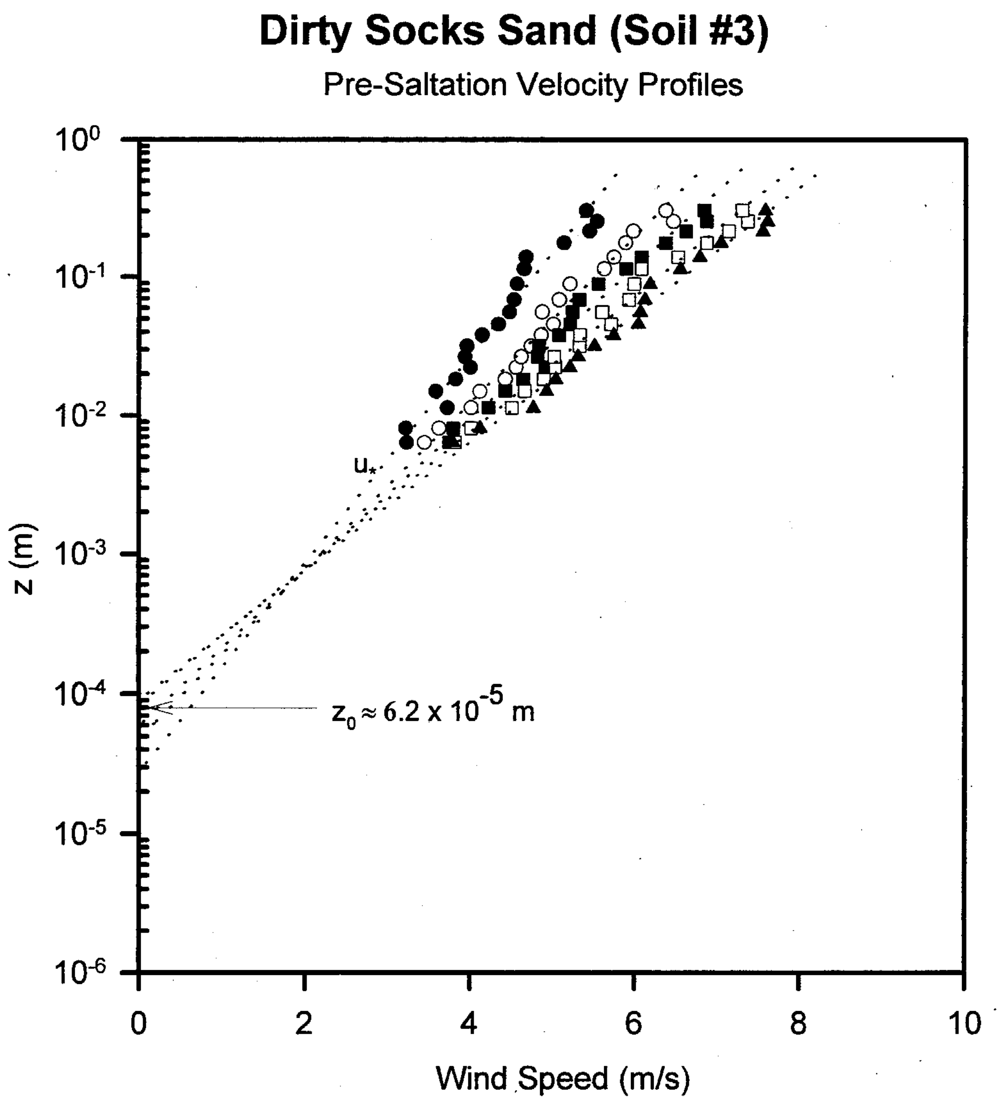

Figure 39. The pre-saltation velocity profiles for Soil #3 indicating the value of z_0 obtained by the intersection of the z-axis. The slope of the velocity profiles then corresponds to a frictional velocity u_* which is related to the shear stress on the soil surface.

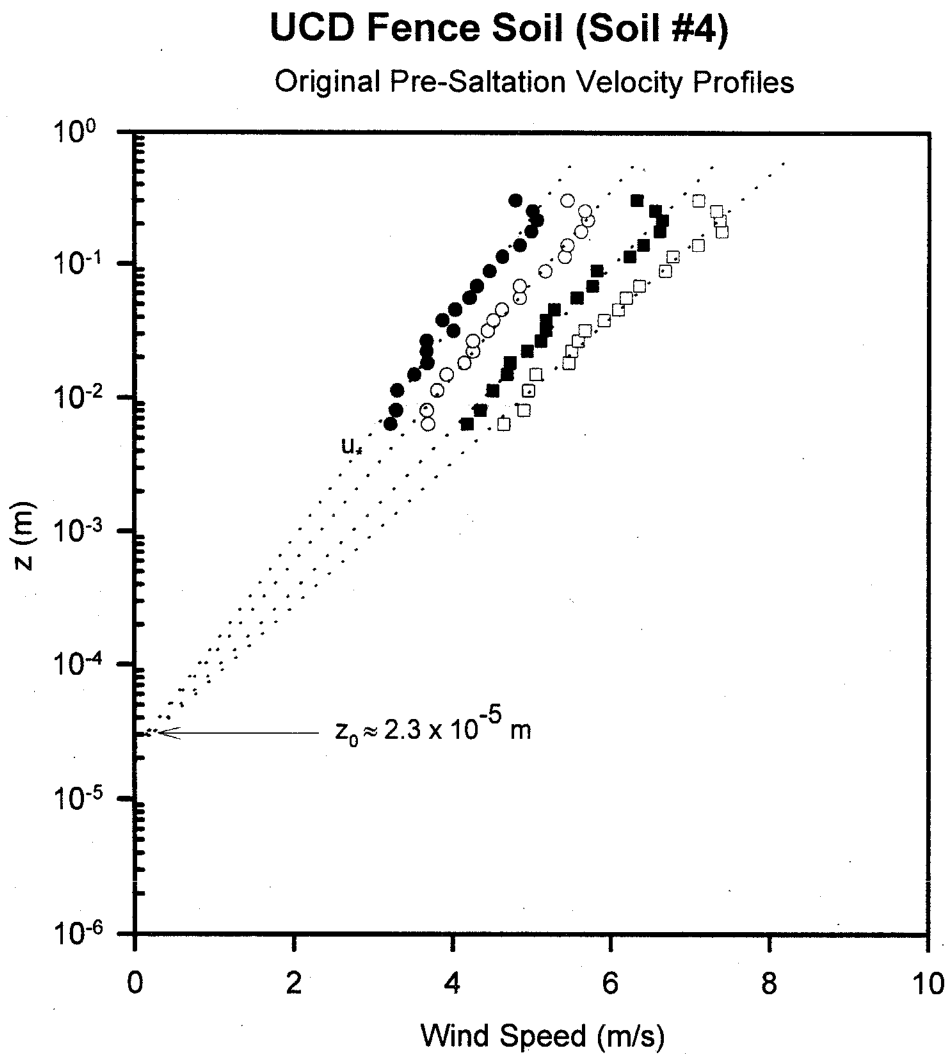

Figure 40. The original pre-saltation velocity profiles for Soil #4 indicating the value of z_0 obtained by the intersection of the z-axis. The slope of the velocity profiles then corresponds to a frictional velocity u_* which is related to the shear stress on the soil surface.

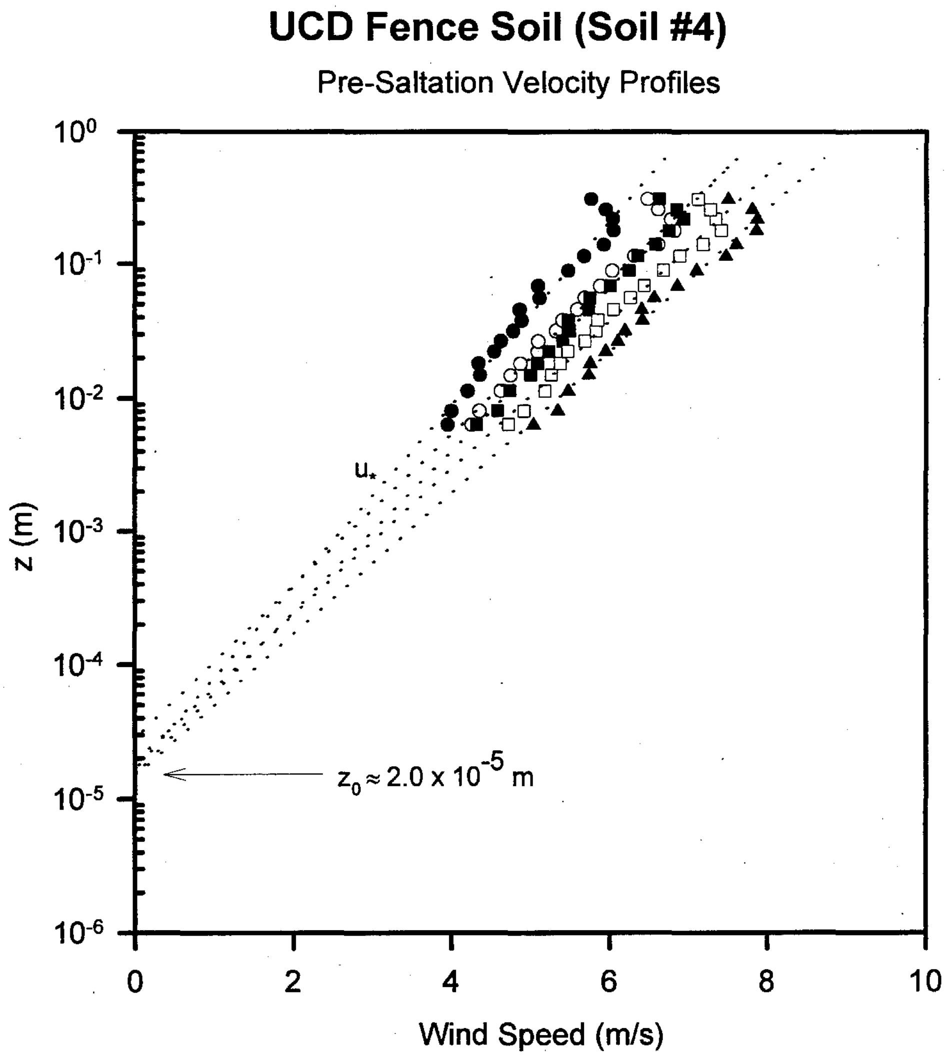

Figure 41. The pre-saltation velocity profiles for Soil #4 indicating the value of z_0 obtained by the intersection of the z-axis. The slope of the velocity profiles then corresponds to a frictional velocity u_* which is related to the shear stress on the soil surface.

Pipe Line Soil (Soil #1) Friction Velocities

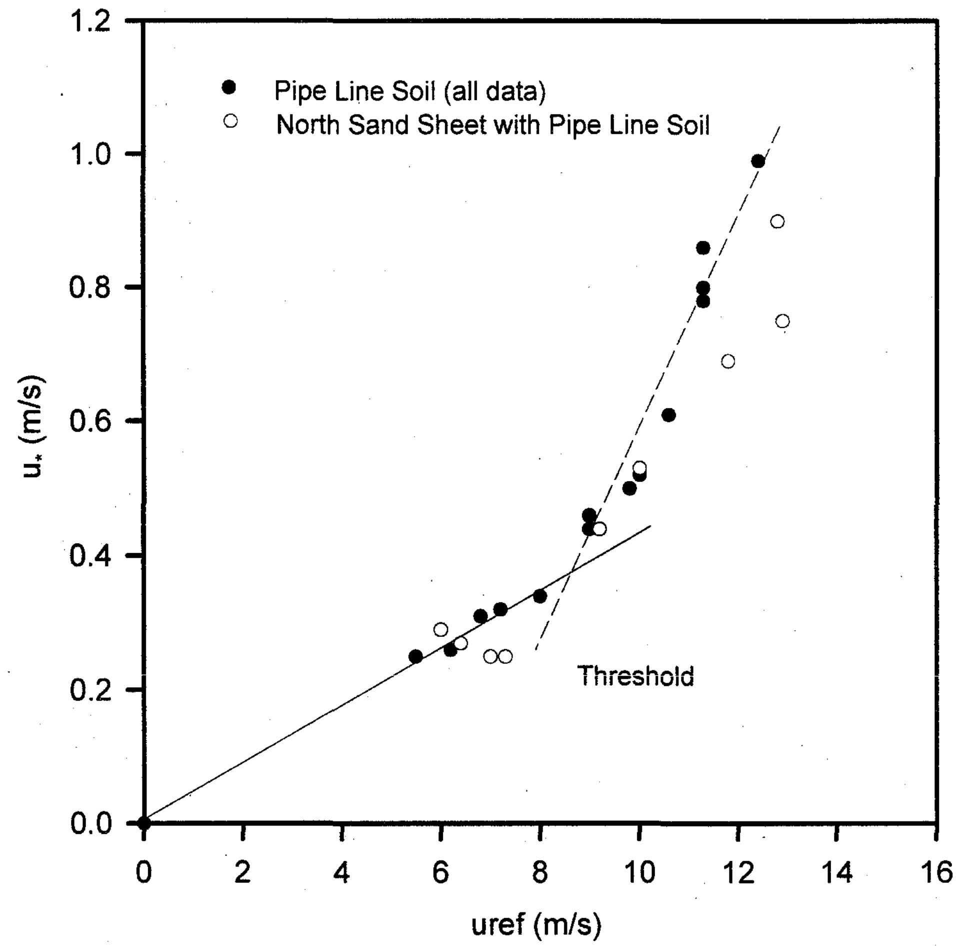

Figure 42. The friction velocity is shown versus the free stream reference velocity in the wind tunnel which is taken at a height of 0.22 m for the Old Pipe Line Soil (Soil #1). In addition, the data is fit with linear fits to correlate free stream in the tunnel with a friction velocity for each soil.

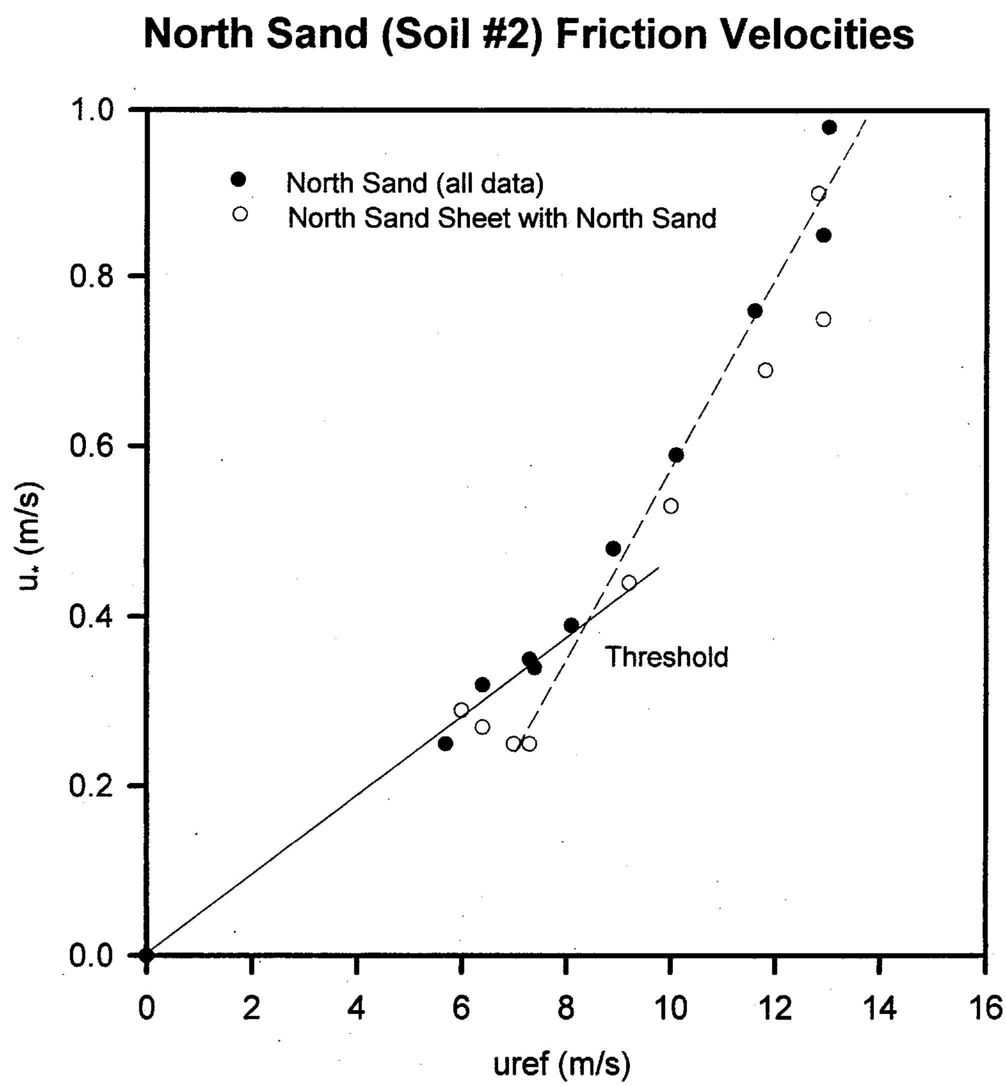

Figure 43. The friction velocity is shown versus the free stream reference velocity in the wind tunnel which is taken at a height of 0.22 m for the North Sand (Soil #2). In addition, the data is fit with linear fits to correlate free stream in the tunnel with a friction velocity for each soil.

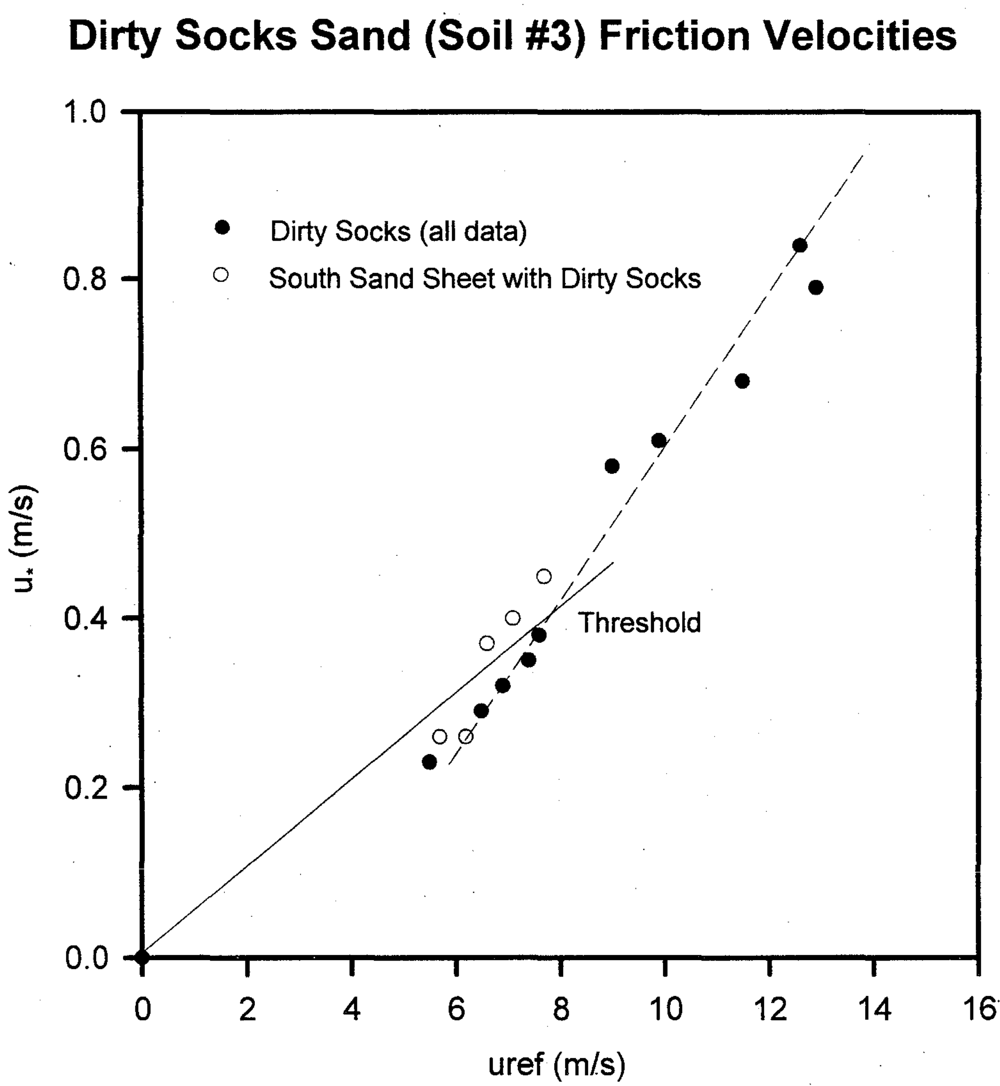

Figure 44. The friction velocity is shown versus the free stream reference velocity in the wind tunnel which is taken at a height of 0.22 m for the Dirty Socks Sand (Soil #3). In addition, the data is fit with linear fits to correlate free stream in the tunnel with a friction velocity for each soil.

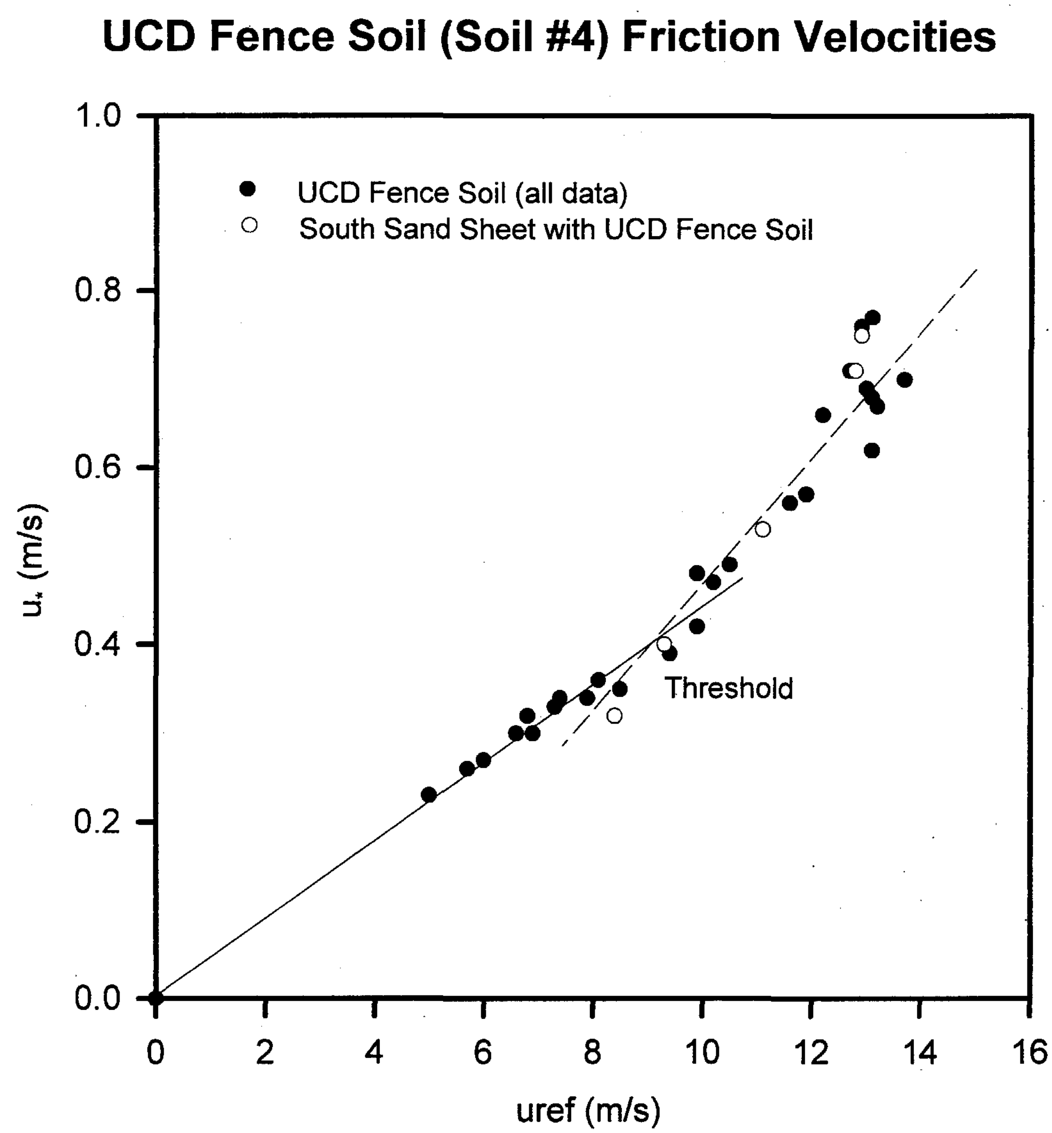

Figure 45. The friction velocity is shown versus the free stream reference velocity in the wind tunnel which is taken at a height of 0.22 m for the UCD Fence Soil (Soil #4). In addition, the data is fit with linear fits to correlate free stream in the tunnel with a friction velocity for each soil.

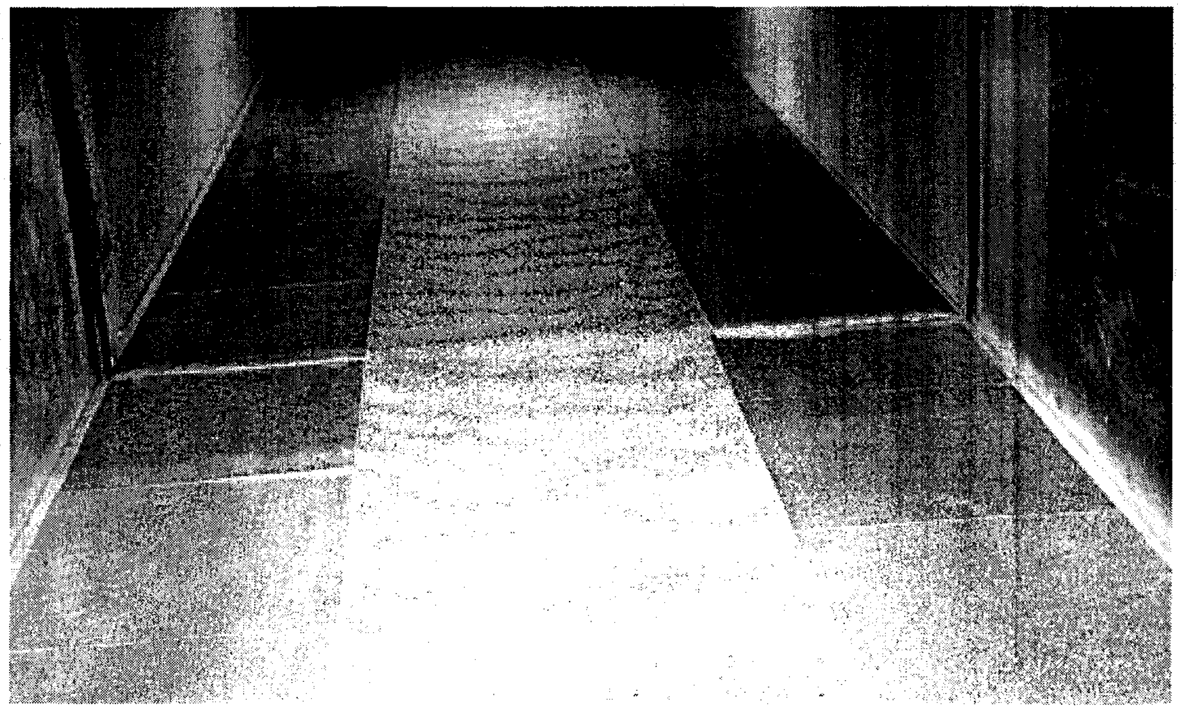

Figure 46. The ripples at high frictional velocities form rapidly as shown in this photograph of the ripple bed formed in Soil #1.

3.4. PM_{10} Loose Soil Emission Rates

Velocity profiles were obtained for each case; however, above threshold conditions z_0 no longer has the same meaning, since movement of the soil causes an increased effective roughness due to saltating particles known z' as shown in Figure 18. The velocity profiles for the four soils above saltation are shown in Figures 47-50. Simultaneously, PM_{10} concentration profiles were obtained for each case at 2.65 m from the beginning of the soil bed and 4.38 m into the soil bed. A typical case of the resulting data is shown in Figures 51-52 (all other similar curves are given in the Appendices A-E). These curves were then analyzed along with the corresponding velocity profiles as in Equations (4)-(6) to obtain emissions rates. For all loose soil emission rates, the control volume was taken as the beginning of the bed to the 4.38 m probe, L = 4.38 m in the calculations and $m_i = 0$. This method of calculation gives a type of average emission rate over the entire soil bed. In addition, emission rates based on a per unit width basis were calculated by not dividing by the length parameter L. In this case, values at L = 2.65 m could be compared to L = 4.38 m in effect looking at the fetch effect on emissions. Two different types of results occur in this comparison; first, those where there is distinctly increasing amounts of PM_{10} along the length of the soil test bed between 2.65 m and 4.38 m, and second, those where the PM_{10} levels remain about the same or decrease slightly. For all of the highest velocities in the tunnel and for all four soils, the latter is the standard—the rate of fall-out and entrainment of PM_{10} have reached an equilibrium state between 2.65 m and 4.38 m in the tunnel. These ideas will be further elaborated upon in the section devoted entirely to the fetch effect on emissions. In general, as expected the emission rates increased with increasing velocity and friction velocity. A summary of these emission rates are shown in Table 4. The values shown in the Table 4 are average values for all studies conducted in which a loose "dry" soil was tested.

Table 4. Loose Soil Emission Rates for the four soils of interest.

Designation	**Description**	**u_* (m/s)**	**uref (m/s)**	**u(10 m) (m/s)**	**E (PM_{10}) ($\mu g/m^2s$)**
Soil # 1	Old Pipe Line	0.47	9.0	12.7	81.5
Soil # 1	Old Pipe Line	0.50	9.8	13.8	2600
Soil # 1	Old Pipe Line	0.61	10.6	15.4	5920
Soil # 1	Old Pipe Line	0.78	11.3	18.1	15200
Soil # 1	Old Pipe Line	0.80	11.32	18.5	7560
Soil # 2	North Sand	0.48	8.9	13.0	24.9
Soil # 2	North Sand	0.59	10.1	14.6	384
Soil # 2	North Sand	0.76	11.6	17.9	1200
Soil # 2	North Sand	0.85	12.9	19.9	1180
Soil # 2	North Sand	0.98	13.0	21.5	1280
Soil #3	Dirty Socks Dune	0.58	9.0	14.3	48.5
Soil #3	Dirty Socks Dune	0.61	9.9	15.2	1120
Soil #3	Dirty Socks Dune	0.68	11.5	17.5	1920
Soil #3	Dirty Socks Dune	0.79	12.9	19.4	2660
Soil #3	Dirty Socks Dune	0.84	12.6	19.1	2580
Soil #4	UCD Fence	0.35	8.5	11.1	35.4
Soil #4	UCD Fence	0.42	9.9	13.2	223
Soil #4	UCD Fence	0.50	11.6	14.3	2230
Soil #4	UCD Fence	0.60	12.4	18.7	1610
Soil #4	UCD Fence	0.70	13.2	19.0	2670

The most surprising result is that under wind stress, the Dirty Socks Dunes Sand (Soil #3) contains a high amount of PM_{10} and is nearly as emissive as the "emissive" soils, Soil #1 and Soil #4. This may result from the deposition of PM_{10} in the sand due to northerly wind storm events in which large amounts of PM_{10} from the UCD Fence Soil fall-out over the sand and become entrained in the grains of sand, thus becoming a potential future source of emissions. This result indicates that Soil #3 can be a large source of emissions and dust storms on Owens Lake. The particle size analysis predicted a slight potential for emissions; however, these results exceed what would have been expected by particle size analysis alone. The most emissive soil is Soil #1, followed by Soil #4 and Soil #3. All three of these soils are potential sources of large PM_{10} events, especially during severe storm events. Observations in the wind tunnel indicate how easily Soil #1 can be transported as values in the wind tunnel greater than 11.5 m/s quickly cleaned out the test bed. For this reason, the largest values tested were around 11.0 m/s for Soil #1, because too much soil loss would ultimately change the test conditions. The most visually emissive soil is the UCD Fence Soil (Soil #4) observed as "white cloud billows" from points of wind stress. The North Sand emits some PM_{10}, although at a rate which is less than any of the other soils tested. All of the soils at the highest wind tunnel speeds rapidly form ripple beds.

The wind forms ridges of sorted particles that are well established very quickly in the tunnel. The height of the ripples and their wavelength are a function of the wind velocity. Since these beds are formed so rapidly, there is no need to consider their time dependence and the effect on the flow after the initial sorting.

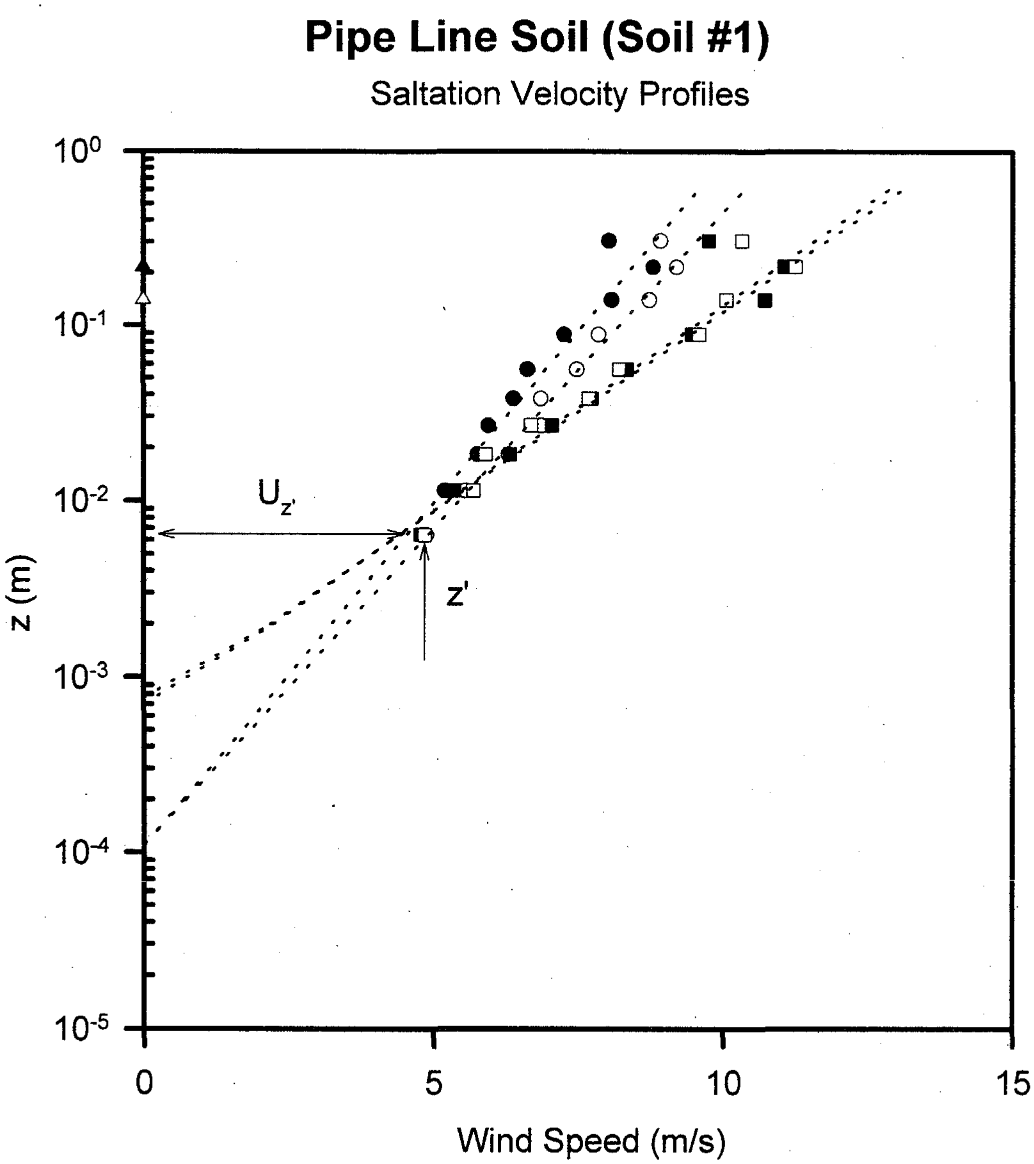

Figure 47. The saltation velocity profiles for Soil #1 indicating the value of z' obtained by the intersection of the lines as well as $U_{z'}$. The slope of the velocity profiles then correspond to a frictional velocity u_* which is related to the shear stress on the soil surface.

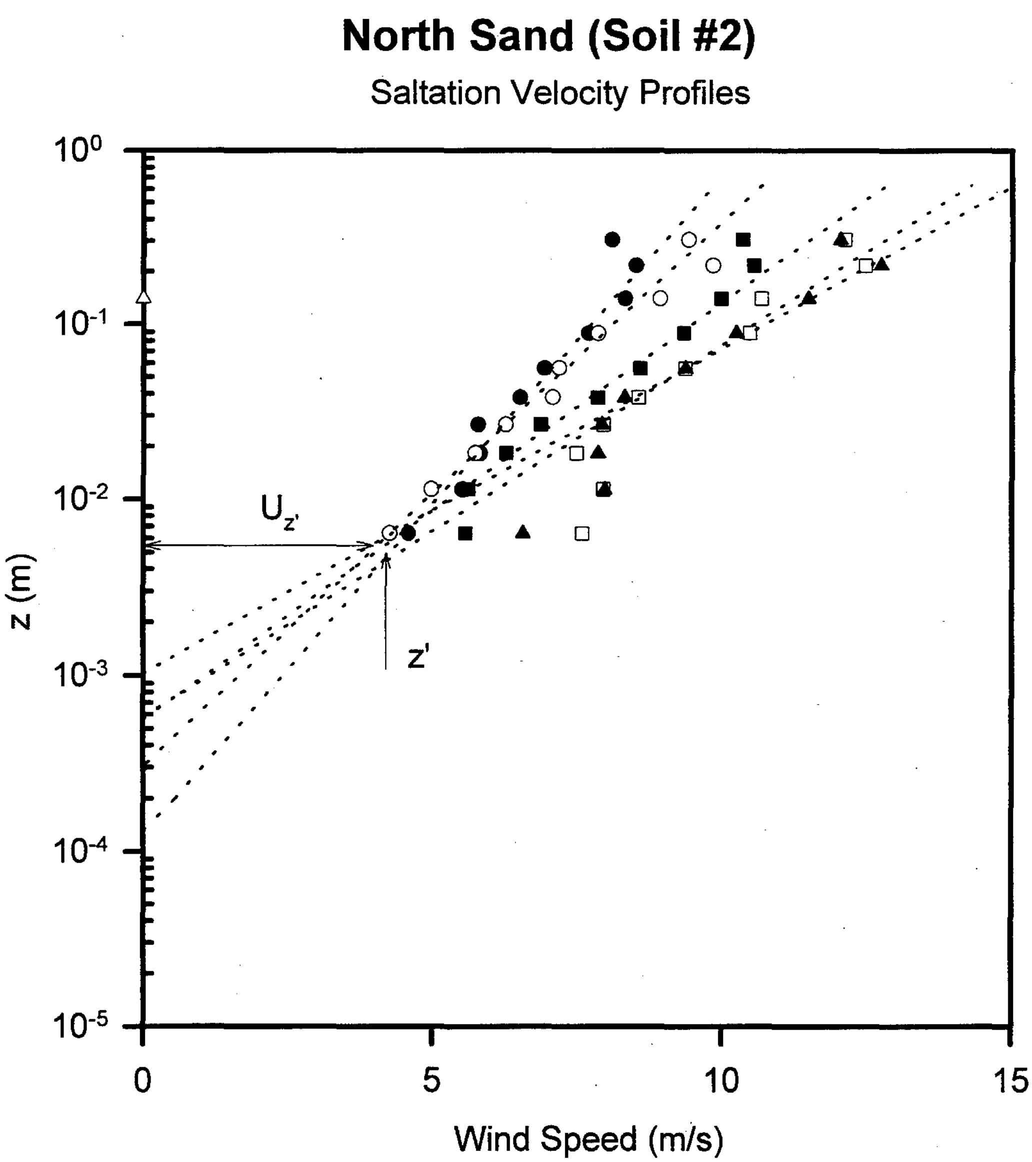

Figure 48. The saltation velocity profiles for Soil #2 indicating the value of z' obtained by the intersection of the lines as well as $U_{z'}$. The slope of the velocity profiles then correspond to a frictional velocity u_* which is related to the shear stress on the soil surface.

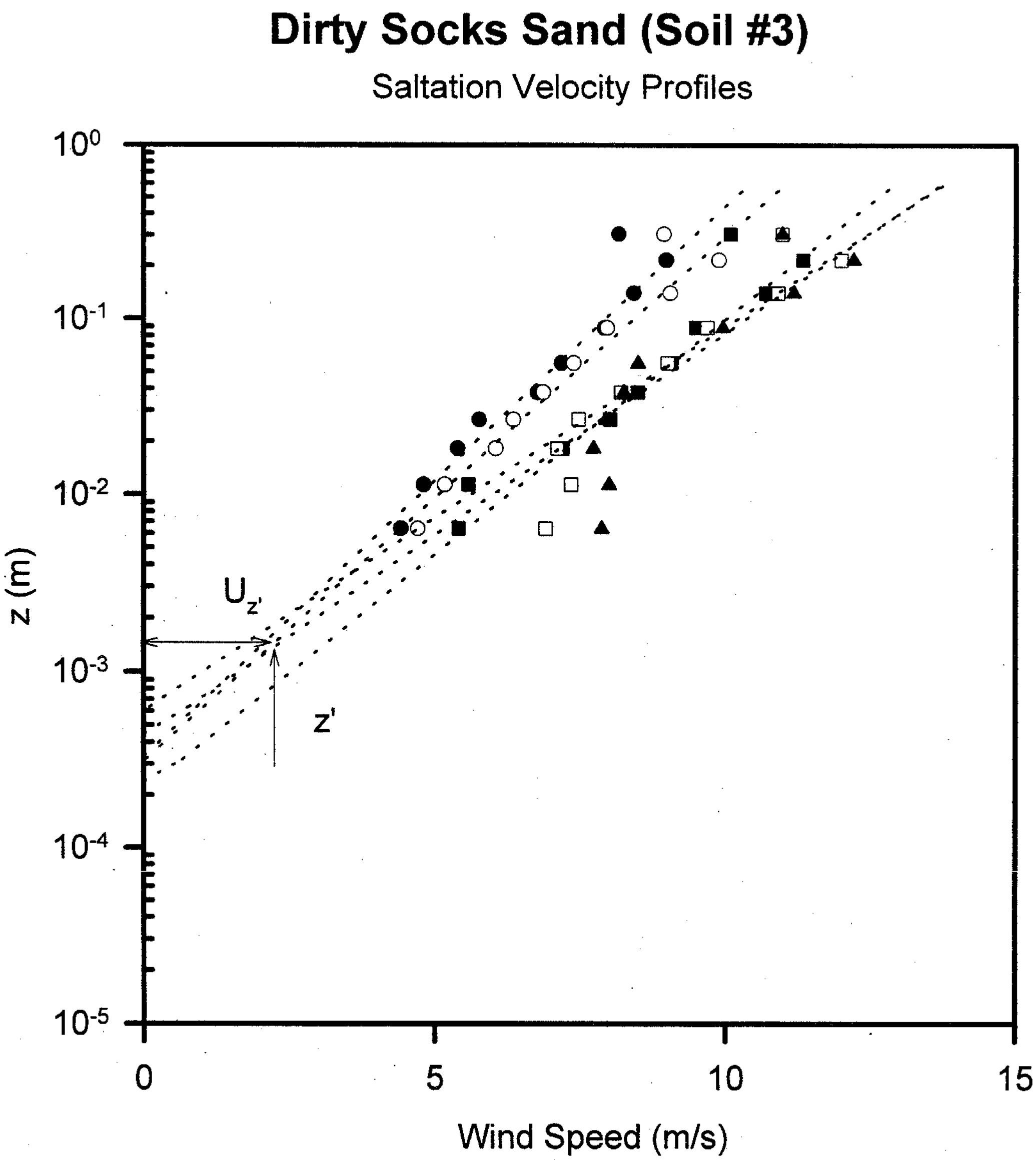

Figure 49. The saltation velocity profiles for Soil #3 indicating the value of z' obtained by the intersection of the lines as well as $U_{z'}$. The slope of the velocity profiles then correspond to a frictional velocity u_* which is related to the shear stress on the soil surface.

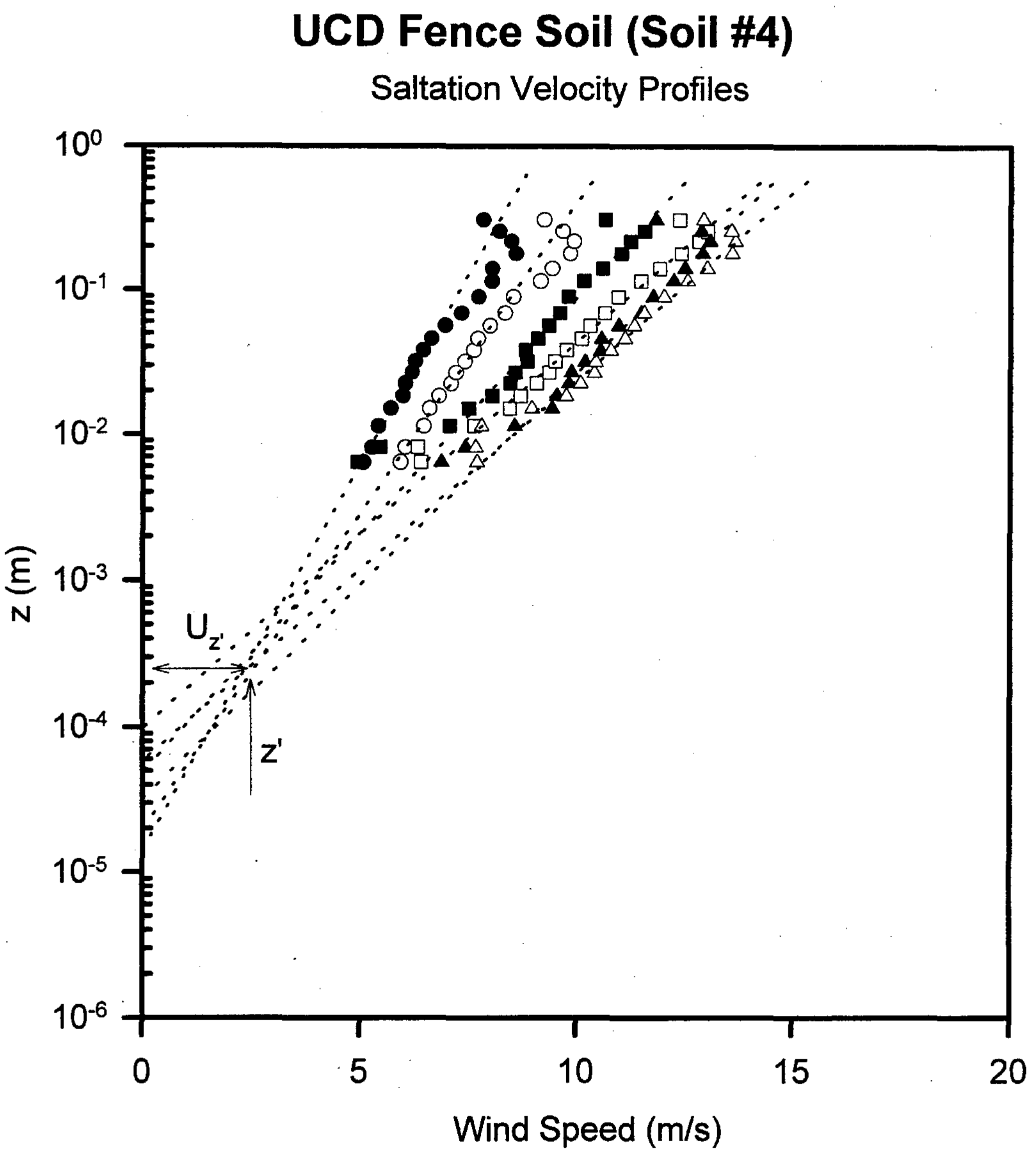

Figure 50. The saltation velocity profiles for Soil #4 indicating the value of z' obtained by the intersection of the lines as well as $U_{z'}$. The slope of the velocity profiles then correspond to a frictional velocity u_* which is related to the shear stress on the soil surface.

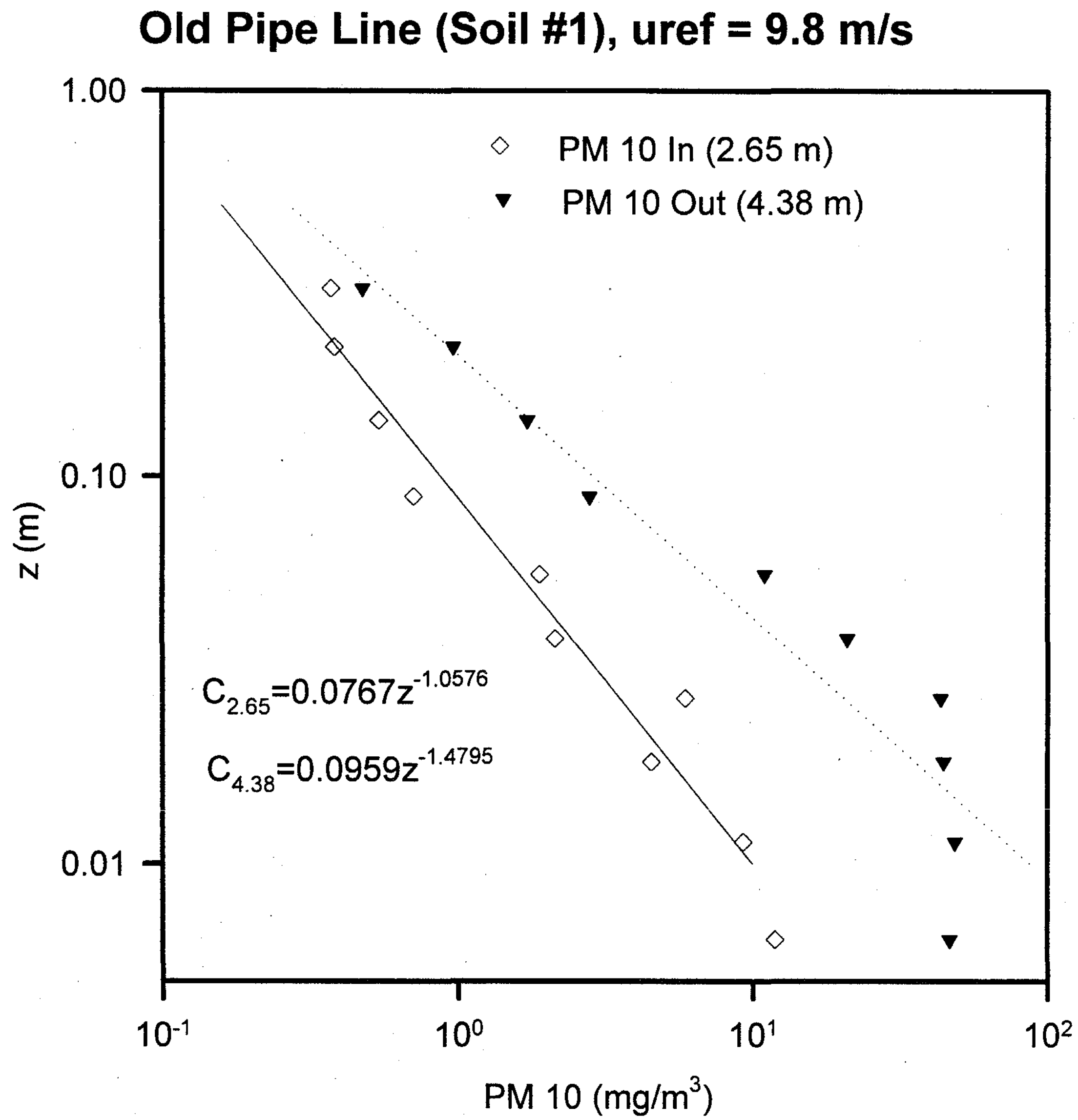

Figure 51. The PM_{10} Concentration profiles for Soil #1 at uref = 9.8 m/s for both the 2.65 m fetch and the 4.38 m fetch distance. These profiles were obtained simultaneously and correlate in time exactly. In this case, there is a gain in the concentration levels between the two probes; however, at the highest velocities, this gain is not seen as in this figure.

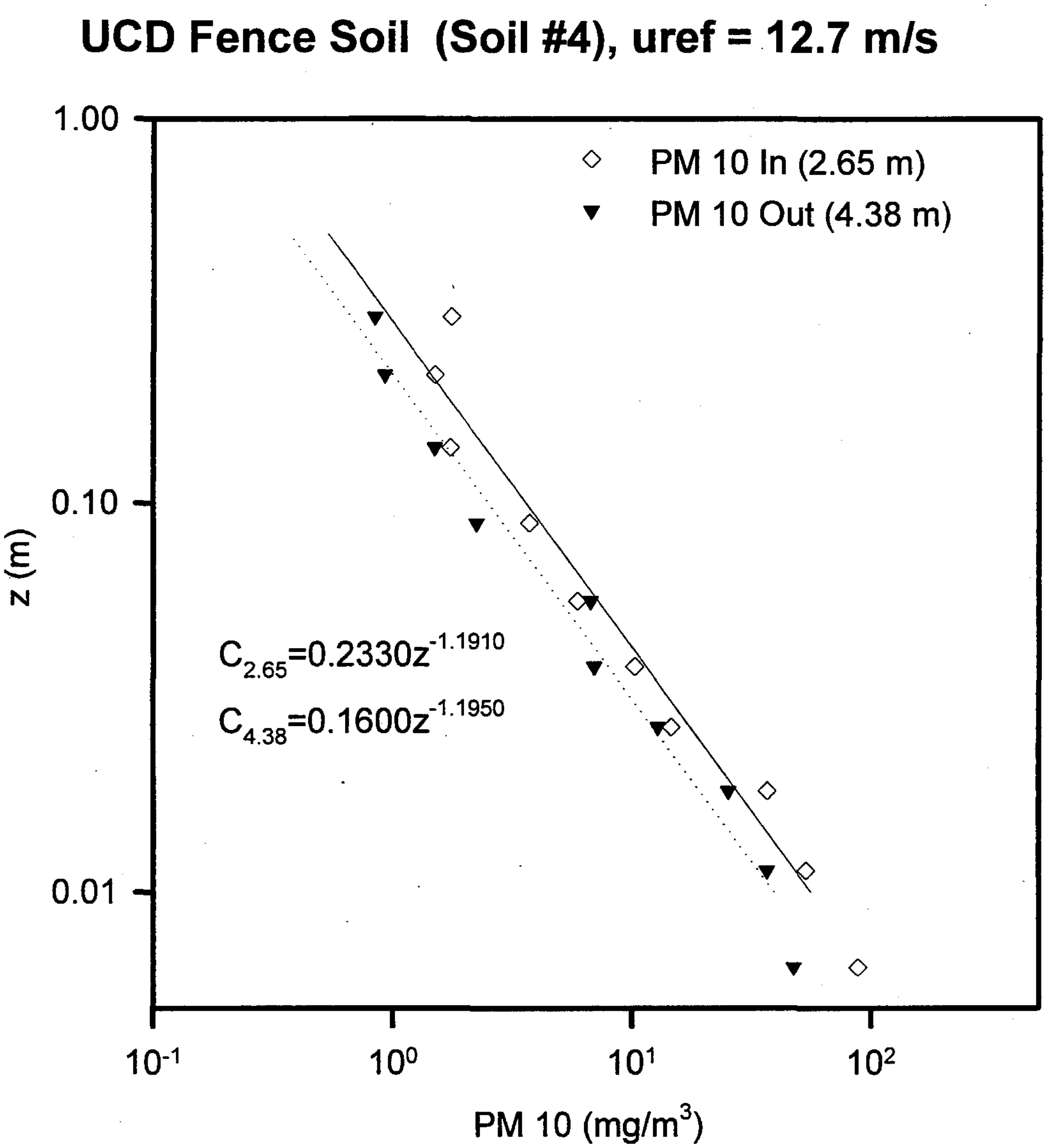

Figure 52. The PM_{10} Concentration profiles for Soil #4 at uref =12.7 m/s for both the 2.65 m fetch and the 4.38 m fetch distance. These profiles were obtained simultaneously and correlate in time exactly. In this case, the concentration levels between the two probes remain about the same, maybe, even a slight decrease is seen.

3.5. Emissions with Upwind Saltation

As discussed previously, one of the proposed mechanisms of enhanced PM_{10} emissions is the scouring of the emissive soils with easily moveable sand particles; in the north part of the lake, the North Sand, and in the south part of the lake, Dirty Socks Sand. To simulate this mechanism, the North Sand was allowed to saltate over the Old Pipe Line Soil and the Dirty Socks Sand was allowed to saltate over the UCD Fence Soil. This would represent strong north and south wind speeds for the two respective cases. These scenarios are known from field observation to be responsible for some of the major dust storms occurring on the lake bed.

The probes again were placed in the same location and concentration profiles obtained (Figure 53-54). The analysis of the last section was reproduced with equations (4)-(6); however, this time the control volume was taken as the volume between the 2.65 m probe and the 4.38 m probe. The integrated profiles at each location were subtracted from each other and divided by L = 1.73 m, in effect capturing those emissions that were due to the emissive soil being bomabarded by sand particles and not those pertaining to the sand movement before the emissive bed. The results are shown below in Table 5.

Table 5. Emission Rates for enhanced saltation for the North and South soils.

Designation	Description	u_* (m/s)	uref (m/s)	u(10 m) (m/s)	E (PM_{10}) ($\mu g/m^2s$)
Soil #2 over Soil # 1	North Sand Sheet	0.44	9.2	12.2	239
Soil #2 over Soil # 1	North Sand Sheet	0.53	10.0	14.2	197
Soil #2 over Soil # 1	North Sand Sheet	0.69	11.8	17.2	11600
Soil #2 over Soil # 1	North Sand Sheet	0.90	12.8	20.6	27600
Soil #3 over Soil # 4	South Sand Sheet	0.32	8.4	10.4	3.58
Soil #3 over Soil # 4	South Sand Sheet	0.40	9.3	11.9	23.2
Soil #3 over Soil # 4	South Sand Sheet	0.53	11.1	15.5	2920
Soil #3 over Soil # 4	South Sand Sheet	0.71	12.8	18.9	5640
Soil #3 over Soil # 4	South Sand Sheet	0.75	12.9	19.4	4620

Saltation has marked effect on the emission rate as expected and is shown in Table 5. This enhancement is likely due to sand particles impacting the soil with ballistic trajectories at a greater frequency than does the saltating soil alone. These impacts throw PM_{10} into the air allowing it to more easily be entrained into the turbulent flow and be transported upward. In addition, agglomerations in the soil are likely abraded into smaller more emissive particles with the coarser sand. In all, enhanced saltation is likely to be an integral mechanism in major emission events at Owens Lake. Plots exemplifying the enhanced emission rates are shown in Figures 55-56. Each of these plots represents those emission rate cases pertaining to a specific location, the North Owens Lake Area and South Owens Lake Area. The North plot contains information on emission rates for Soil #1 and Soil #2 and Soil#2 over Soil #1. The South plot contains information on emission rates for Soil #3 and Soil #4 and Soil #3 over Soil #4. The enhancement in emission rates by introducing saltating sand up stream of the emissive soils is indicated by the trend lines.

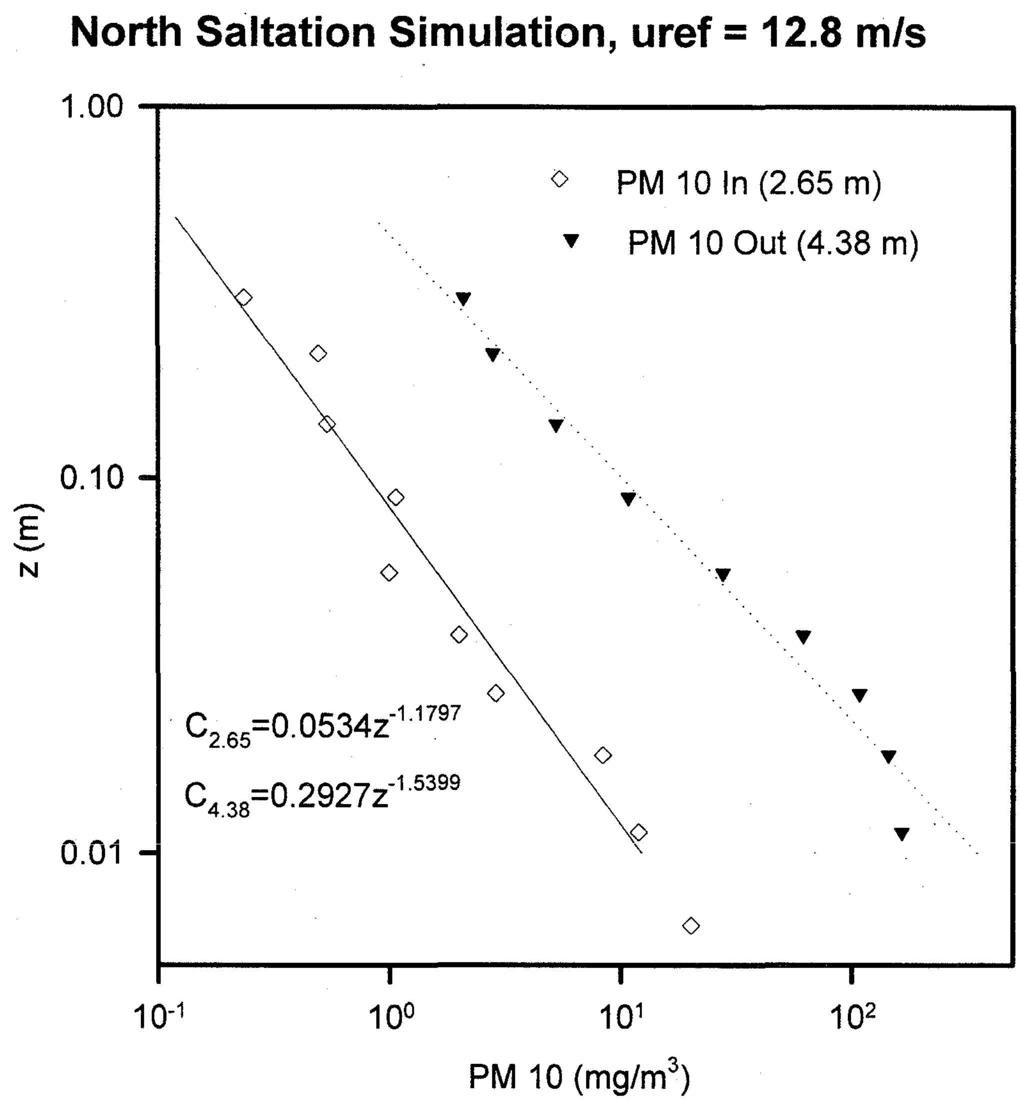

Figure 53. The PM_{10} Concentration profiles for Soil #2 over Soil #1 at uref =12.8 m/s for both the 2.65 m fetch and the 4.38 m fetch distance. These profiles were obtained simultaneously and correlate in time exactly. In this case, the concentration levels between the two probes increase dramatically due to the enhanced saltation, and also because the 2.65 m location represents the emissions from the North Sand (Soil #2) which does not have very much PM_{10}.

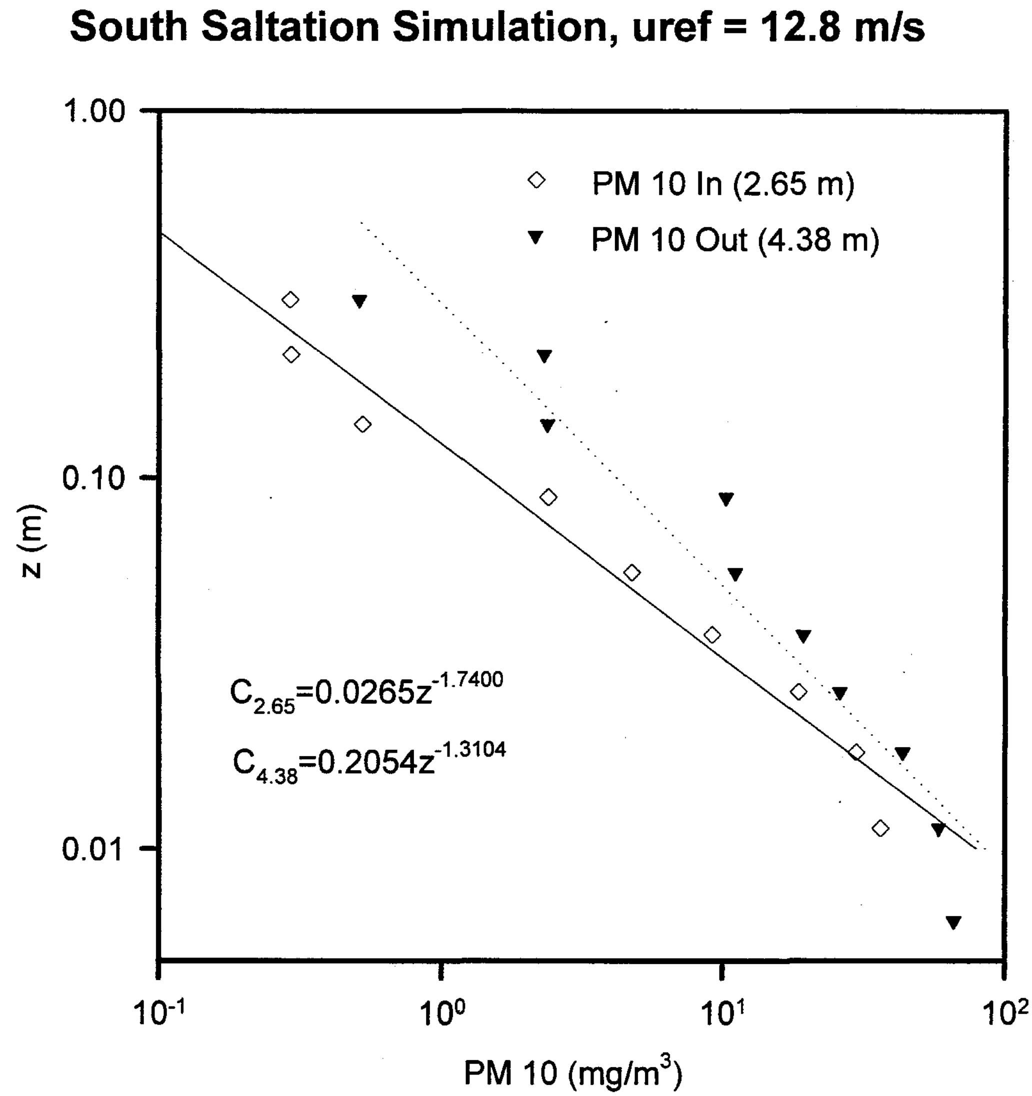

Figure 54. The PM_{10} Concentration profiles for Soil #3 over Soil #4 at uref =12.8 m/s for both the 2.65 m fetch and the 4.38 m fetch distance. These profiles were obtained simultaneously and correlate in time exactly. In this case, the concentration levels between the two probes increase due to the enhanced saltation; however, because the 2.65 m location represents the emissions from the Dirty Socks Sand (Soil #2) which contains a lot of PM_{10} we do not see as dramatic of differences as with the North Sand Sheet case.

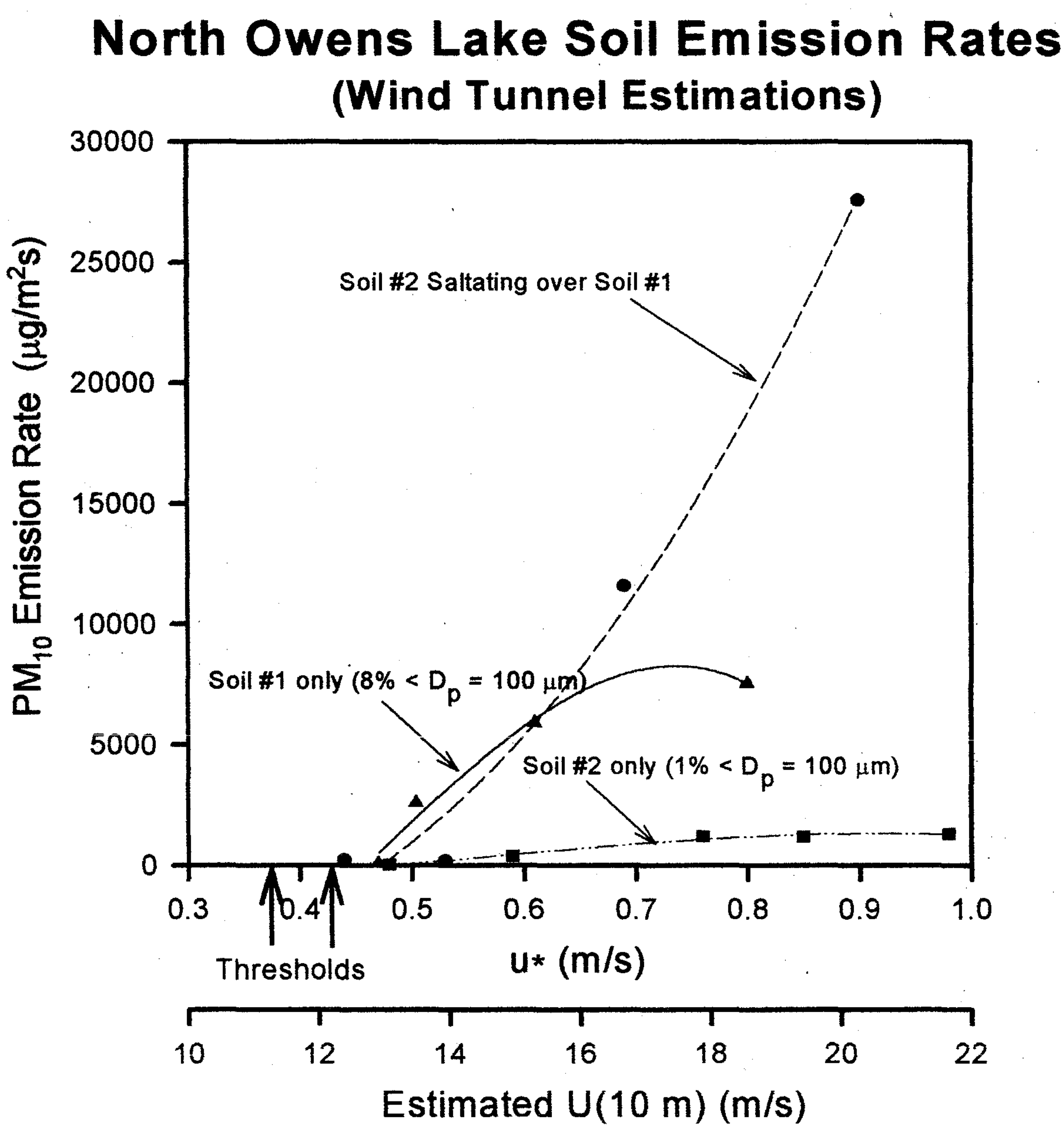

Figure 55. The PM_{10} emission rates versus the friction velocity for all the North Soils are shown above. The effect of enhanced saltation (Soil #2 over Soil #1) is quite apparent as the emission rates are dramatically higher for the enhanced saltation over those rates for Soil #1 and Soil #2 alone.

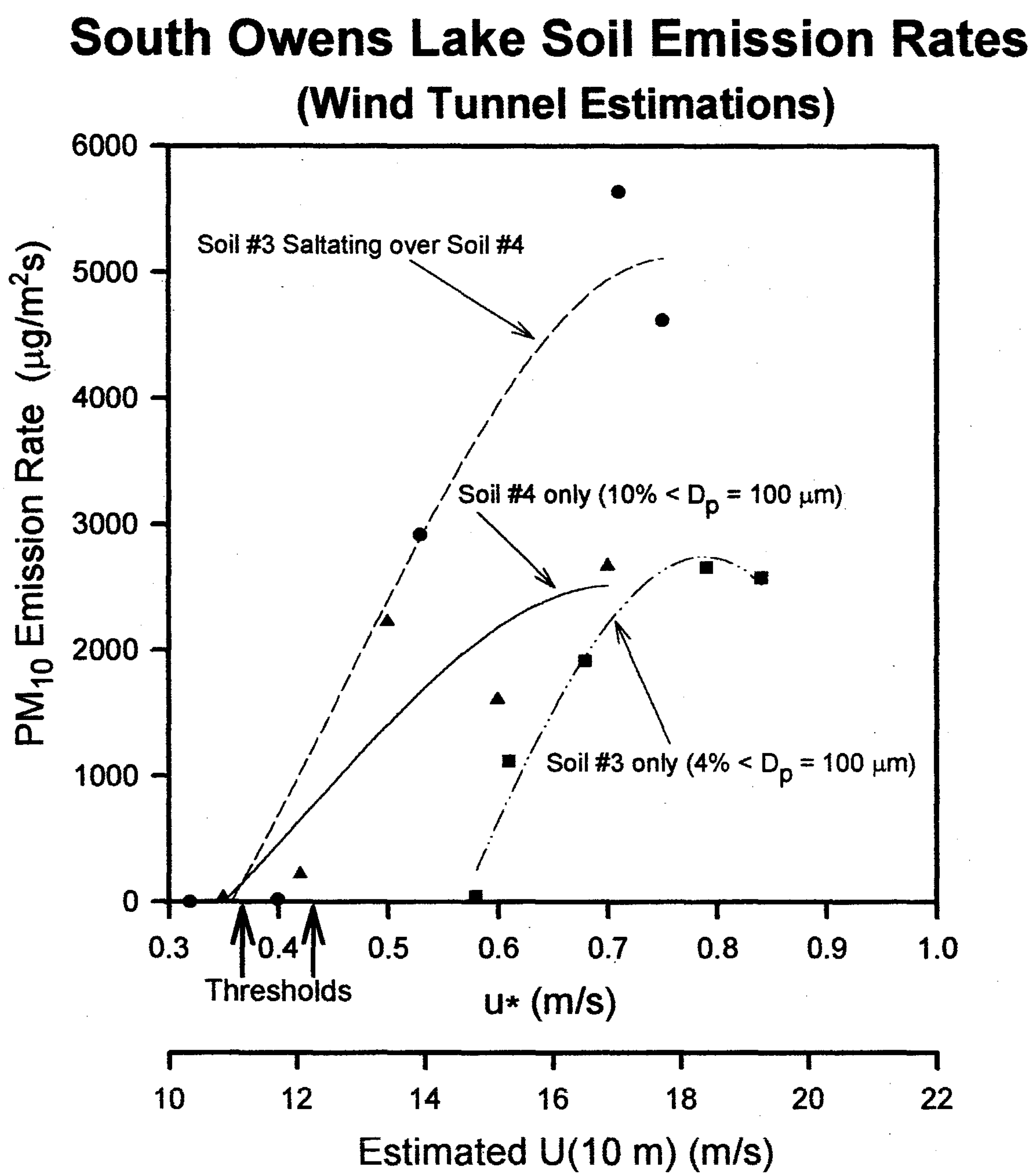

Figure 56. The PM_{10} emission rates versus the friction velocity for all the South Soils are shown above. The effect of enhanced saltation (Soil #3 over Soil #4) is quite apparent as the emission rates are dramatically higher for the enhanced saltation over those rates for Soil #3 and Soil #4 alone.

3.6. Sand Fluxes

In addition, total sand fluxes Q for the beds of sand in the loose soil emissions and for the enhanced saltation were calculated from data gathered using the sand traps with Equations (7)-(9). Profiles of the sand flux q were obtained for each case and are shown in Figures 57-60. The total sand flux calculated from these curves is shown in Figures 61 and 62. The curves are plotted versus the normalized friction velocity form given in Equation (9). Ideally, if a linear fit is made with the normalized form, a slope of 2.61 should result; however, in the study done to produce Equation (9) glass spheres of all the same diameter were used and not for a dust-type material. The slopes for a linear fit in our study range from approximately 0.4 to 0.9 which is less than the slope predicted with Equation (9). This discrepancy is likely due to the dust content in our sands—there is wide range of distribution of particle sizes and the geometry is not spherical, like the glass-sphere model. In fact, the total sand flux Q fits the normalization with a quadratic equation reasonably well. With a quadratic fit (Figures 63-64), it is quite obvious that the sand flux for both cases of enhanced saltation decreases in comparison to the sand case alone.

A likely mechanism for this result is that "sand on sand" impacts are more elastic and movement is facilitated, while "sand on soil" collisions are more plastic and impede the momentum of the particles that are moving through the soil. Another aspect of interest is that at high velocities, there is a "plateau effect", that is, the sand flux does not increase, but levels off. The sand particles probably embed themselves deeper into the soil and cease to move more often statistically.

North Sand (Soil #2) Sand Flux

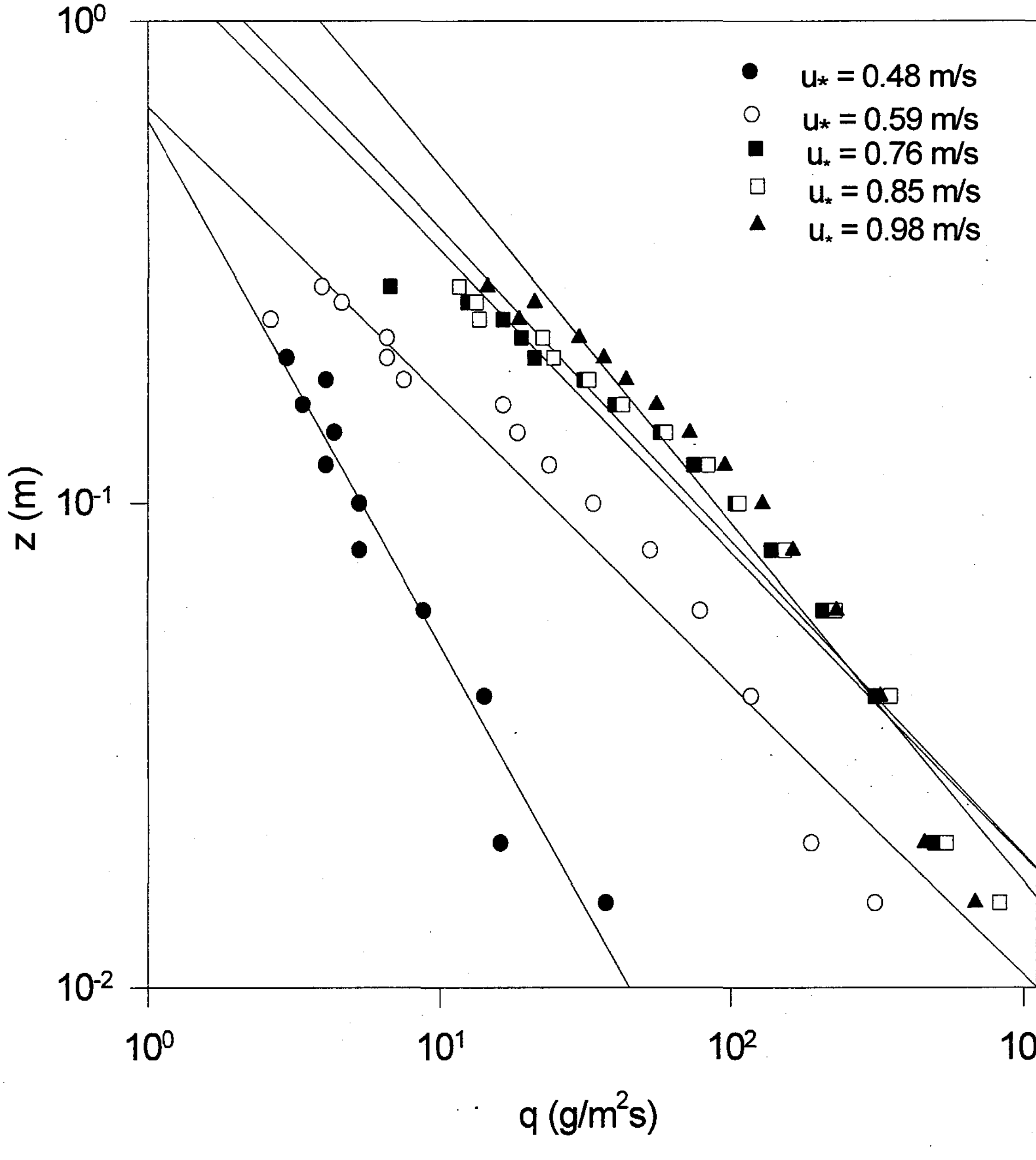

Figure 57. The sand fluxes for different friction velocities versus the height for the North Sand are shown above. The sand fluxes increase to a limit where they approach about the same value above a certain friction velocity.

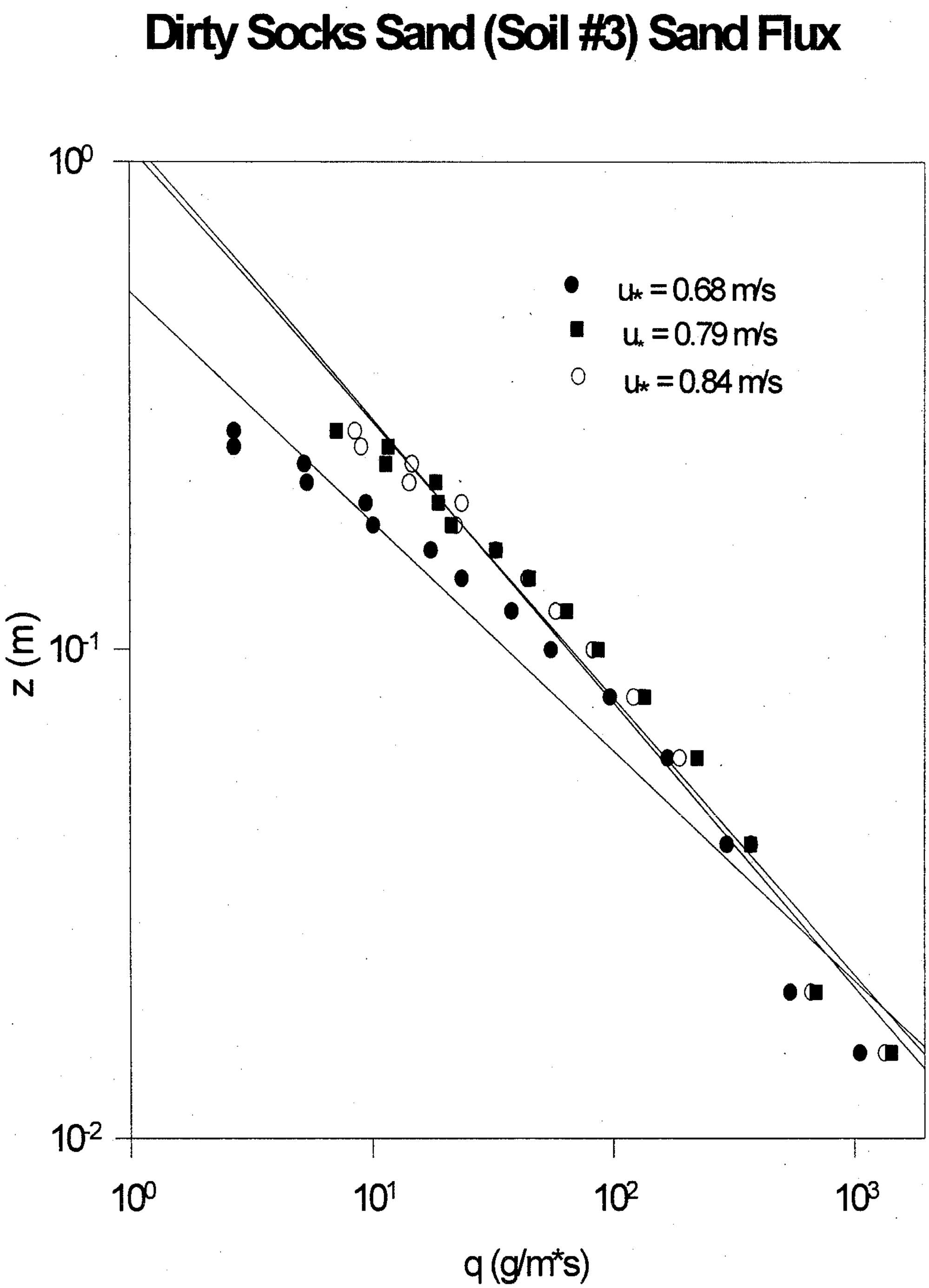

Figure 58. The sand fluxes for different friction velocities versus the height for the Dirty Socks Sand are shown above. The sand fluxes increase to a limit where they approach about the same value above a certain friction velocity.

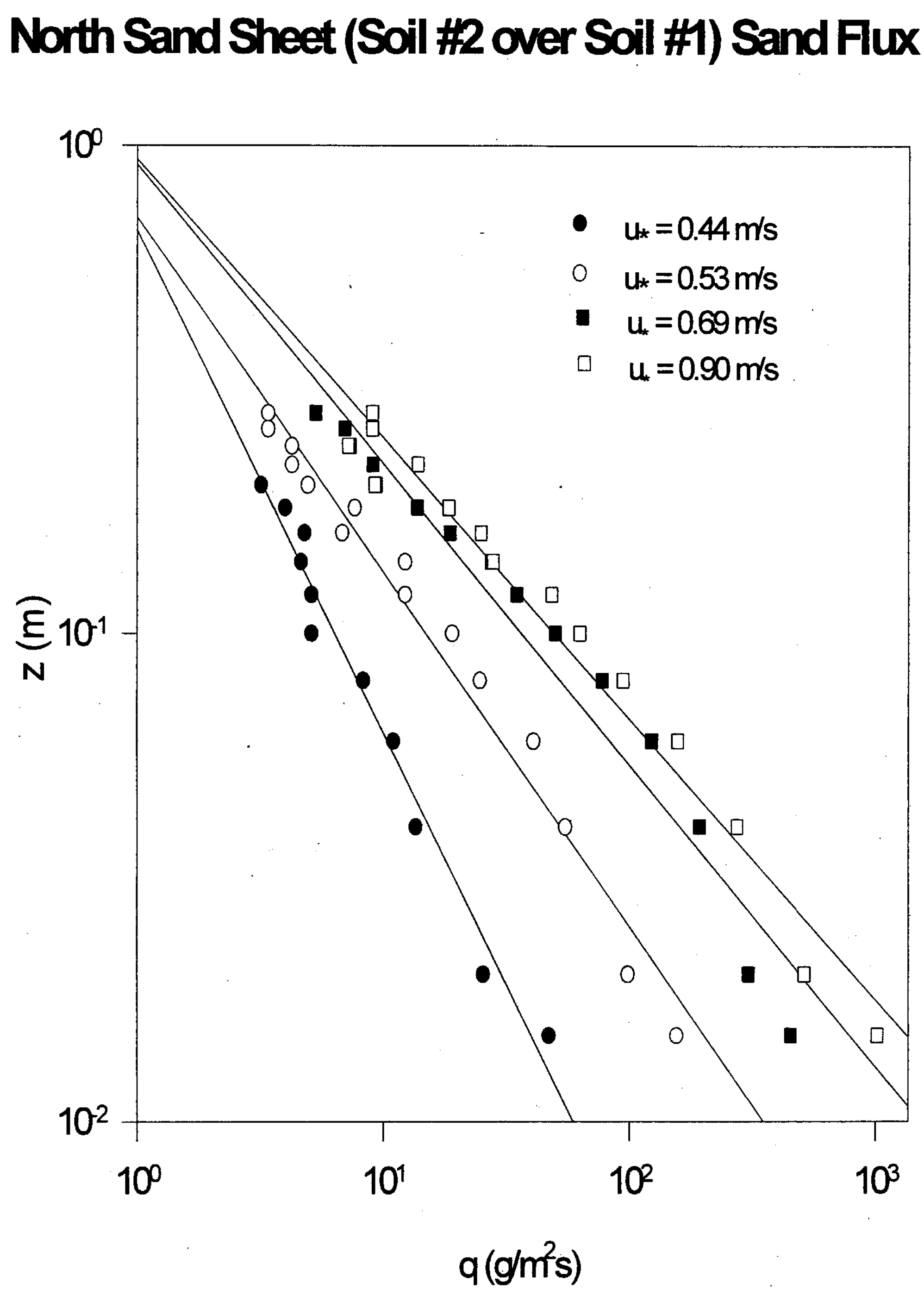

Figure 59. The sand fluxes for different friction velocities versus the height for the North Sand Sheet simulation with Soil#2 saltating over Soil #1 are shown above. The sand fluxes increase to a limit where they approach about the same value above a certain friction velocity.

South Sand Sheet (Soil #3 over Soil #4) Sand Flux

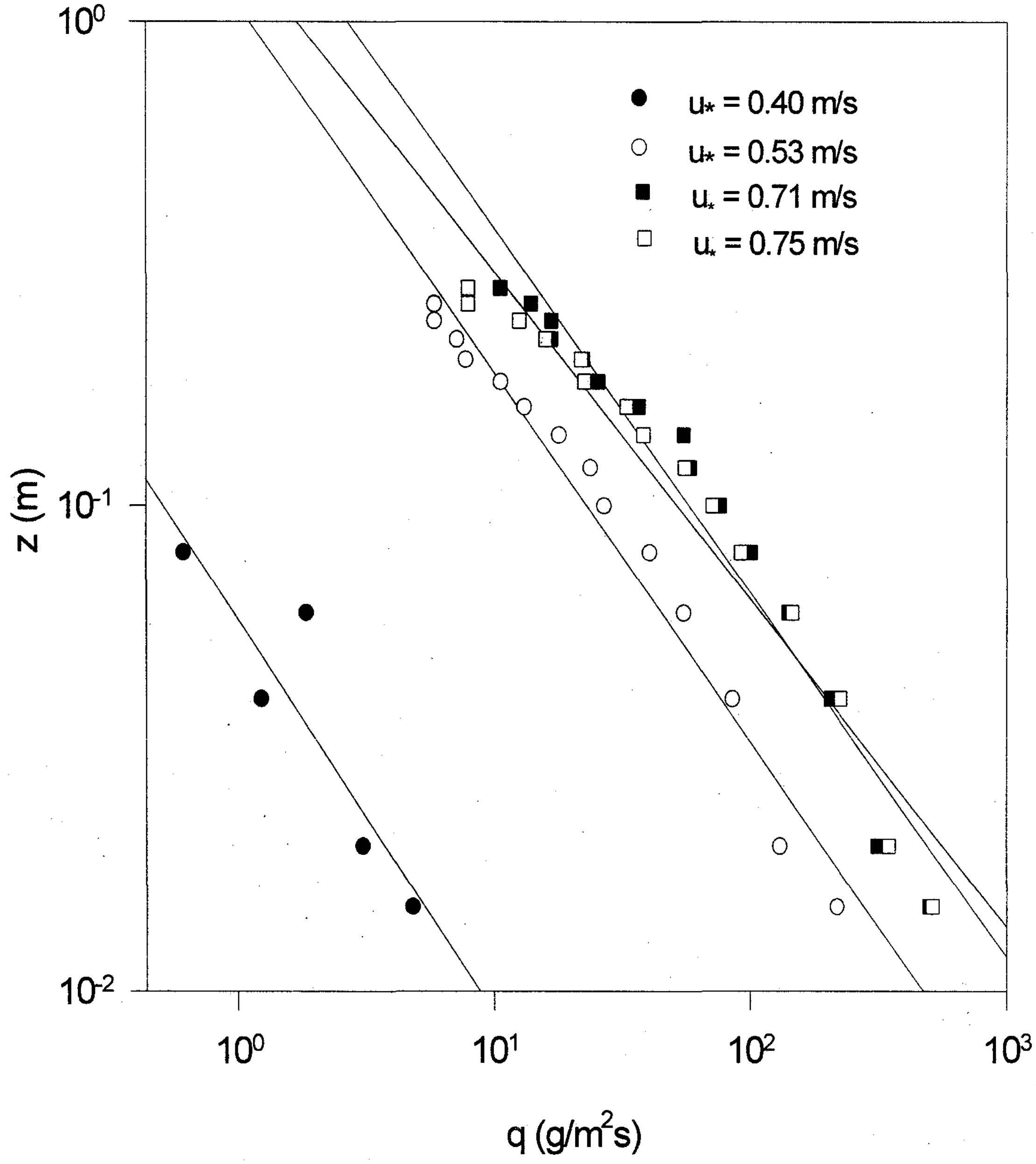

Figure 60. The sand fluxes for different friction velocities versus the height for the South Sand Sheet simulation with Soil#3 saltating over Soil #4 are shown above. The sand fluxes increase to a limit where they approach about the same value above a certain friction velocity.

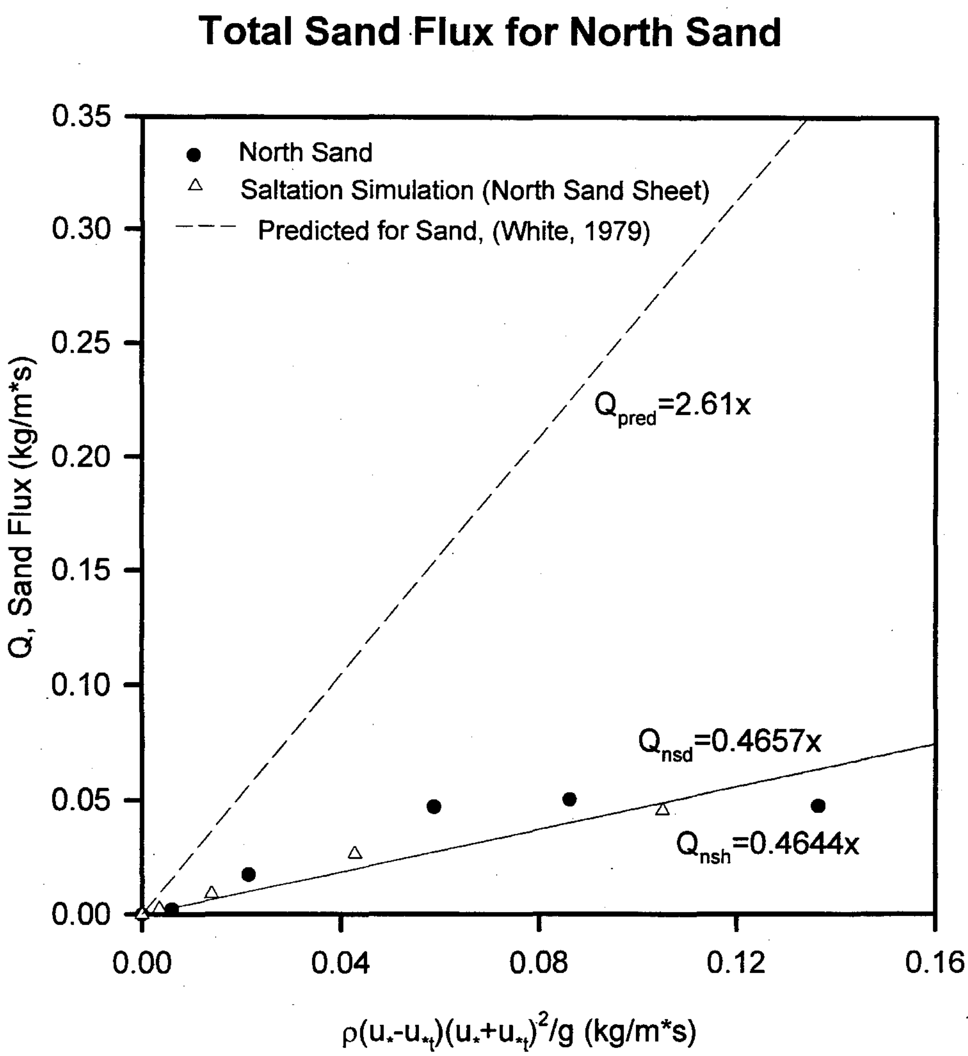

Figure 61. The total sand fluxes versus the normalized friction velocity for the North Sand Sheet simulation and the North Sand are shown above. The total sand fluxes increases with friction velocity for both cases; however, the linear coefficients are much smaller than that expected for sand only material from White, 1979 for small glass spheres.

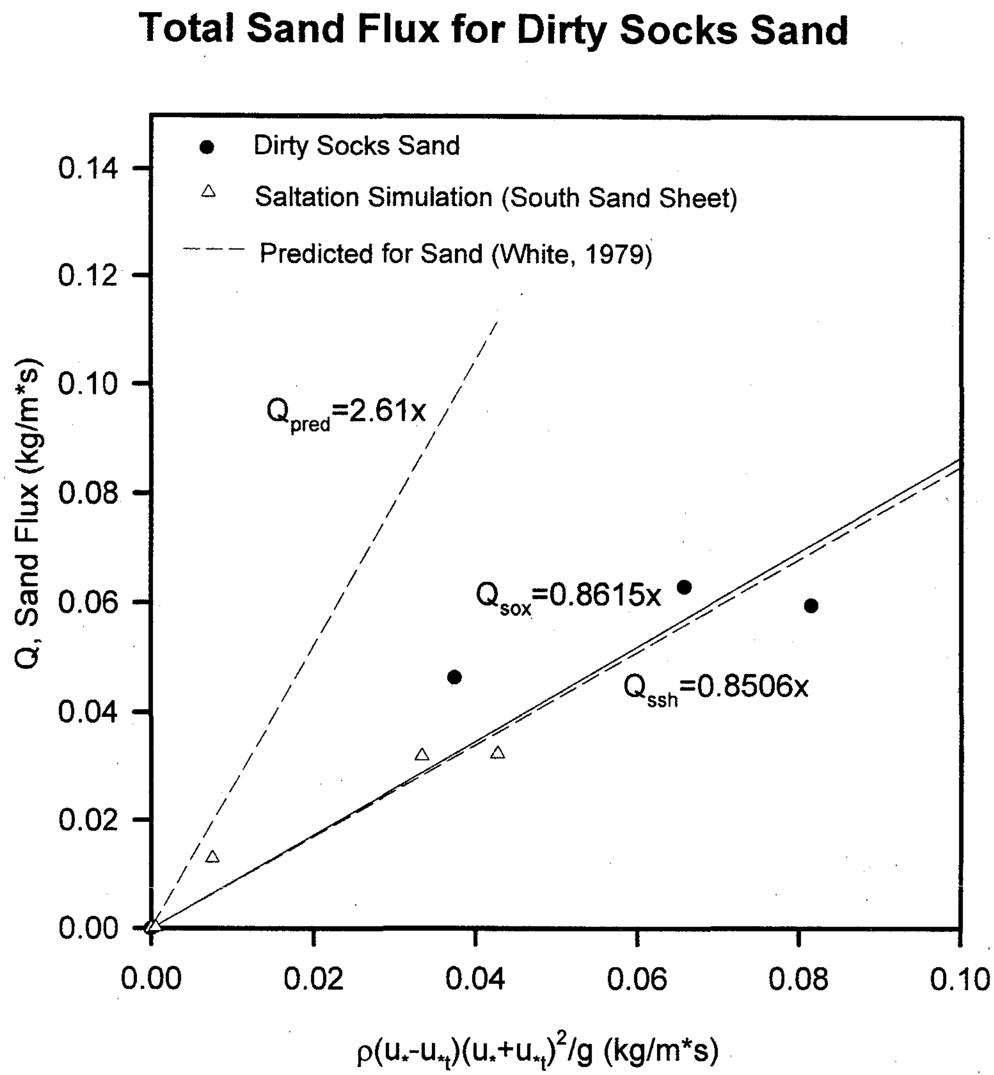

Figure 62. The total sand fluxes versus the normalized friction velocity for the South Sand Sheet simulation and the Dirty Socks Sand are shown above. The total sand fluxes increases with friction velocity for both cases; however, the linear coefficients are much smaller than that expected for sand only material from White, 1979 for small glass spheres.

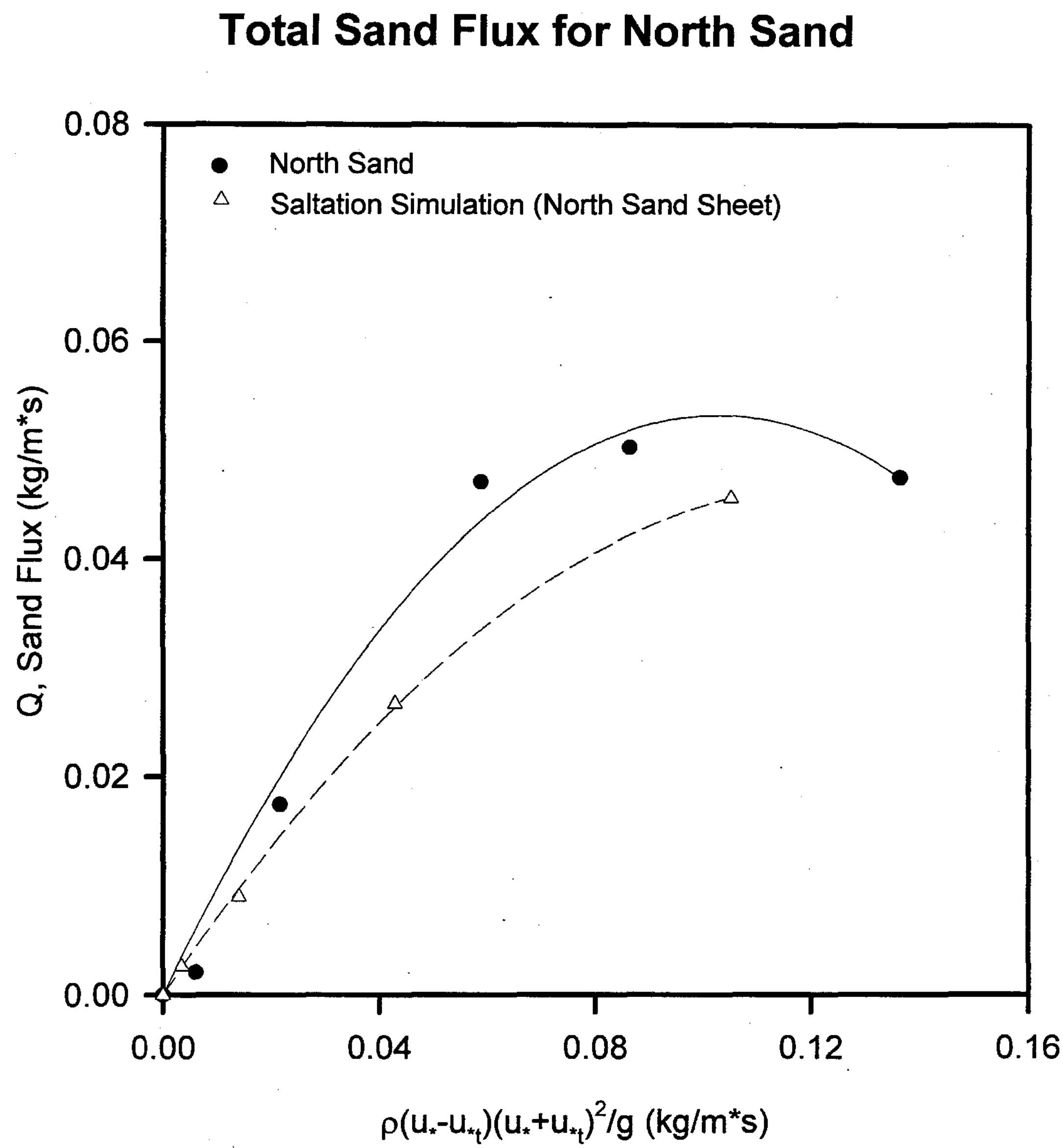

Figure 63. The total sand fluxes versus the normalized friction velocity for the North Sand Sheet simulation and the North Sand are shown above. The total sand fluxes increases with friction velocity for both cases; however, with the quadratic fit, it is apparent the total sand flux is greater for the case in which sand alone is saltating.

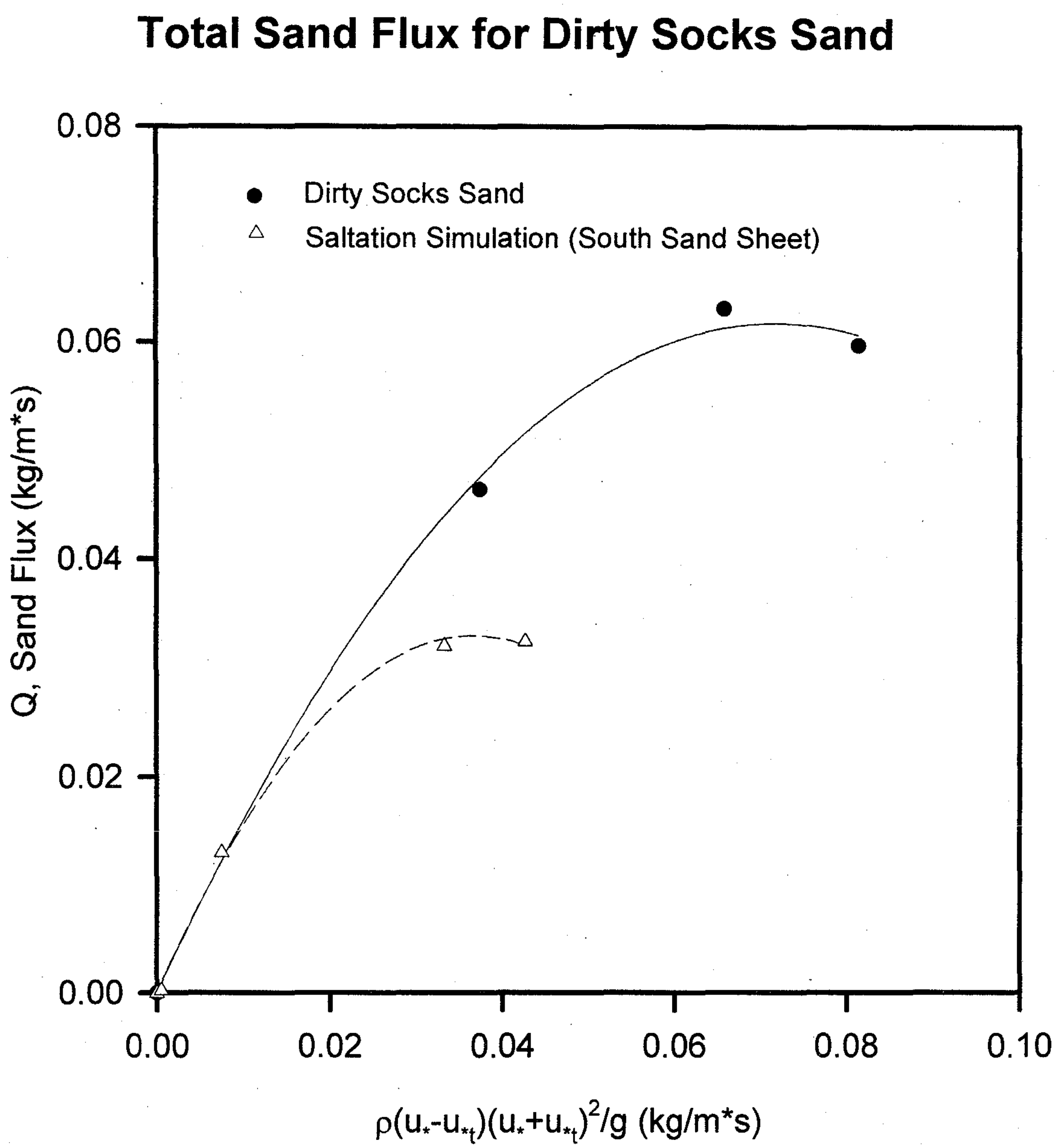

Figure 64. The total sand fluxes versus the normalized friction velocity for the South Sand Sheet simulation and the Dirty Socks Sand are shown above. The total sand fluxes increases with friction velocity for both cases; however, with the quadratic fit, it is apparent the total sand flux is greater for the case in which sand alone is saltating.

3.7. Fetch Studies

In studying the loose soil emissions, it became apparent that the emissions of soils increase over the soil bed, but not continuously at all speeds. Sometimes, equilibrium is reached between the 2.65 m and 4.38 m sampling probe at the higher speeds. The results between 2.65 m and 4.38 m probe inspired studies in which the fetch effect of the UCD Fence Soil and the Dirty Socks Sand were explored, since emission rates from these soils actually appeared to show not only equilibrium, but fall-out at the highest speeds. Initially, the UCD Fence Soil was tested by probing simultaneously between 0.6 m and 1.5 m, between 1.5 m and 2.65, and between 2.65 and 4.38 m. The velocity was recorded at each location in the tunnel and the free stream velocity maintained at a constant rate of 10.5 m/s giving approximately the same friction velocity. The velocity profiles for this test are shown in Figure 65. The slopes of the velocity profiles are reasonably constant. However, possibly due to dust loading, the free stream velocity obtained by the traversing probe earlier in the tunnel is higher than in the test section at 4.38 m, 14.0 m/s at 0.6 m compared to 10.5 m/s at 4.38 m along the bed. At a 10.5 m/s free stream velocity as measured at 4.38 m, the equilibrium state was not witnessed, but instead a steady increase in the emissions observed, Figure 66.

A more comprehensive study was then undertaken which included probing only between 0.6 m and 1.2 m and between 1.2 m and 2.65 m for many different free stream velocities and combining those results with the previously obtained values between 2.65 m and 4.38 m from the loose soil emission studies. The emission rate per unit width values were then grouped into the respective frictional velocity categories and then plotted versus fetch length x. The plots are shown in Figure 67. These curves represent a system in which emissions increase with fetch limited to the strength of the shear velocity. Once a certain shear velocity is exceeded and there is large amount of particles in the air, the system reaches a saturation or equilibrium in which fall-out and entrainment of new PM_{10} are about equal.

The question is whether this is an artifice of the wind tunnel or if this is a natural occurring phenomenon on Owens Lake dependent on the soil type. To answer this question it is important to look at the other fetch studies conducted. For the Dirty Socks Sand, the probes were placed between 0.6 m and 1.2 m and compared with the 2.65 m and 4.38 m values for the loose soil emissions (Figure 68). Likewise, the other four cases, North Sand, Old Pipe Line and the North Sand Sheet and South Sheet were plotted versus their fetch for 2.65 m and 4.38 m (Figures 69-72). For the individual soils without enhanced saltation, all curves show the same trend with tunnel saturation at the highest friction velocities and a transition to this equilibrium state. However, the point at which saturation equilibrium occurs is not directly related to how much PM_{10} is in the air as one observes higher levels of PM_{10} in the Pipe Line Soil. For the Pipe Line Soil the transition from increasing concentration across the bed to a "plateau" occurs between approximately 10 mg/m*s and 38 mg/m*s at 2.65 m; for the UCD Fence Soil it occurs between 3 mg/m*s and 7 mg/m*s at 2.65; for the North Sand it occurs between 3 mg/m*s and 4.5 mg/m*s at 2.65 m; and for the Dirty Socks Sand it occurs between 2 mg/m*s and 9 mg/m*s. Likewise, for the combined cases, there does not appear to be the implication of saturation.

A relevant experiment to consider is the South Sand Sheet Simulation. The Dirty Socks Sand and the UCD Fence Soil according to the loose soil emission studies have similar amounts of PM_{10}; however, no signs of saturation in the combined study are observed. Saturation would likely occur if this result simply depended on too many particles in the air in the confined wind tunnel space. More likely, these saturation points result directly from the dynamics of the near surface where entrainment and fall-out become equal due to the large loading of particles near the surface. Each soil and study has slightly different dynamical considerations, and thus, different saturation points are obtained. In most of these studies, the boundary layer of concentration is growing and we still see greater values at the higher heights downstream, but near the surface a smaller amount of concentration is observed, thus forming a crossing of the concentration curves as in Figure 73. In all, the fetch becomes a dynamical consideration in predicting how emissive soil surfaces should be treated; as point sources, continuous sources, or recurring continuous sources.

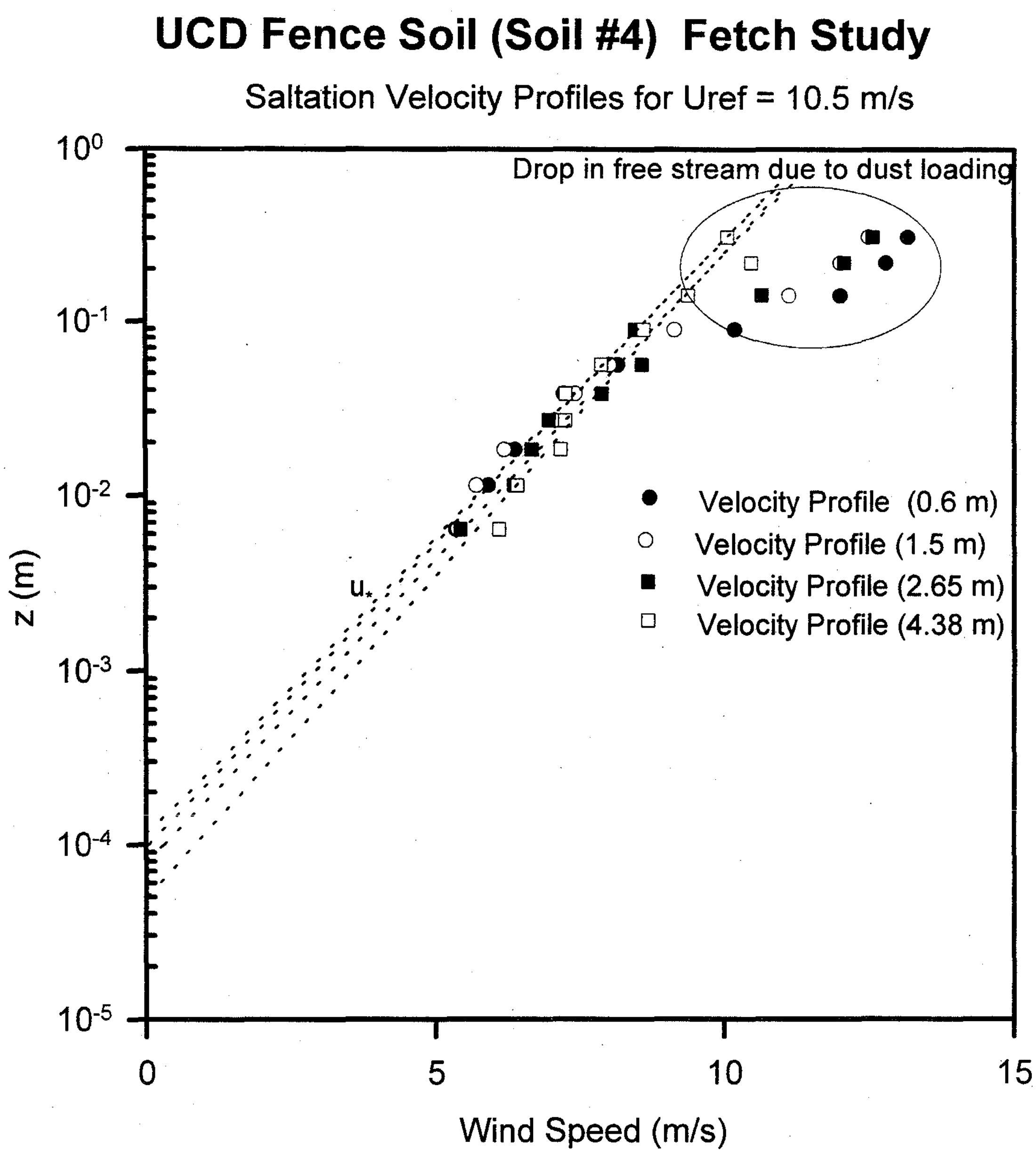

Figure 65. The velocity profiles for the initial UCD Fence Soil fetch study in which sets of different locations in the tunnel were tested as indicated on the plot at approximately the same free stream velocity. In addition, in this study, the possibility of dust loading effecting the free stream is observed as the free stream drops continuously down the tunnel.

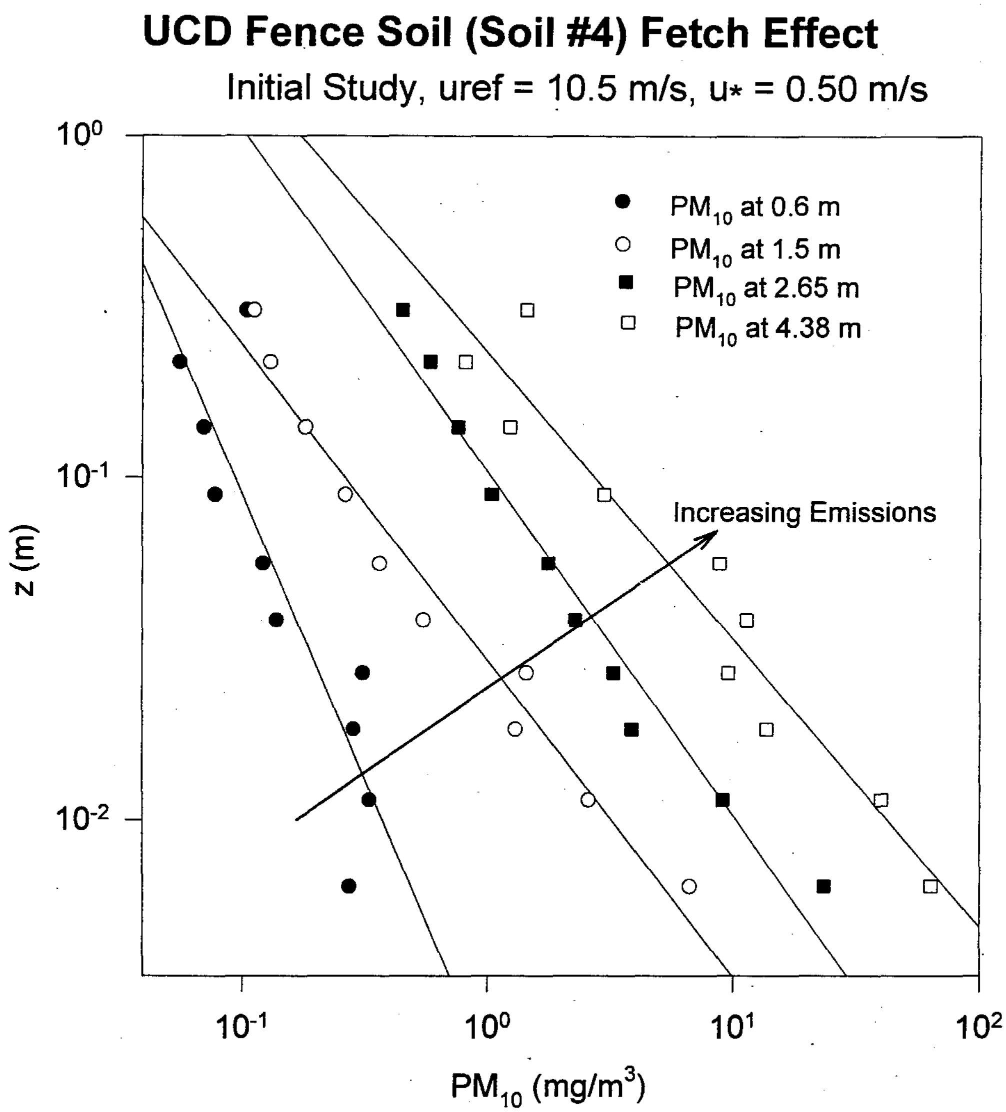

Figure 66. The PM_{10} Concentration profiles for Soil #4 for uref =10.5 m/s for fetch distances of 0.6 m, 1.5 m, 2.65 m and the 4.38 m distance. In this case, the concentration levels increase throughout the length of the tunnel and equilibrium is not reached.

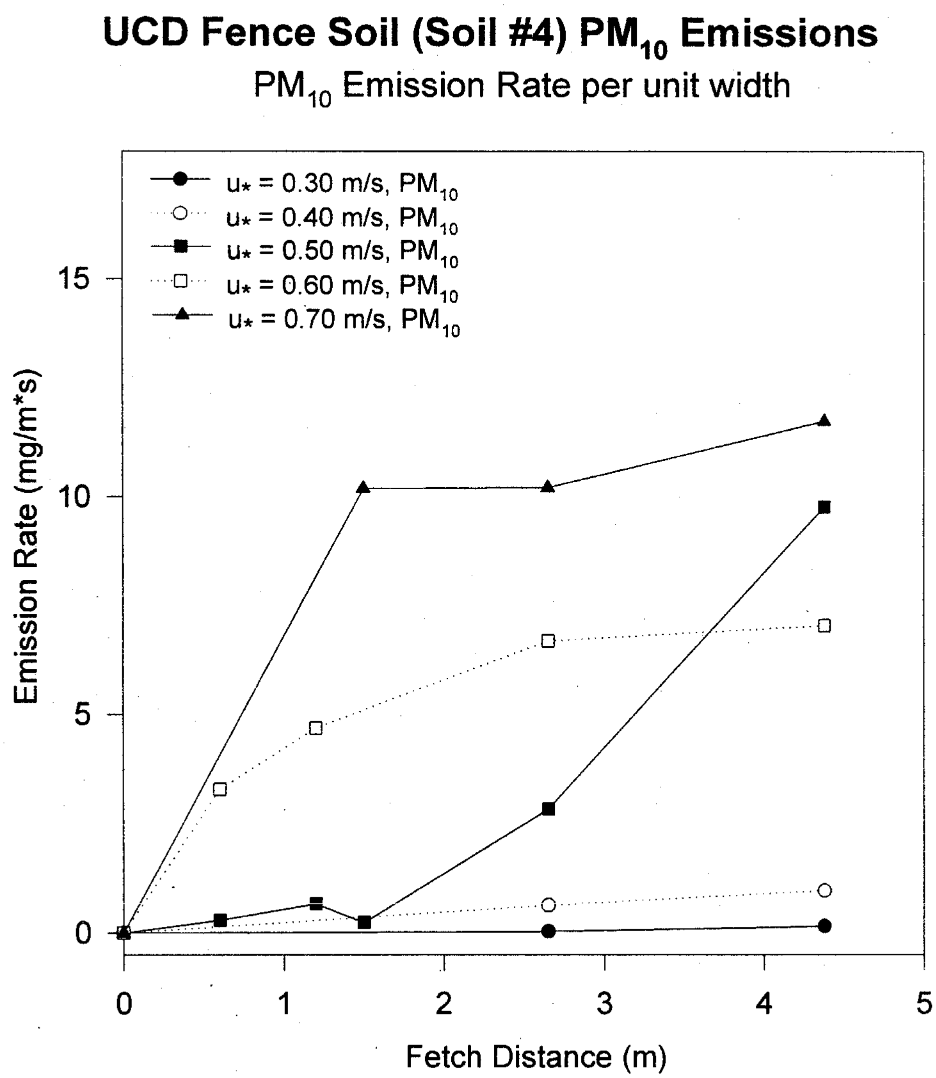

Figure 67. The PM_{10} emission rates per unit width for the UCD Fence Soil along the soil fetch are shown above for different friction velocities. There is a distinct friction velocity at which there is a transition from continuously increasing emissions to an equilibrium state. Above this transition, in the equilibrium range, there is the possibility of fall-out as well.

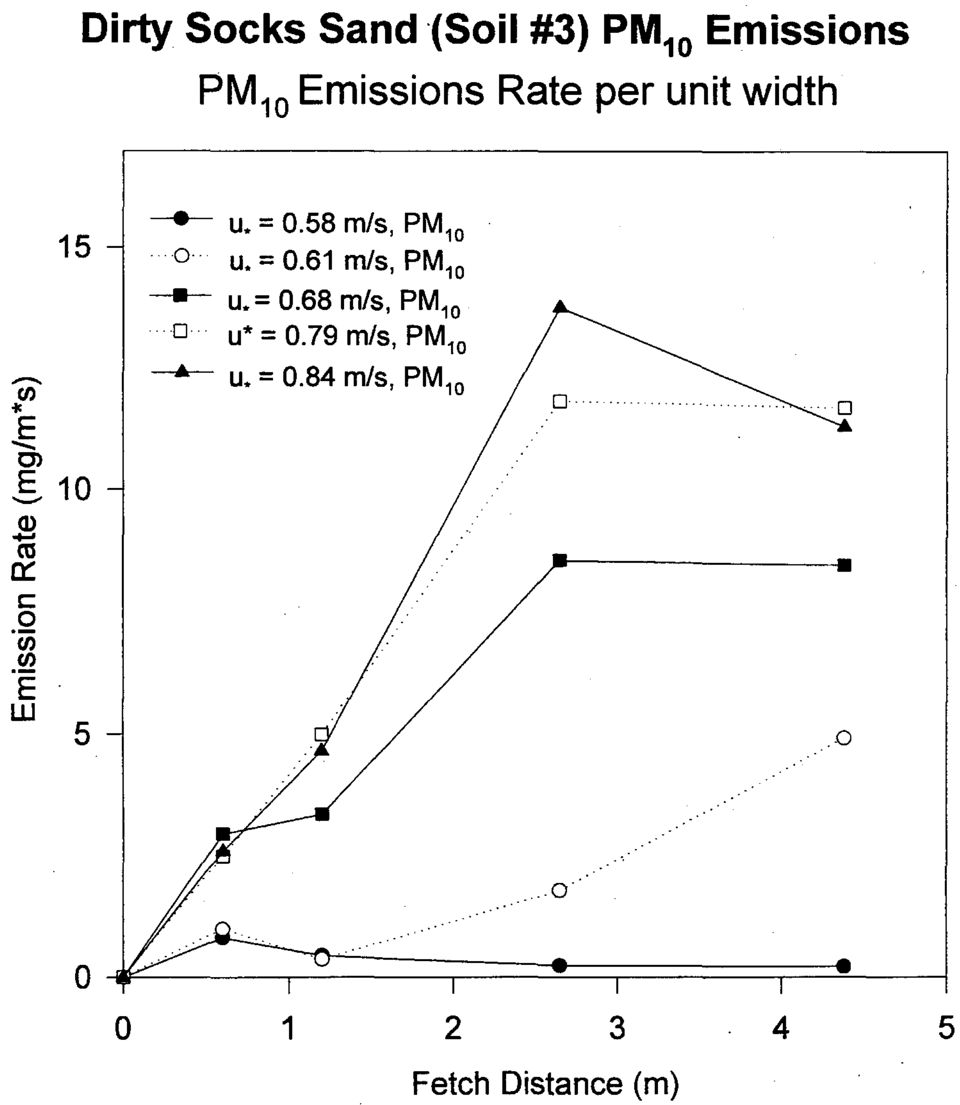

Figure 68. The PM_{10} emission rates per unit width for the Dirty Socks Sand along the soil fetch are shown above for different friction velocities. There is a distinct friction velocity at which there is a transition from continuously increasing emissions to an equilibrium state. Above this transition, in the equilibrium range, there is the possibility of fall-out as well.

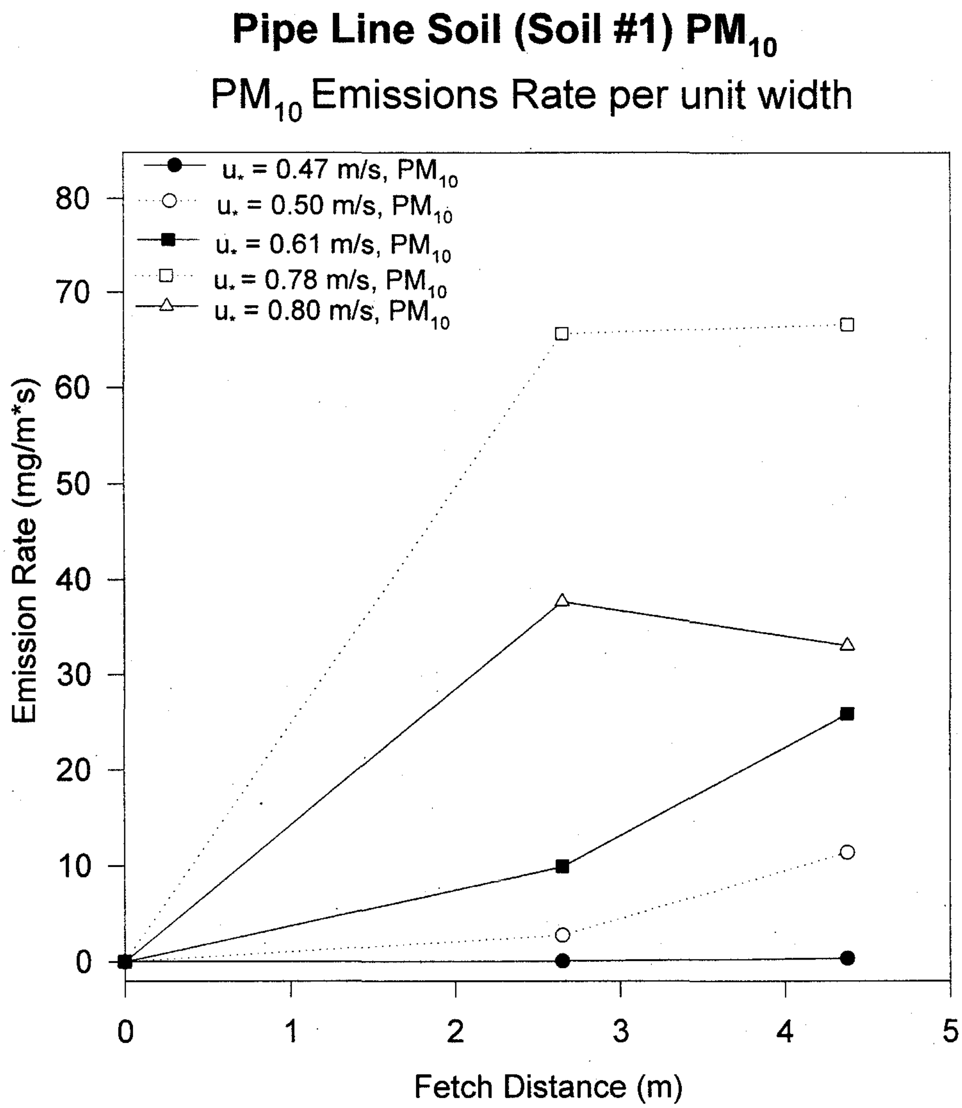

Figure 69. The PM_{10} emission rates per unit width for the Pipe Line Soil along the soil fetch are shown above for different friction velocities. There is a distinct friction velocity at which there is a transition from continuously increasing emissions to an equilibrium state. Above this transition, in the equilibrium range, there is the possibility of fall-out as well.

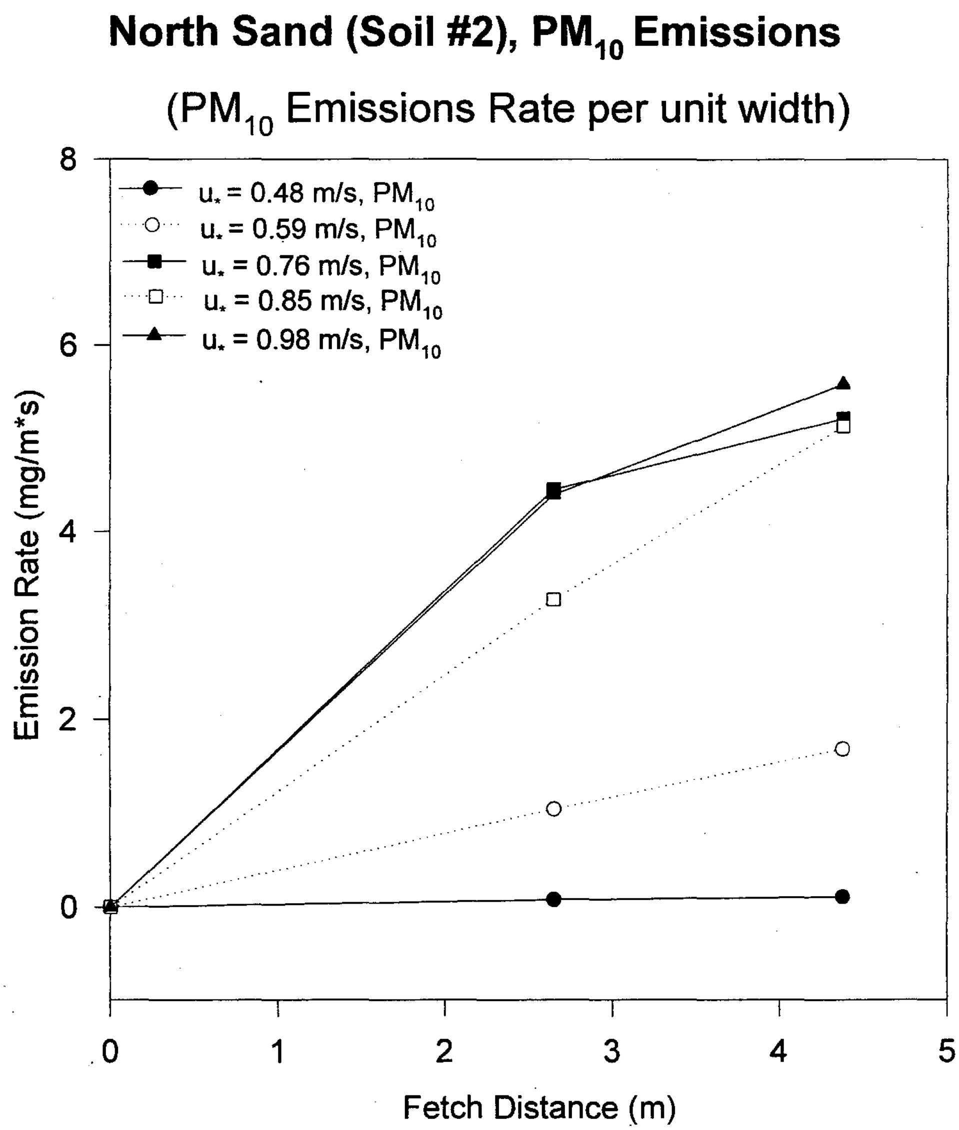

Figure 70. The PM_{10} emission rates per unit width for the North Sand along the soil fetch are shown above for different friction velocities. There is a distinct friction velocity at which there is a transition from continuously increasing emissions to an equilibrium state. Above this transition, in the equilibrium range, there is the possibility of fall-out as well.

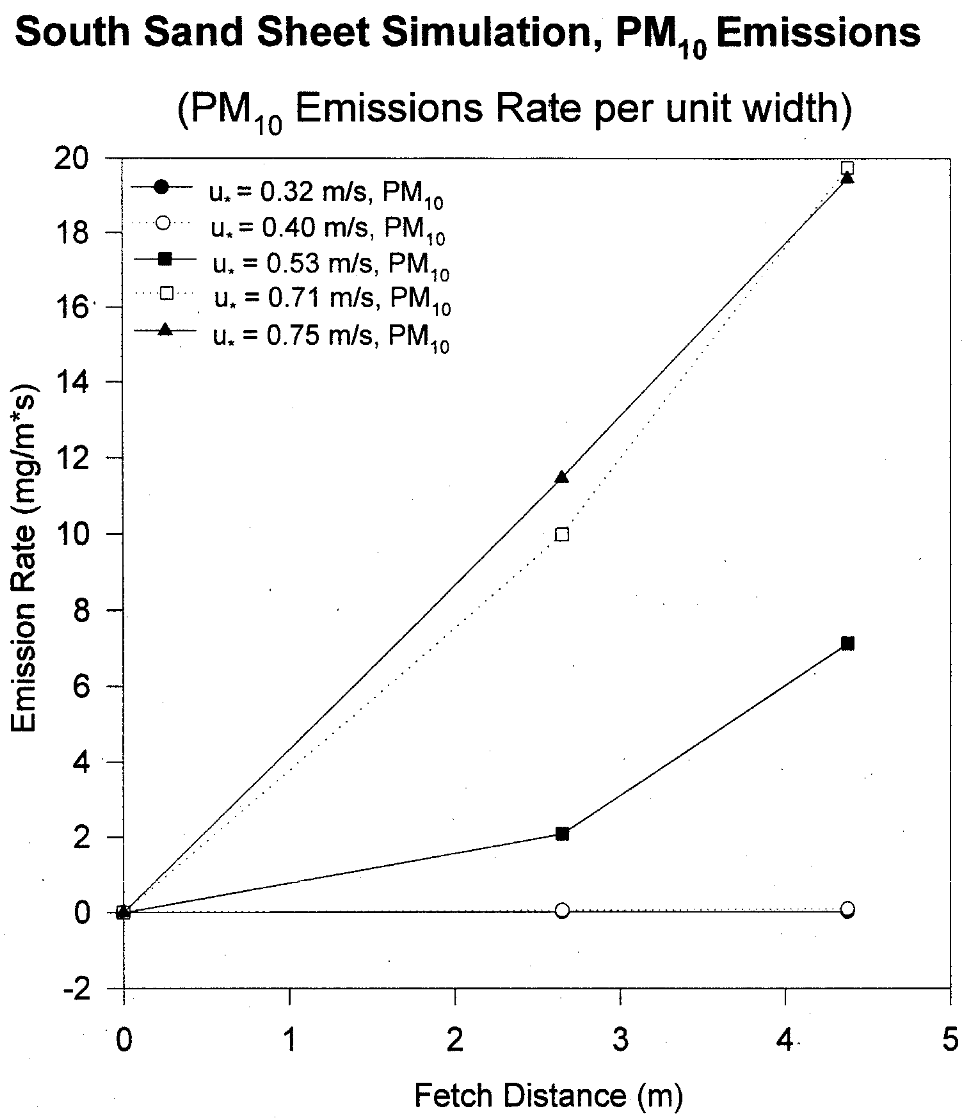

Figure 71. The PM_{10} emission rates per unit width for the South Sand Sheet Simulation along the soil fetch are shown above for different friction velocities. There is not a distinct friction velocity at which there is a transition from continuously increasing emissions to an equilibrium state. Instead, emissions continually increase in the tunnel for all friction velocities due to the enhancement of saltation on emissions.

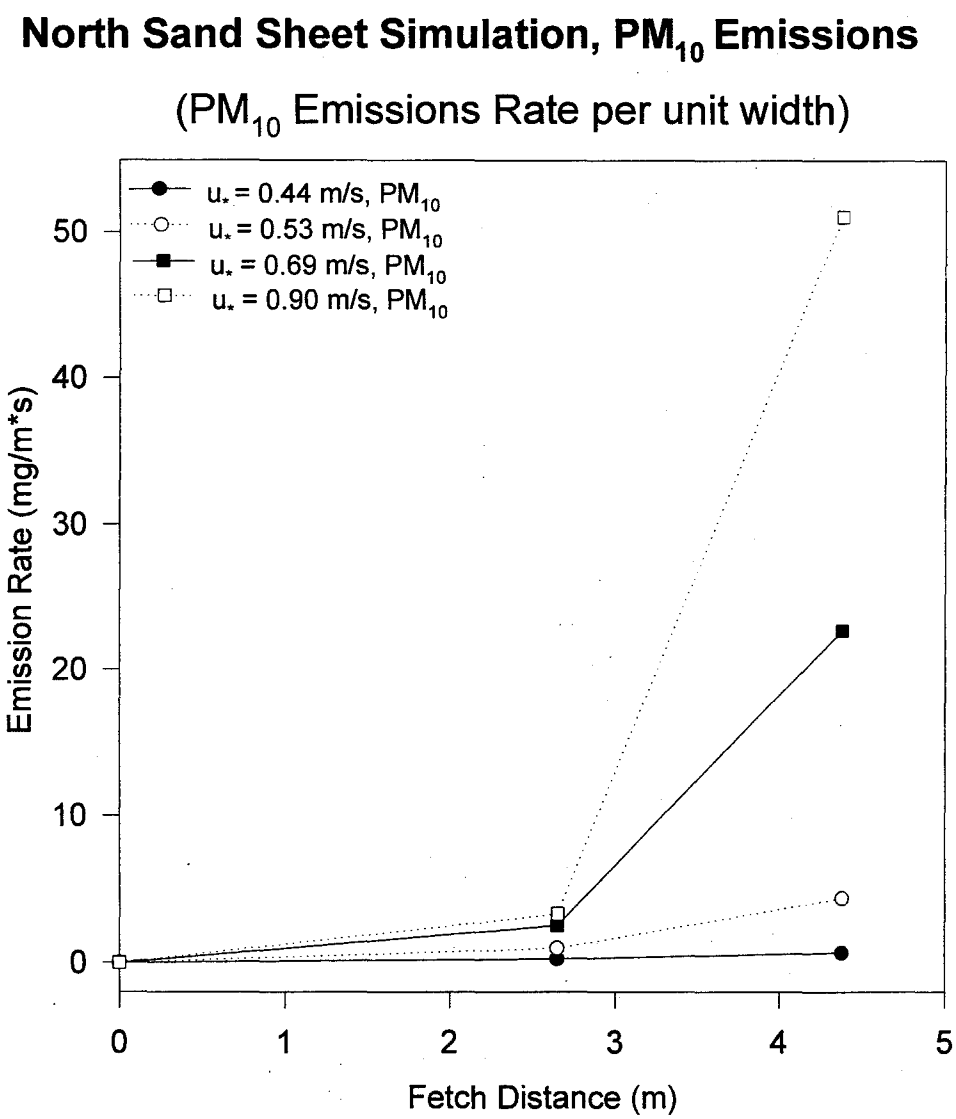

Figure 72. The PM_{10} emission rates per unit width for the North Sand Sheet Simulation along the soil fetch are shown above for different friction velocities. There is not a distinct friction velocity at which there is a transition from continuously increasing emissions to an equilibrium state. Instead, emissions continually increase in the tunnel for all friction velocities due to the enhancement of saltation on emissions.

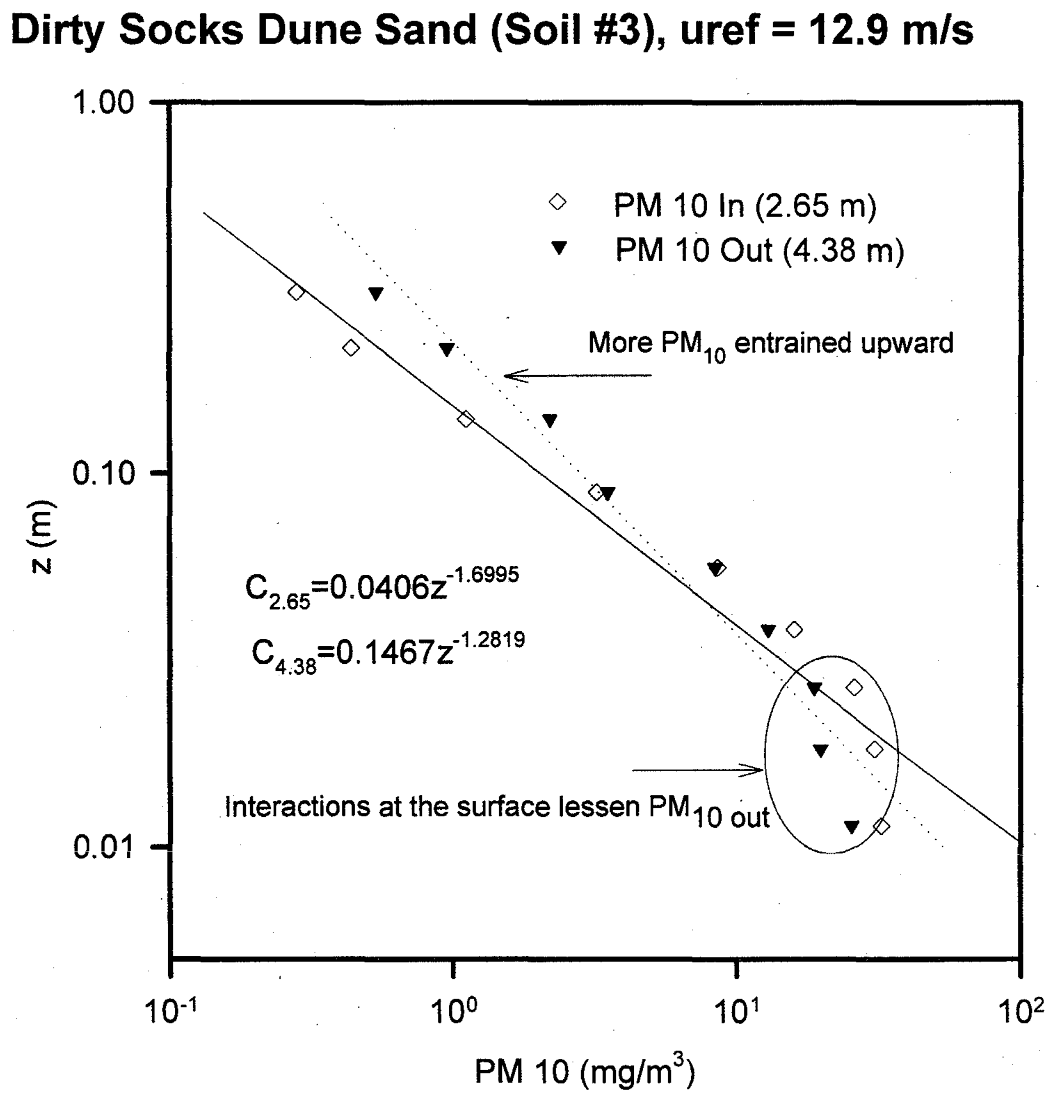

Figure 73. The PM_{10} Concentration profiles for Soil #3 at uref = 12.9 m/s for both the 2.65 m fetch and the 4.38 m fetch distance. These profiles were obtained simultaneously and correlate in time exactly. In this case, there is a gain in the concentration levels for the higher heights, however, a loss at the lower heights due to the interaction of PM_{10} at the surface.

3.8. Moisture Content Studies

The moisture content studies were performed for the UCD Fence Soil and Pipe Line Soil. The amount of residual moisture of the air dried UCD Fence Soil was around 13-16% corresponding well with the moisture content obtained by Wallace laboratories. The moisture content then was varied from 16% to about 25.5 % with the velocity and friction velocity held constant at one of the highest shear rates previously investigated (about 0.70 m/s) for the loose soil emissions. The constancy of the shear velocity is shown in Figures 74 and 75. As expected, increasing moisture content has a dramatic effect on the emission rates; the emission rates with respect to moisture content for the UCD Fence Soil are plotted in Figure 76 and shown in Table 6. Likewise, the Pipe Line Soil in its air dried state contained 3.9% residual moisture content and then was tested in a range of 3.9% to 9.8% moisture content at a constant velocity and shear velocity (around 0.60 m/s). Again, a similar trend is shown in a plot of emission rates versus moisture content for the Pipe Line Soil (Figure 76 and Table 6). The increased moisture becomes attached to the small particulate keeping it from becoming a source of airborne PM_{10}. As the moisture content increases more and more small particles are bonded to the moisture until saturation is reached in which no PM_{10} is available for emissions. This is the trend shown in the plots; a 10% increase in moisture content above the air dried value results in, approximately, an order of magnitude difference in the emission rates. If moisture can effectively be introduced at Owens Lake at a constant rate, it is viable that it can act as a mechanism to decrease emissions.

Table 6. Emission Rates for the Moisture Content Studies for Soil #1 and Soil #4.

Designation	Description	%Moist. Content	u_* (m/s)	uref (m/s)	u(10 m) (m/s)	E (PM_{10}) ($\mu g/m^2 s$)
Soil # 1	Old Pipe Line	3.9	0.61	10.6	15.4	5920
Soil # 1	Old Pipe Line	5.8	0.65	10.7	16.5	1880
Soil # 1	Old Pipe Line	7.6	0.60	10.7	15.9	755
Soil # 1	Old Pipe Line	9.8	0.58	10.9	15.8	481
Soil # 4	UCD Fence Soil	14.5	0.71	13.0	19.4	3690
Soil # 4	UCD Fence Soil	19.0	0.69	12.6	18.8	2500
Soil # 4	UCD Fence Soil	19.5	0.65	12.5	18.1	1140
Soil # 4	UCD Fence Soil	22.5	0.70	12.7	18.4	919
Soil # 4	UCD Fence Soil	25.5	0.69	13.2	18.4	251

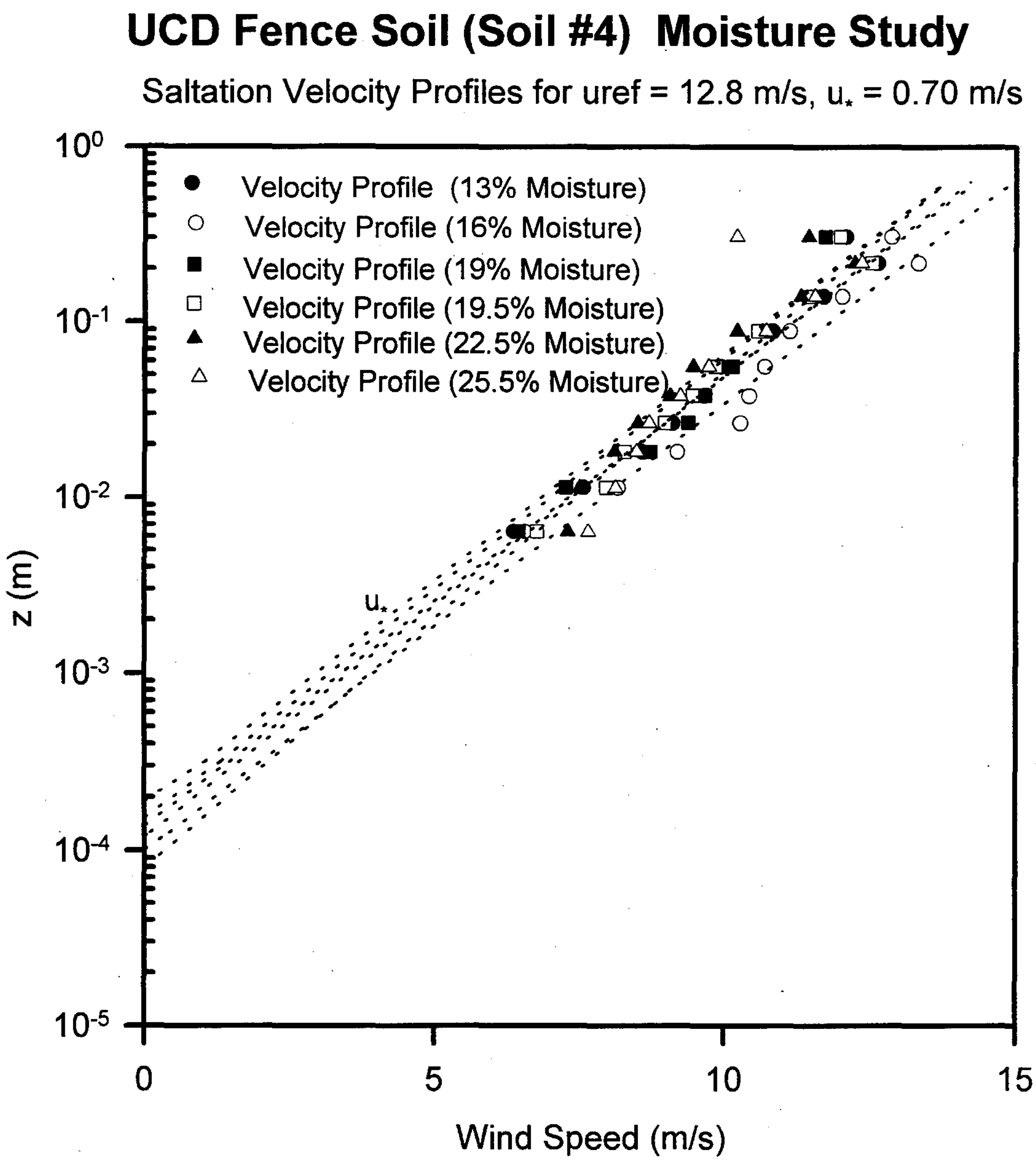

Figure 74. The velocity profiles for the UCD Fence Soil moisture study in which sets of different moisture contents were tested as indicated on the plot at approximately the same free stream velocity.

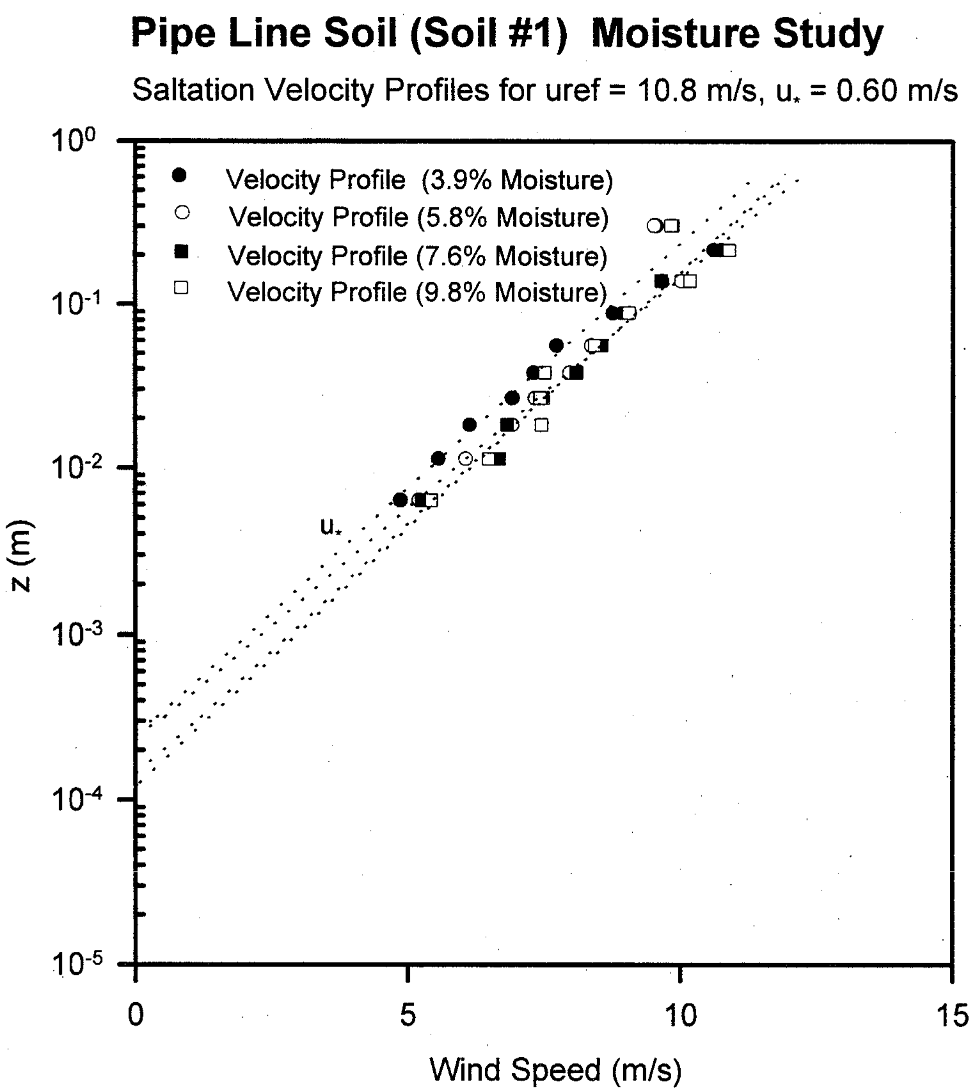

Figure 75. The velocity profiles for the Pipe Line Soil moisture study in which sets of different moisture contents were tested as indicated on the plot at approximately the same free stream velocity.

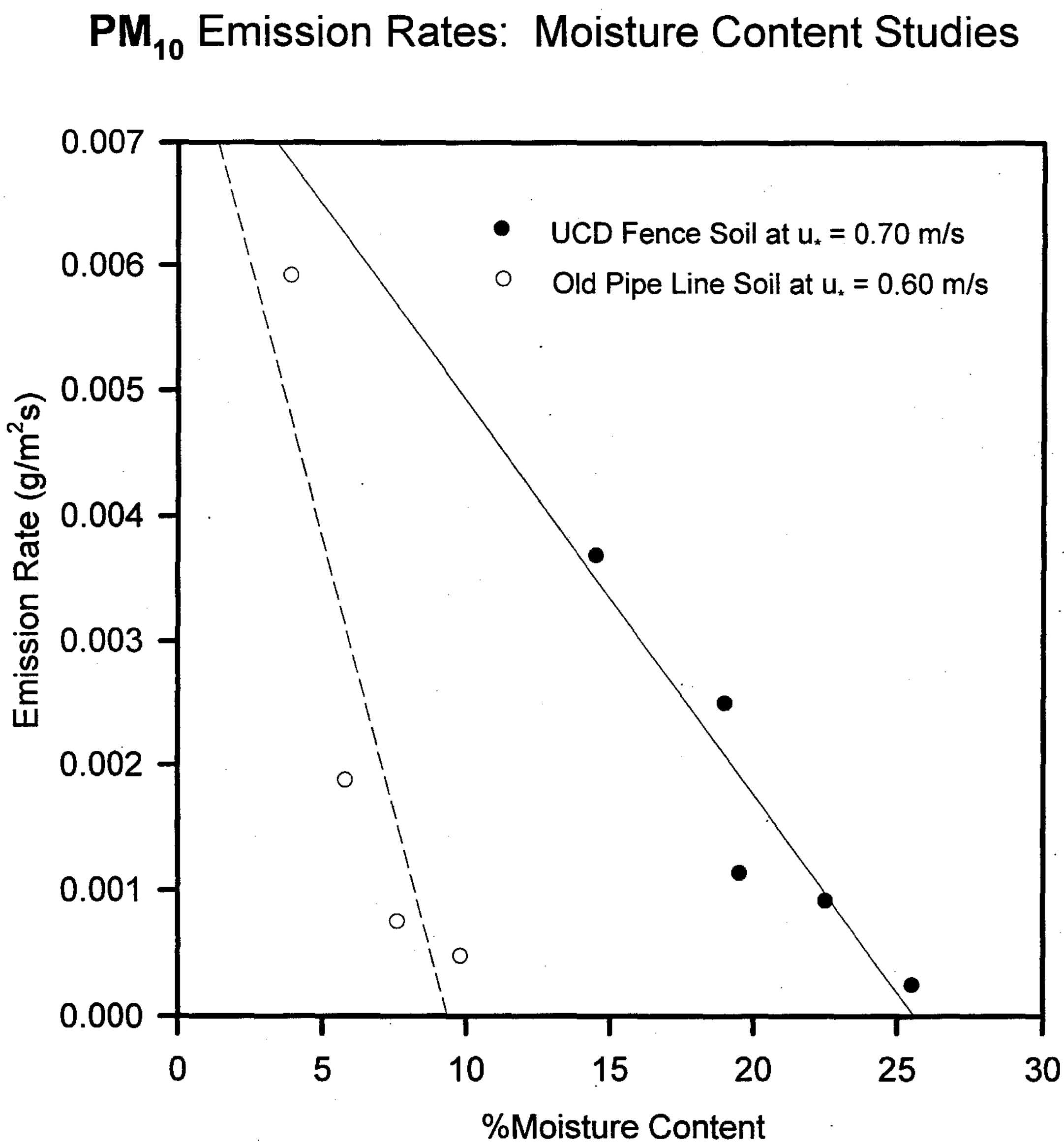

Figure 76. The emission rates versus the %Moisture Content for the moisture study in which different moisture contents were tested at approximately the same free stream velocity or friction velocity. The constant friction velocity gives high emissions for the initial air-dried soil; thereafter, with increasing moisture content a sharp decline in emissions is seen for both soils.

3.9. $PM_{2.5}$ Studies

In lieu of the new emission standards set by the EPA, some limited $PM_{2.5}$ tests were performed on the soils found to be most emissive in the current tests, specifically, the UCD Fence Soil and the Old Pipe Line Soil. The test procedure repeated is for loose soil emissions. The analysis is the same and the emission rates are shown in Table 7.

Table 7. Emission Rates for $PM_{2.5}$ for Soil #1 and Soil #4.

Designation	Description	u_* (m/s)	uref (m/s)	u(10 m) (m/s)	E ($PM_{2.5}$) ($\mu g/m^2 s$)
Soil # 1	Old Pipe Line	0.44	9.0	11.9	62.1
Soil # 1	Old Pipe Line	0.52	10.0	13.6	427
Soil # 1	Old Pipe Line	0.86	11.3	18.3	2670
Soil # 1	Old Pipe Line	0.99	12.4	20.9	5550
Soil # 4	UCD Fence Soil	0.36	8.1	10.3	3.10
Soil # 4	UCD Fence Soil	0.47	10.2	13.7	36.3
Soil # 4	UCD Fence Soil	0.57	11.9	15.2	110
Soil # 4	UCD Fence Soil	0.68	13.1	18.6	667

The $PM_{2.5}$ emission rates for the Old Pipe Line Soil are much larger than the emission rates for the UCD Fence Soil and both are large. A ratio of the percentage of $PM_{2.5}$ to PM_{10} for the same friction velocities are shown in Figures 77 and 78. The ratio is always less than one, as expected, since everything that is $PM_{2.5}$ should be measured as PM_{10}. With increasing friction velocity the ratio between the two increases steadily due to the fact that small agglomerations are abraded into smaller and smaller particles with the increased movement of the bed—particles which would have been PM_{10} are released as $PM_{2.5}$ size particles. In all, the calculated rates indicate that $PM_{2.5}$ levels will likely far exceed the EPA standards on strong wind days.

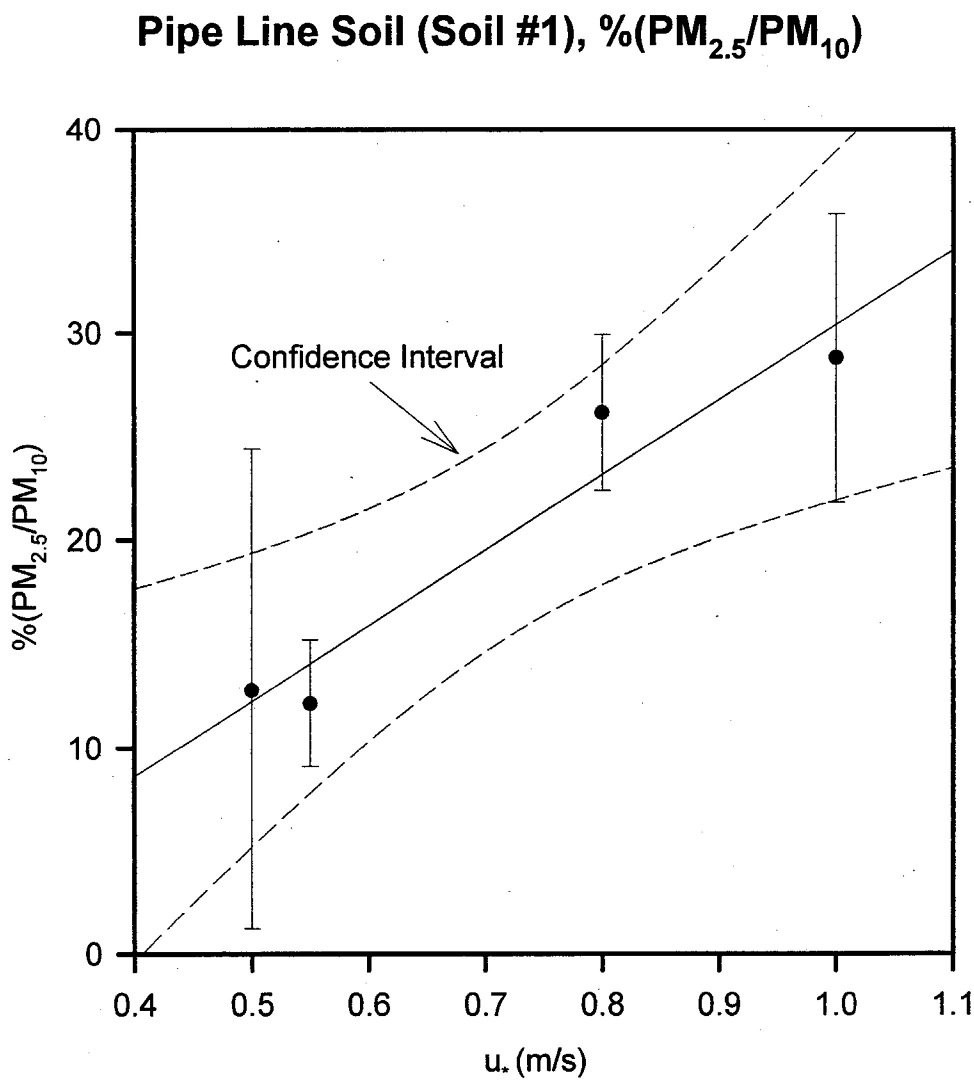

Figure 77. The %($PM_{2.5}$/PM_{10}) versus the friction velocity. The percentage slowly rises with greater friction velocity (shear stress) indicating the smaller particles are being abraded into even smaller particles.

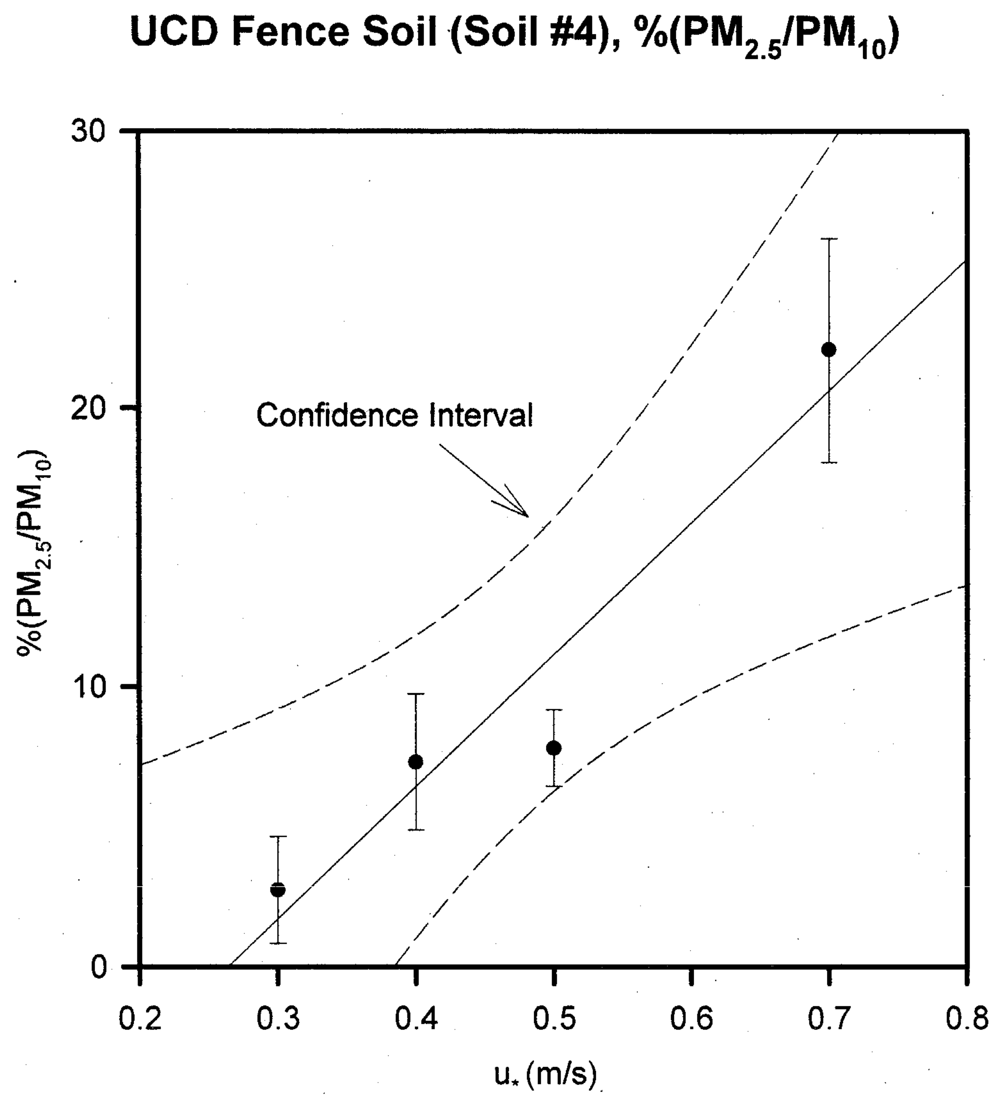

Figure 78. The %($PM_{2.5}$/PM_{10}) versus the friction velocity. The percentage dramatically rises with greater friction velocity (shear stress) indicating the smaller particles are being abraded into even smaller particles.

3.10. Crust Studies

Experimentally, one of the more difficult studies on surface variability involved developing a crust. Both qualitative and quantitative information was obtained in this study. Small scale crusts were developed with evident efflorescent salt crusts. The cycle of saturating and drying resulted in a large hard crust from the UCD Fence soil that was tested in the wind tunnel (Figure 26.). The procedure for testing is mentioned in the previous sections. The emissions from the crust alone for different shear velocities were tested. The concentration levels show very little emissions; however, there is a critical point at which the emissions jump slightly, but are inconsequential in comparison to the Loose Soil Emissions (Figure 79). At about uref = 5 m/s, at a probe height of 0.013 m the concentrations begin to increase; however, emissions do not increase at the 0.22 m height until about uref = 9 m/s indicating vertical transport is weak. The crust did not break for any of these tests. The two point velocity profiles were used to obtain law of the wall fits and an estimation of the surface roughness (Figure 80). The crust z_0 is much larger than the loose soils and is around 7.9×10^{-5} m.

Next, a bed of Dirty Socks Sand was placed behind the crust to provide saltating sand particles to scour the surface. Again, the two probes were set-up at 4.38 m in the test bed and at heights of 0.013 m and 0.22 m. In addition, a bed of Dirty Socks Sand with no crust in front of the bed was tested first to obtain a background amount of emissions at 4.38 m to compare with the two-bed results. This background test was performed, since PM_{10} emissions from the sand could overshadow any enhanced emissions if the enhanced emissions were small. With the two beds, the emissions were quite large as expected, and mostly due to the Dirty Socks Sand. The concentrations versus uref for both tests are shown on one plot (Figure 81). Power law fits were performed to the two points of recorded emissions for each velocity, since these fits had been the correct ones in the previous studies. Law-of-the-wall equation fits were performed for the corresponding velocity profiles. Using these crude fits, emission rates were calculated for both the background test and the abrasion of the crust with Dirty Socks Sand. These emission rates were plotted versus uref (Figure 82). Both Figures 81 and 82 show that there is enhanced emission due to scouring particles abrading the top surface of the crust which consists primarily of fine sediments (Figure 83). However, this hard crust did not incur much damage and remained intact. Likely as mentioned in AeroVironment, 1992, these crusts break apart by the expansion and contraction of the desert diurnal cycle creating cracking and breaking in the crust. This method of exposure was not a viable means in the laboratory setting. So, finally the crust was fractured manually (Figure 84) by compressing the surface slightly with weight.

Once the crust is broken apart, the first series of tests was repeated. Again, velocity profiles were fit with the law-of-the-wall equation and an estimate of z_0 obtained as 3.0×10^{-4} m (much rougher surface) (Figure 85). At a critical speed the emissions begin to increase (uref = 6.0 m/s) and then rapidly increase, however, not nearly as dramatic as the loose-soil emissions (Figure 86). In fact, the most dramatic act with a broken crust is the tumbling of the broken crust pieces (Figure 83). At critical values upward of uref = 12.0 m/s, some of the crust pieces are lifted up and thrown away from the surface exposing a softer surface which is not entirely moveable in itself, although it easily can be abraded to a loose-soil without much work. Under other parts of the crust, there were areas of loose soil. Likely, on the lake, the hard crusts are weakened by the sand abrasion, broken apart by expansion and contraction associated with the diurnal cycle or other non-aeolian events (i.e., chemical reactions, ultraviolet radiation, etc.), tumbled apart by high winds, and then abraded into loose soils which result in the high emission rates previously attained.

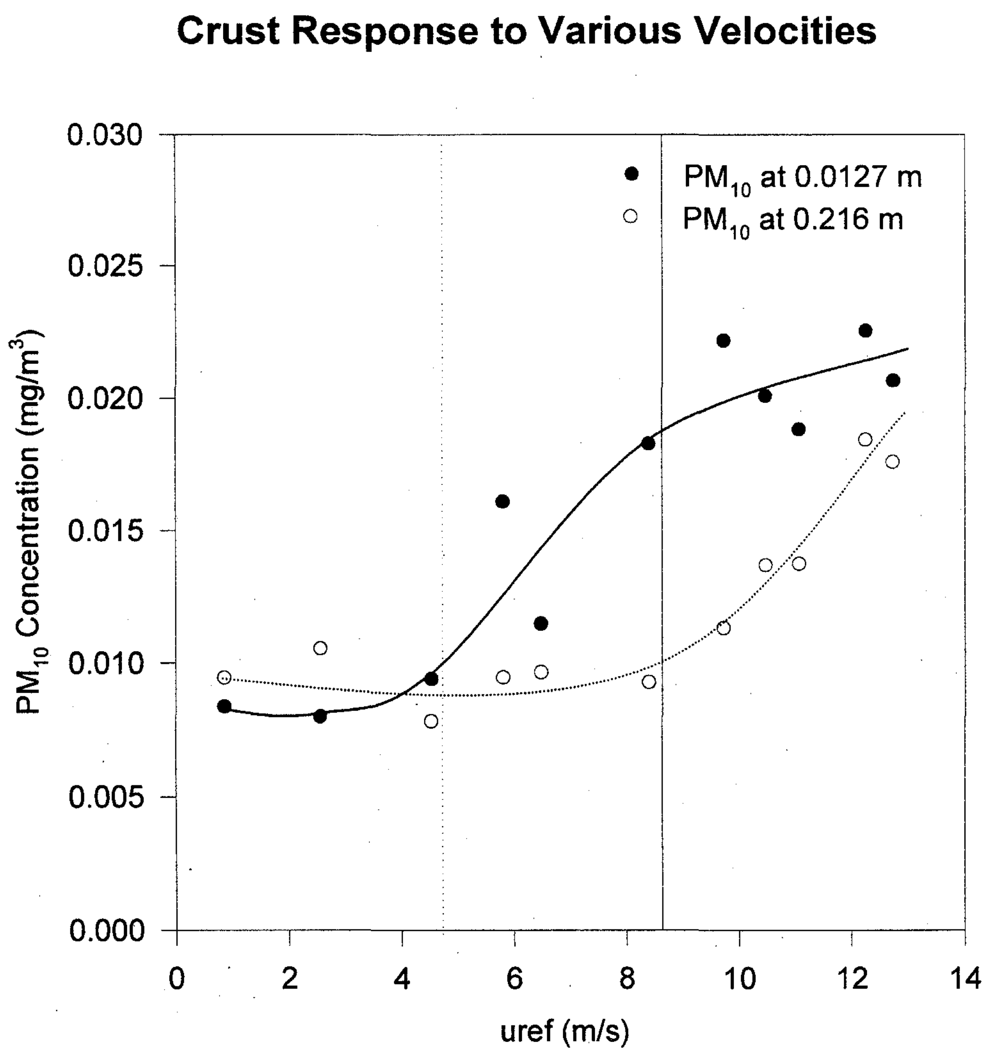

Figure 79. The PM_{10} concentrations versus uref. The concentrations are not large for the hard crust subjected to wind alone; however, there is a distinct moment at which emissions become more noticeable at 0.013 m and at 0.22 m as indicated by the lines on the plot.

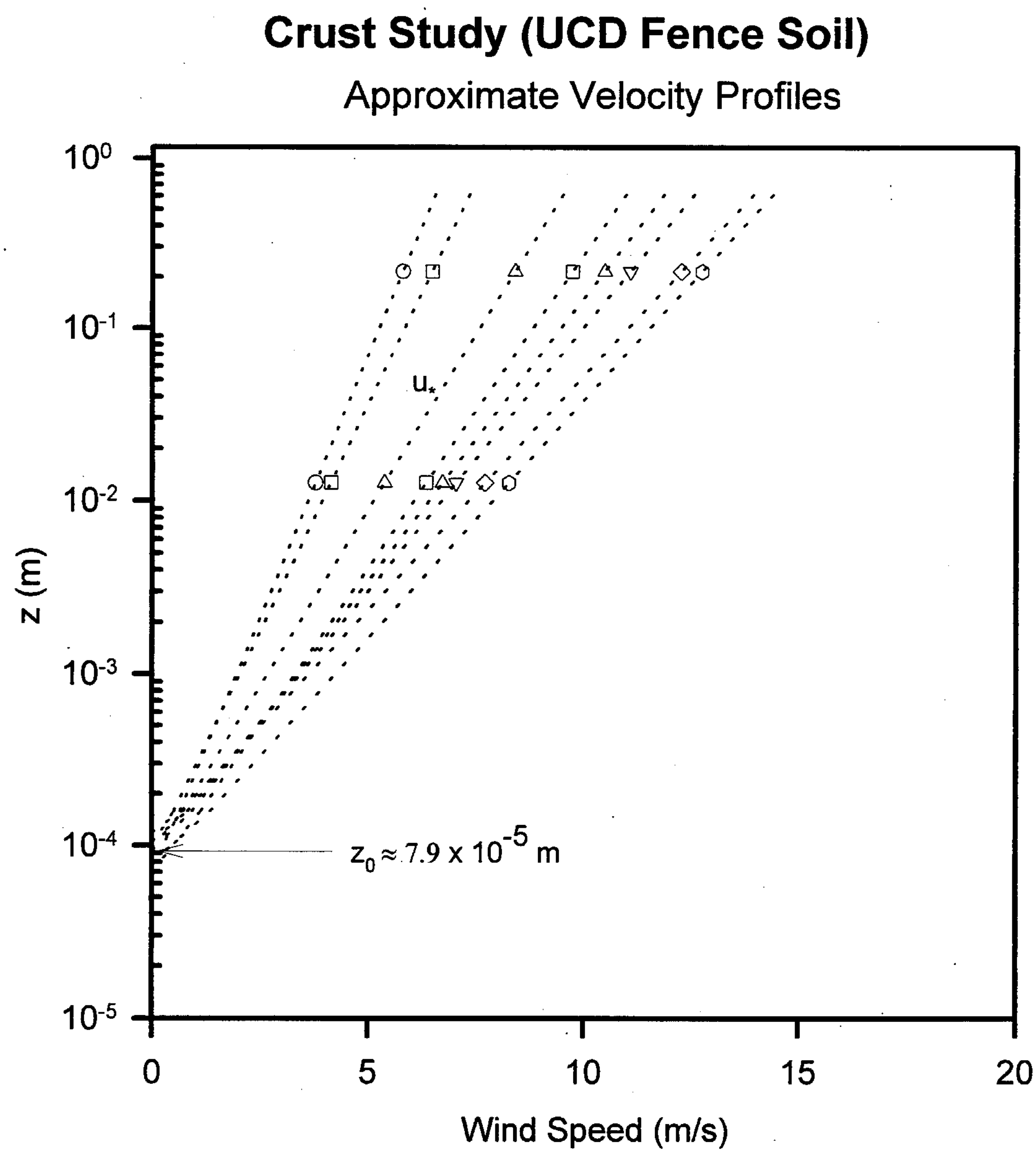

Figure 80. Approximate velocity profiles based on two sampling heights and the Law-of-the-Wall Equation Curve fit. Since there is no saltation, all values of velocity could be used to obtain a wide range. Though only two experimental points were obtained, there is a good focus at the z-axis and the ability to obtain an approximate $z_0 = 7.9 \times 10^{-5}$ m.

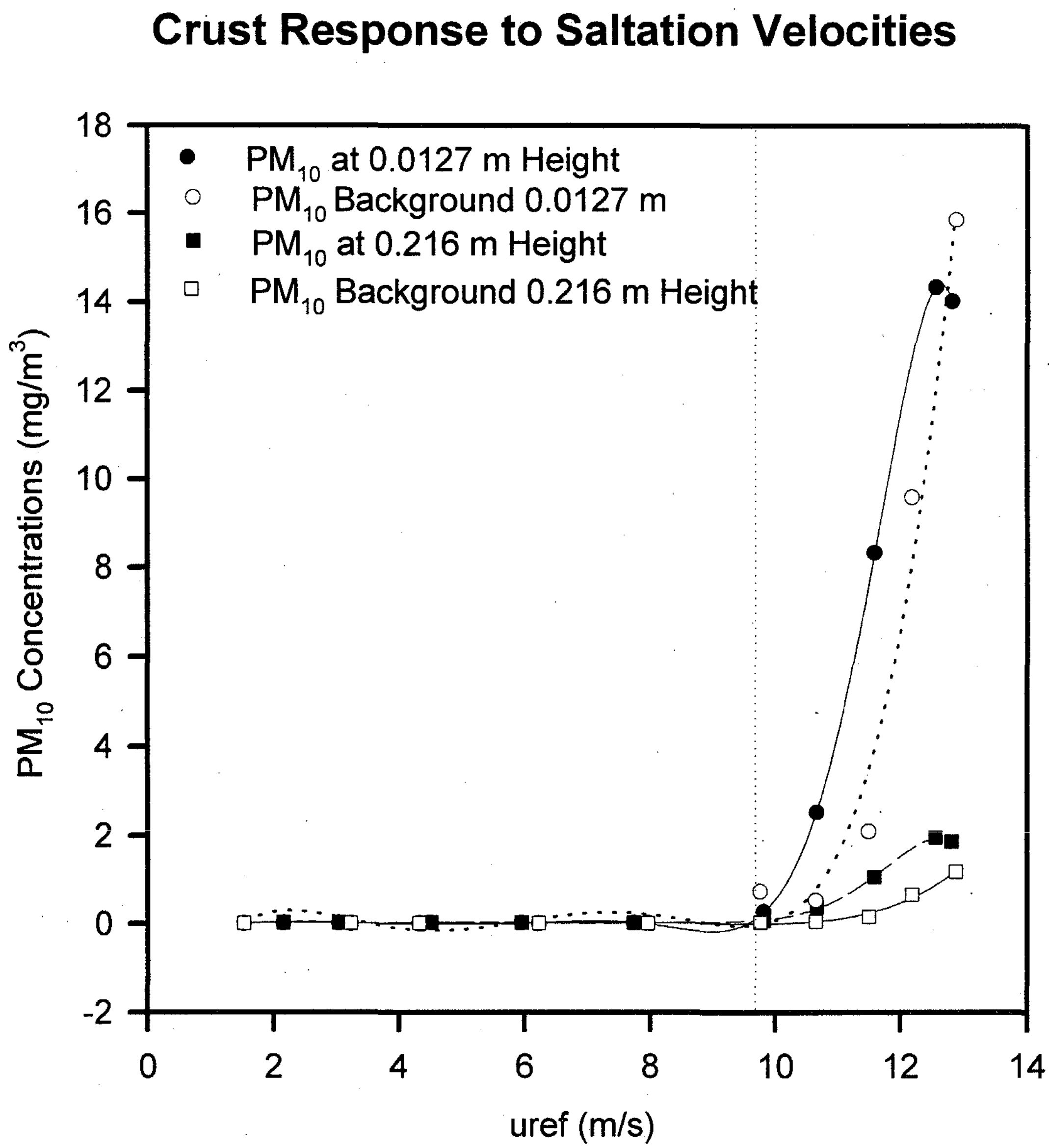

Figure 81. Concentration profiles based on two sampling heights for a UCD Fence Soil crust with Dirty Socks Sand saltating over the crust, and for Dirty Socks Sand with no crust in front of the sand ("Background"). When plotted against the reference speed in the wind tunnel, there appears to be a slight enhancement in emissions due to the saltating sand over the crust. The complete quantitative amount is hard to estimate though, because of the large amount of PM_{10} from the Dirty Socks Sand.

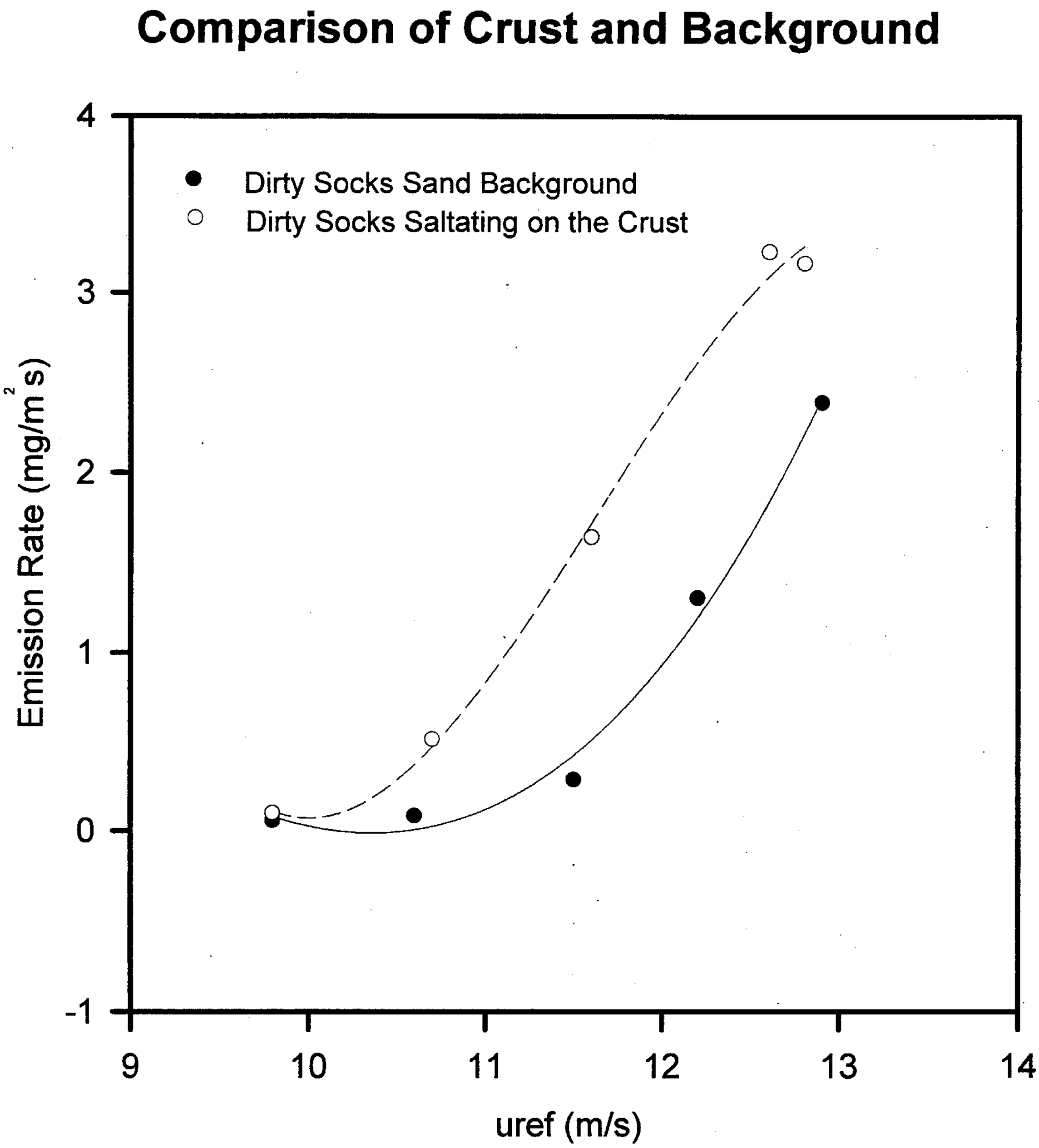

Figure 82. Emission rates based on two sampling heights for a UCD Fence Soil crust with Dirty Socks Sand saltating over the crust, and for Dirty Socks Sand with no crust in front of the sand ("Background"). When plotted against the reference speed in the wind tunnel, there appears to be a slight enhancement in emissions due to the saltating sand over the crust. The complete quantitative amount is hard to estimate though, because of the large amount of PM_{10} from the Dirty Socks Sand.

a)

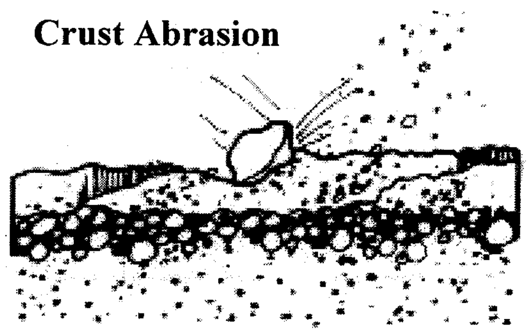

b)

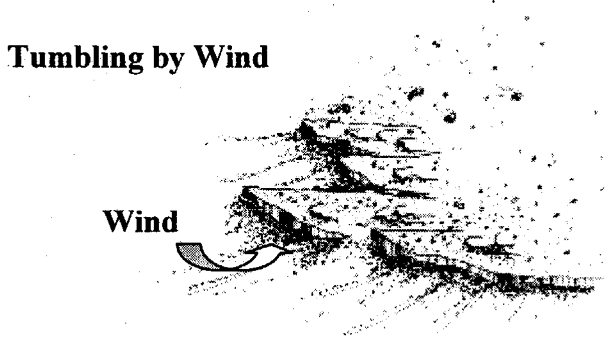

Figure 83. The hard crust emissions were studied in the tunnel and two mechanisms were noted as being important in the emissions from the crust: a) the abrasion of the crust by saltating particles and the possible abrasion of the softer crust underneath and b) the tumbling of the top layer of the crust exposing loose soils and softer crusts underneath the top layer (Kohen et al., 1994).

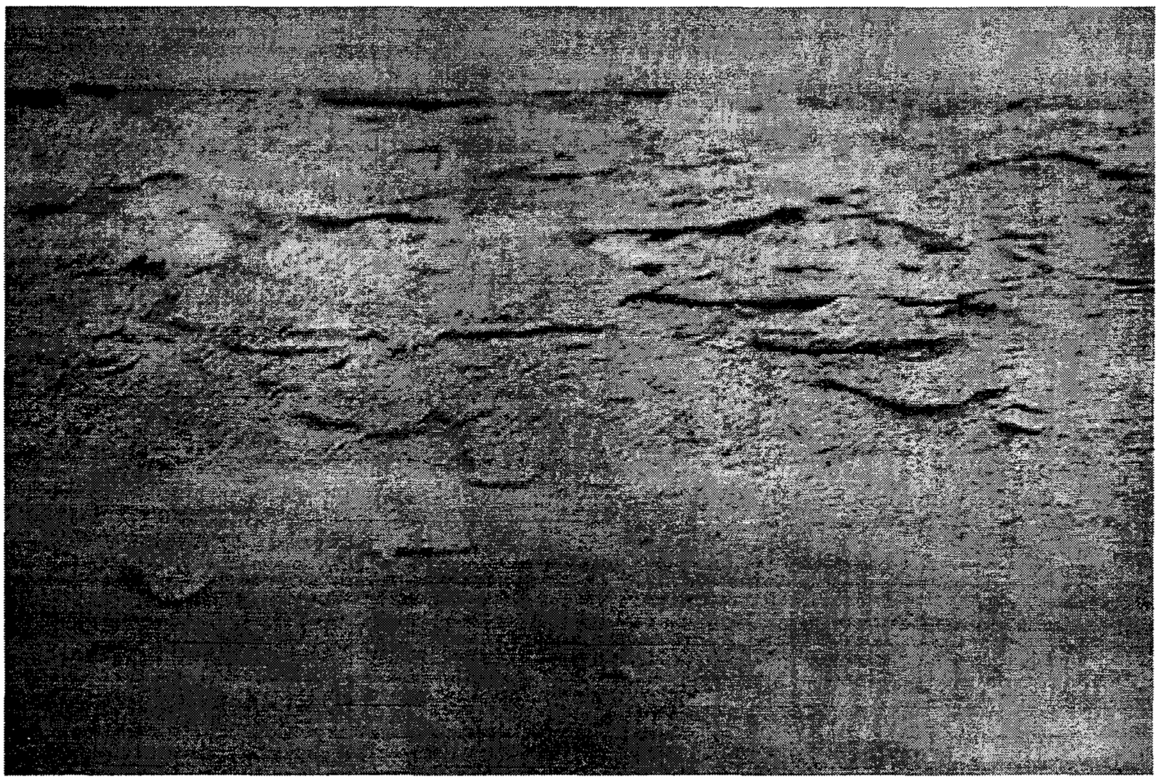

Figure 84. The hard crust was broken manually with pressure once it would not break through wind shear or saltation. The emissions for this crust were then tested for various wind velocities.

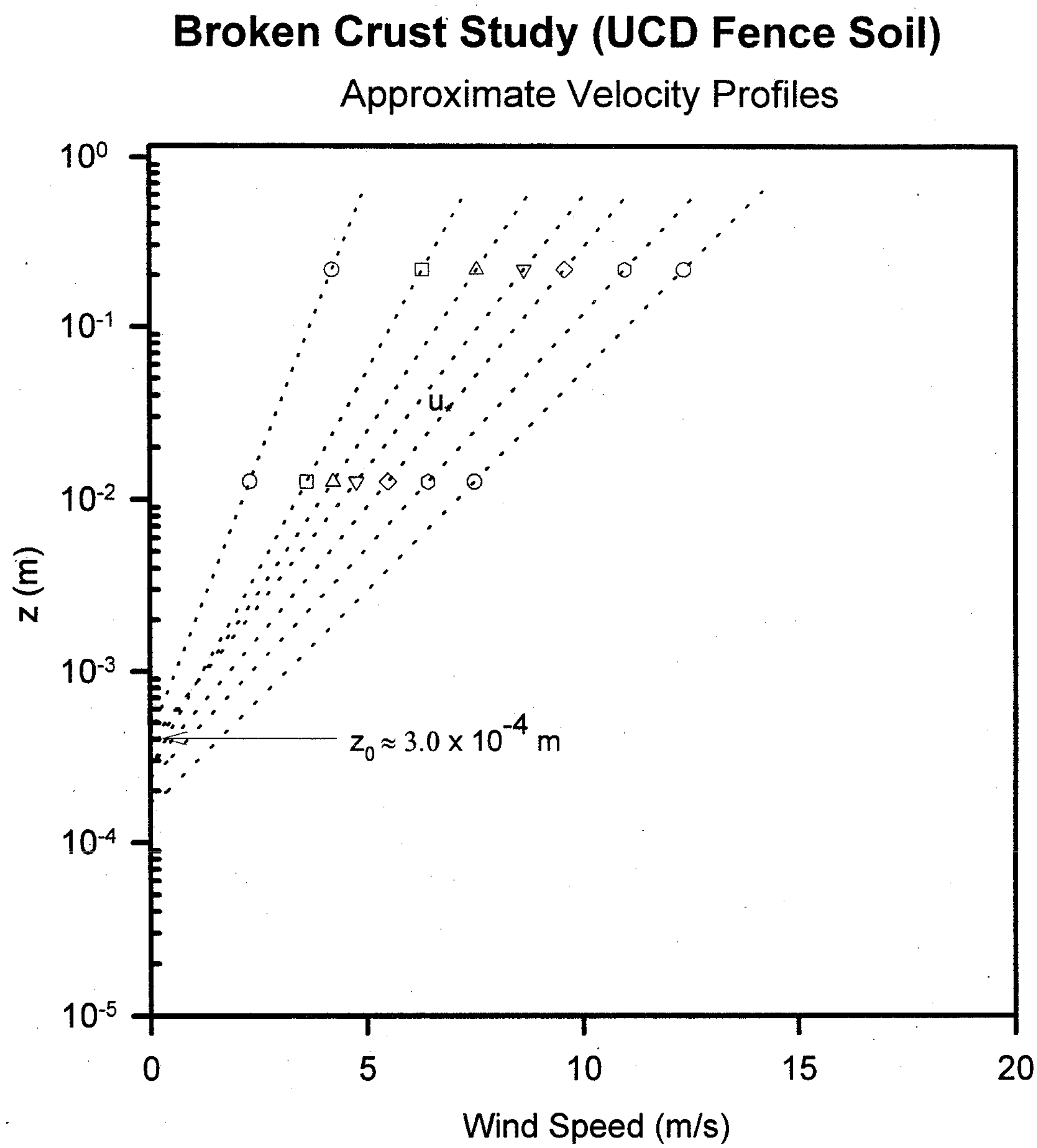

Figure 85. Approximate velocity profiles based on two sampling heights and the Law-of –the-Wall equation curve fit for a broken crust. Since there is primarily no saltation, all values of velocity could be used to obtain a wide range. Though only two experimental points were obtained, there is a good focus at the z-axis and the ability to obtain an approximate $z_0 = 3.0 \times 10^{-4}$ m.

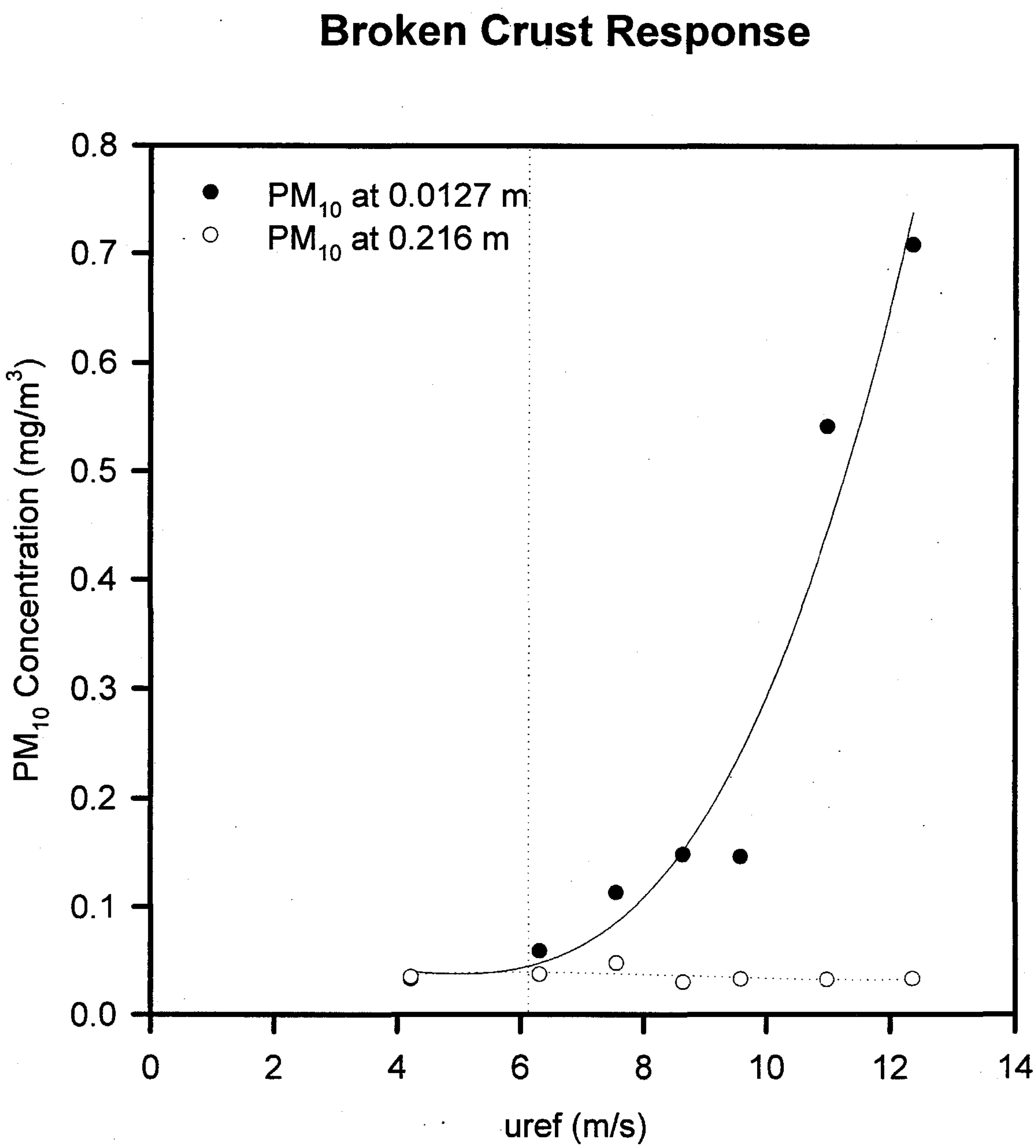

Figure 86. The PM_{10} concentrations versus uref for a broken crust. The concentrations are not very large for the hard broken crust when subjected to wind alone; however, there is a distinct moment at which emissions become more noticeable at 0.013 m as indicated by the line on the plot. These concentrations are greater than the emissions for the unbroken hard crust, but still are not high concentrations in comparison to the loose soil emissions.

3.11. Stability Studies

There were no significant results obtained on the effect of heating instabilities on threshold conditions. The bed was heated to give the required instability with the methods described in Section 2.6.9.; however, the method requires more iterations in order to obtain the type of desired results described previously. Some temperature profiles and velocity profiles with heating were obtained, but none of any consequence to the Owens Lake soils. The one year length allotted on this contract simply did not allow the meticulous attention that this part of the experiment required.